8-2004

Environment-Induced Degradations in a Target Structural Material for Transmutation Applications

Ramprashad Prabhakaran
University of Nevada, Las Vegas

ENVIRONMENT-INDUCED DEGRADATIONS IN A TARGET STRUCTURAL MATERIAL FOR TRANSMUTATION APPLICATIONS

by

Ramprashad Prabhakaran

Bachelor of Engineering in Mechanical Engineering
University of Madras, Chennai, India
May 2001

A thesis submitted in partial fulfillment
of the requirements for the

Master of Science Degree in Mechanical Engineering
Department of Mechanical Engineering
Howard R. Hughes College of Engineering

Graduate College
University of Nevada, Las Vegas
August 2004

Thesis Approval Page
Provided by the Graduate College

ABSTRACT

Environment-Induced Degradations in a Target Structural Material for Transmutation Applications

by

Ramprashad Prabhakaran

Dr. Ajit K. Roy, Examination Committee Chair
Associate Professor of Mechanical Engineering
University of Nevada, Las Vegas

This investigation is focused on the evaluation of stress corrosion cracking (SCC) and localized corrosion behavior of Type 422 stainless steel in aqueous environments at ambient and elevated temperature. The results of constant load SCC testing using smooth specimens showed no failure in the neutral solution but a threshold stress of 97 ksi was observed in the 90°C acidic environment. SCC testing by the slow-strain-rate test method indicate that the time-to-failure, true failure stress and ductility parameters were gradually reduced with increasing temperature, showing more pronounced effect in the acidic solution. The application of a controlled cathodic potential showed further reduction in the magnitude of these parameters indicating a detrimental effect on the cracking due to hydrogen generation. The results of cyclic potentiodynamic polarization testing revealed pits and crevices on the specimen surface, showing more active (negative) critical pitting potential in the 90°C acidic solution, as expected. Metallographic and fractographic evaluations showed secondary cracks at the gage section and a combination of ductile/brittle failures at the primary fracture face, respectively.

TABLE OF CONTENTS

LIST OF TABLES

LIST OF FIGURES

ACKNOWLEDGMENTS

This work was performed under the able guidance of my advisor, Dr. Ajit K. Roy. It was my privilege and pleasure to work with him on this project and I would like to express my gratitude to him for his invaluable contributions.

I would like to thank Dr. Anthony E. Hechanova, Dr. Brendan J. O'Toole and Dr. Satish C. Bhatnagar, for their valuable suggestions and support throughout this investigation.

I would like to acknowledge the assistance offered by my associates in the Materials Performance Laboratory. I would also like to express my appreciation to my parents for their sacrifices, persistent support and boundless confidence in me.

Finally, I would like to acknowledge the United States Department of Energy for the financial support, under Grant Number: DE-FG04-2001AL67358.

CHAPTER 1

INTRODUCTION

Dwight D. Eisenhower outlined his vision for nuclear energy during his historical address at 470th Plenary Meeting of the United Nations on December 8, 1953. Subsequently, international efforts to utilize nuclear technology for the development of mankind began with the conception of International Atomic Energy Agency. Radioactive materials play an important role on human lives. Today, nuclear technology is being used in many applications including medicine, industry, consumer products, scientific research, agriculture, energy, environmental protection, law enforcement and public safety.

Even though the nuclear technology offers several benefits, the disposal of radioactive waste arising from nuclear-power production or from the dismantling of nuclear weapons poses a severe challenge to many nations employing this technology.[1-3]

In countries such as France, United Kingdom and Japan, spent nuclear fuel (SNF) is being reprocessed to extract uranium and plutonium for further use. The United States adapted a policy to place the high-level radioactive waste (HLRW) and SNF in the proposed geologic repository, near Las Vegas, Nevada, without re-processing and therefore, without destroying the plutonium and minor actinides.[4]

The environmental concern over nuclear waste management presents a formidable barrier to increased use of nuclear energy for various applications in the United States at a time when there is global climatic change and there is an increased need for energy independence. At present, the waste that results from nuclear-power reactors will take more than 10,000 years to decay to the natural radioactive levels of uranium ore. The nuclear reactors currently operating in the United States are expected to produce more than 90,000 metric tons of nuclear waste, thereby exceeding the current statutory limit at the Yucca Mountain repository. Thus, if there is a modest growth in the generation of electricity using the nuclear-power plants, the nation needs to construct and license additional repositories in the near future.[5] Hence, alternative paths should be vigorously pursued for future handling of SNF resulting from these reactors.

Globally, significant efforts are ongoing to reduce the half-lives of SNF by a process known as transmutation. Transmutation is currently being practiced in Europe, in particular, Russia, Sweden, Switzerland and France. During this past decade, these countries have made significant progress in partitioning and transmuting the long-lived actinides from SNF. Due to these advances, U.S. national laboratories had begun to explore the transmutation concept as an alternative waste management strategy. The transmutation of SNF, shown in Figures 1.1 and 1.2, would provide the benefit of disposing substantially less radioactive waste inside the proposed geologic repository at the Yucca Mountain site.

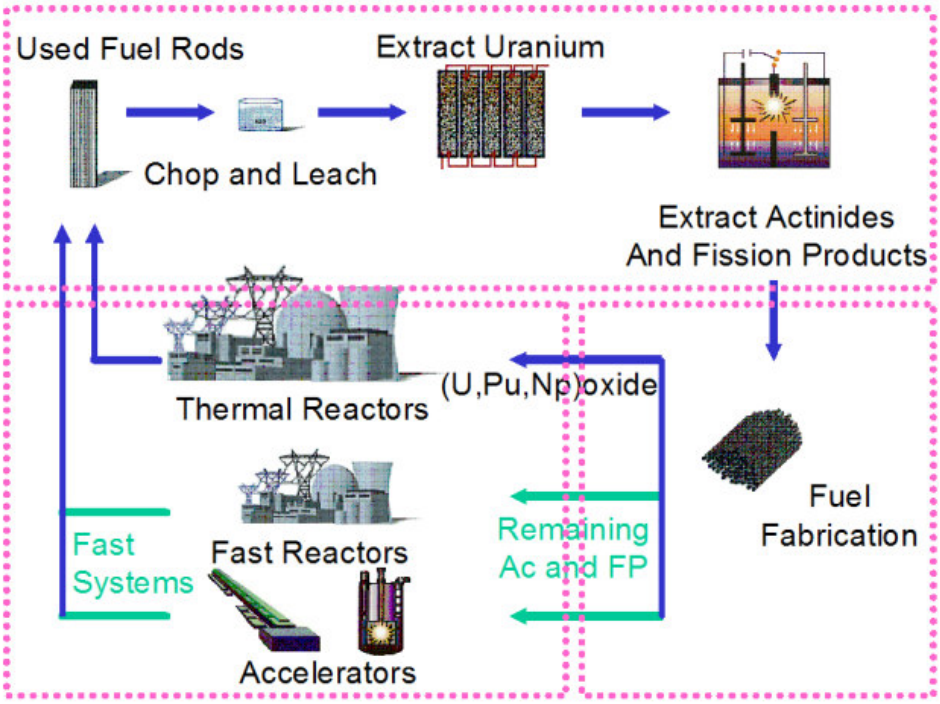

Figure 1.1: Transmutation Approach

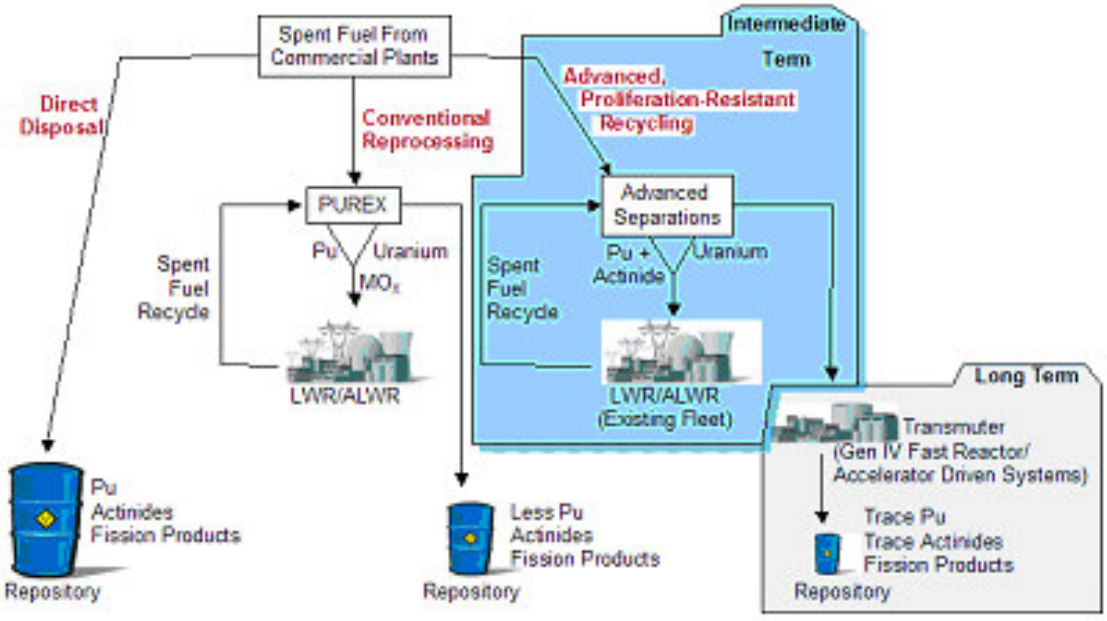

Figure 1.2: SNF Management Approach

Several research projects are ongoing to determine to feasibility of using accelerator driven systems (ADS) concept for the process of transmutation of SNF.[6,7,8] An ADS system consists of an accelerator for high-energy proton generation, a spallation target to produce neutrons and a subcritical blanket. A heavy material is preferred for the target to increase the number of spallation neutrons. In addition, liquid metal targets are considered to solve heat removal and radiation damage problems. The lead-bismuth-eutectic alloy (Pb: 55.2 wt % Bi) is a candidate for the target material. Martensitic steels containing 9-12 % Cr class are considered as candidate target structural materials.

Transmutation enables elimination or reduction of undesirable radioactive isotopes and actinides from SNF.[9] Transmutation refers to the transformation of SNF by impingement of neutrons generated by direct bombardment of accelerator driven proton beam onto a target material such as molten lead-bismuth-eutectic (LBE) that may be contained inside a structural configuration made of a martensitic steel such as Alloy EP-823, Alloy HT-9 and Type 422 stainless steel (SS), by a process known as spallation, as shown in Figure 1.3.

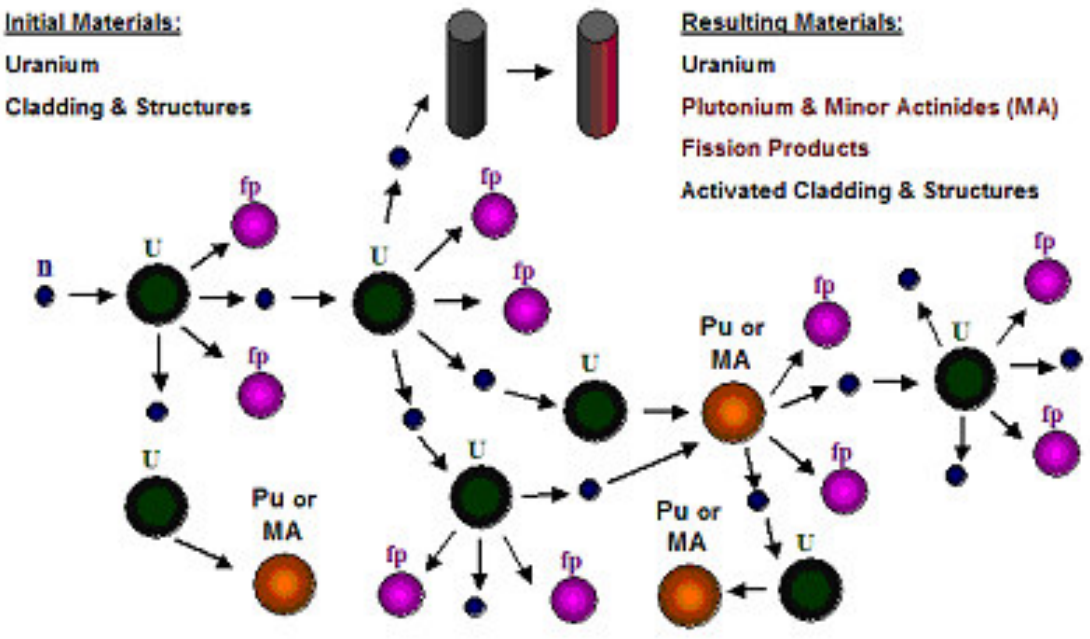

Figure 1.3: Separation of Fission Products and Actinides

Molten LBE is a very effective nuclear coolant because of its low melting temperature, low vapor pressure, good neutron yield, low neutron absorption, high boiling temperature, high atomic number and good heat removal.[10] The Russians have developed an extensive knowledge on LBE by virtue of its use as a coolant in their alpha-class submarines. Further, LBE has been identified to be an efficient spallation target source during the transmutation process.

Martensitic stainless steels are candidates for structural materials in future high-power spallation neutron sources, ADS facilities as well as in fusion reactors.[11-14] Compared to the austenitic stainless steels, this class of material is favorable due to their high mechanical strength and lower susceptibility to void swelling, irradiation creep and high-temperature helium embrittlement. However, the points of concern are possible problems with welding, irradiation at low temperatures and hydrogen embrittlement due to their

lower solubility. An increase in ductile-to-brittle transition temperature (DBTT) by helium has also been observed with these materials. Since the spallation neutron source will result in an abundant amount of hydrogen and helium, it is very important to perform a detailed investigation. Hydrogen is effectively retained in martensitic stainless steels even at elevated temperatures due to its trapping. The presence of hydrogen increases the hardness and thereby, reduces the ductility.[15]

The molten LBE has the tendency to corrode most engineering materials in the form of liquid metal corrosion and embrittlement.[16] Hence, liquid metal corrosion has to be considered while selecting the appropriate containment materials for the target. This phenomenon manifests itself in numerous ways: dissolution, compound formation, and liquid penetration at grain boundaries. The corrosion process depends upon various factors such as time of exposure, temperature, thermal gradient, flow velocity, solid and liquid compositions.[17] Several studies addressing the issue of corrosion of the steel in the presence of either lead or LBE have been published in the literature.[18-26]

During the transmutation process, significant amount of stress, heat, hydrogen and helium can be generated and hence, the structural material may be subjected to various environment-induced degradations such as stress corrosion cracking (SCC), hydrogen embrittlement (HE) and localized (pitting and crevice) corrosion in the susceptible environments.[15, 27]

So far, very little work has been performed in the United States to identify and characterize the structural material that can contain the target at hostile environments and temperature. Therefore, it is appropriate to evaluate the performance of a candidate structural material, namely, Type 422 SS in molten LBE environment. Simultaneously,

the corrosion behavior of this alloy in aqueous environments of different pH is required to be evaluated to establish the baseline data that can be compared to those evaluated in the molten LBE, to achieve a thorough understanding of the corrosion behavior of Type 422 SS.

This investigation in aimed at elucidating the effect of environmental and mechanical variables on environment-induced degradations of Type 422 SS in aqueous environments using different state-of-the-art testing techniques. The metallurgical and fractographic evaluations of this material, as determined by surface analysis techniques, have also been presented in this thesis. Currently, tests are ongoing at the Los Alamos National Laboratory (LANL) to evaluate the SCC susceptibility in the presence of molten LBE. Based on the overall data obtained in the aqueous environments and the molten LBE, the most viable structural material will eventually be selected for transmutation applications.

CHAPTER 2

TEST MATERIAL, SPECIMENS AND ENVIRONMENTS

2.1. Test Material

Stainless steels are strong, weldable and corrosion resistant structural materials. Several grades of stainless steels have been used for construction of nuclear facilities. In the past, numerous martensitic stainless steels have been developed for the fast breeder and fusion reactor programs. Martensitic stainless steels containing 9-12 weight percent (wt %) of chromium are recognized to be the leading candidate structural materials for the first wall.[28-30] The presence of at least 9 wt % of chromium has been proved to optimize the requirements for enhanced corrosion resistance and reduced irradiation-embrittlement tendency.[15] Martensitic stainless steels are essentially alloys of chromium and carbon that can develop a body-centered-cubic (bcc) or body-centered-tetragonal (bct) crystal structure in the hardened martensitic condition. They are ferromagnetic and hardenable by heat-treatments.

A comparison of the stress-strain curves for different types of SS are shown in Figure 2.1, indicating the enhanced strength in the martensitic stainless steels, compared to the other types of stainless steels. The effect of the testing temperature on the yield strength (YS) and creep strength (CS) for different types of SS is shown in Figure 2.2. These data indicate that the martensitic stainless steels can retain its high YS and CS even at the elevated temperatures.[31]

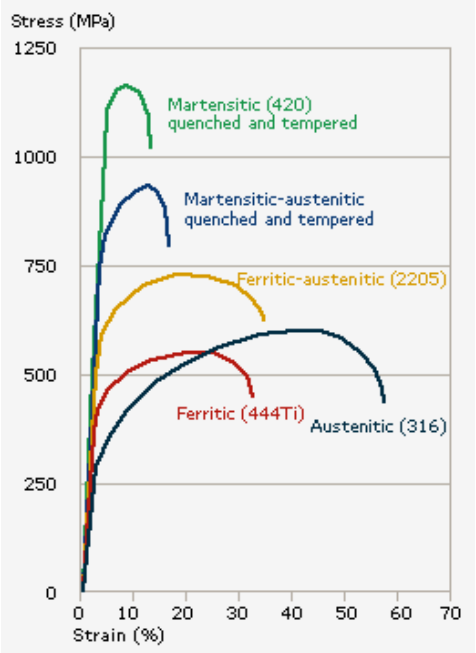

Figure 2.1: Stress-Strain Curves for Different Types of SS at 25°C [31]

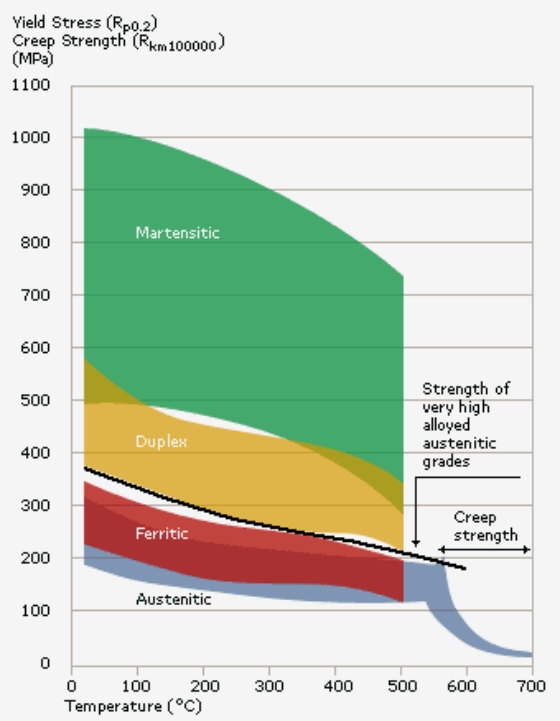

Figure 2.2: Effect of Temperature on YS and CS for Different Types of SS [31]

Martensitic Type 422 SS is a candidate structural material to hold the molten LBE during the transmutation process. It has higher mechanical strength, lower thermal expansion, higher swelling resistance, lower work hardening index, higher thermal conductivity, higher resistance to irradiation creep and helium-embrittlement and better liquid-metal compatibility than the austenitic stainless steels.[32-34] Type 422 SS can possess high strength and toughness at temperatures up to 1200°F (650°C). Besides nuclear applications, it can also be used for highly stressed components such as the turbine blades and high-strength fasteners for applications in the corrosive environments due to its ability to be heat-treated in large sections. Further, it has high damping capacity and good resistance to fatigue, thermal shock and hot pressurized molecular hydrogen.[35-37] The Table 2.1 provides the basic information on Type 422 SS.[38]

Table 2.1: Basic Information on Type 422 [38]

Category	Steel
Class	Stainless Steel
Type	Martensitic Standard
Common Name	Chromium Steel
Designations/ Standards	**U.S.**: AISI 422, AMS 5655, ASTM A565, SAE 51422, SAE J467, UNS S42200 **Germany**: DIN 1.4935 **Japan**: JIS SUN 616

The high strength and hardness values associated with Type 422 SS can be primarily attributed to the presence of relatively high carbon content. In addition, it has carbide-forming elements such as molybdenum, vanadium and tungsten for the high-temperature strength. The improved corrosion resistance of this alloy is primarily due to the presence of chromium oxide protective film. The chromium and carbon contents are balanced to

ensure a martensitic structure following the hardening operation. Molybdenum, nickel and nitrogen are added to improve the mechanical strength and localized corrosion resistance. Nitrogen can also improve the formability and ductility and can maintain the desired metallurgical microstructure without forming excessive free ferrite.[39] The mechanical and thermal properties of Type 422 SS are shown in Tables 2.2 and 2.3, respectively.[38]

Table 2.2: Mechanical Properties of Type 422 SS [38]

Properties	**Value at 25°C**
Poisson's Ratio	0.27 to 0.30
Density	7800 kg/m^3
Specific Gravity	7.8
Elastic Modulus	190 - 210 GPa (27557 - 30457 ksi)
Tensile Strength	965 MPa (139.96 ksi)
Yield Strength	760 MPa (110.23 ksi)
Elongation	13 %
Reduction in Area	30 %

Table 2.3: Thermal Properties of Type 422 SS [38]

Properties	**Value at 0 - 100°C**	**Value at 0 - 500°C**
Thermal Expansion	11.2 * 10^{-6}/°C	11.9 * 10^{-6}/°C
Thermal Conductivity	23.9 W/m-K	27.3 W/m-K
Specific Heat	460 J/Kg-K	-

Experimental heats of Type 422 SS were custom-melted by a vacuum-induction-melting (VIM) practice and were subsequently processed into round bars. The heat-treatment of Type 422 SS is similar to that of carbon and low-alloy steels. In order to

achieve maximum corrosion resistance and strength, these bars were austenitized at 1850°F (1010°C) for 1 hour, followed by an oil-quench. Type 422 SS has high hardenability due to its high alloy content; hence, it can be quenched in either oil or air. Oil quenching can improve the ductility and can reduce delayed cracking.[25, 40] The austenitized bars were then tempered at 1150°F (621°C) for 1.25 hours and were subsequently air-cooled. The purpose of quenching and tempering was to achieve a fully-tempered fine-grained martensitic microstructure without any retained austenite. The chemical composition of Type 422 SS tested in this study is shown in Table 2.4.

Table 2.4: Chemical Composition of Type 422 SS (wt %)

Heat Number	C	Mn	P	S	Si	Cr	Ni	Mo	Cu	V	W	Fe
2051	0.21	0.55	0.013	0.005	0.51	12.83	0.73	0.98	0.002	0.22	0.93	Bal

Bal: Balance

2.2. Test Specimens

Cylindrical smooth and notched specimens (4-inch overall length, 1-inch gage length and 0.25-inch gage diameter) of Type 422 SS were machined from the heat-treated bars in such a way that the gage section was parallel to the longitudinal rolling direction. It is known that imperfections such as notch or dents can be present in machined specimens, which can influence the performance of test specimens. In view of this rationale, a V-shaped notch of 0.156-inch diameter, with an angle of 60º and a maximum depth of 0.05 inch around the diameter was added to the center of the gage section of the test specimen to study the effect of stress concentration. A gage length to gage diameter (l/d) ratio of 4 was maintained for both smooth and notched specimens according to the ASTM

Designation E 8.[41] The schematic view (Figure 2.3) and detailed dimensions of smooth and notched specimens, are shown in Figures 2.4 and 2.5, respectively.

(a)

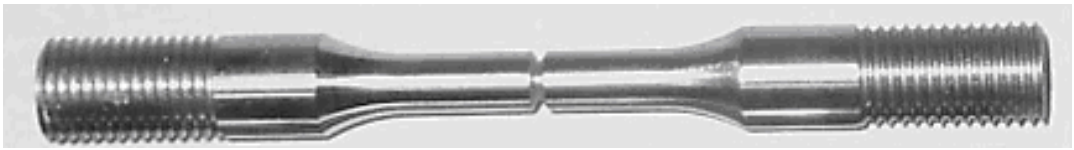

(b)

Figure 2.3: Schematic View of (a) Smooth and (b) Notched Cylindrical Specimens

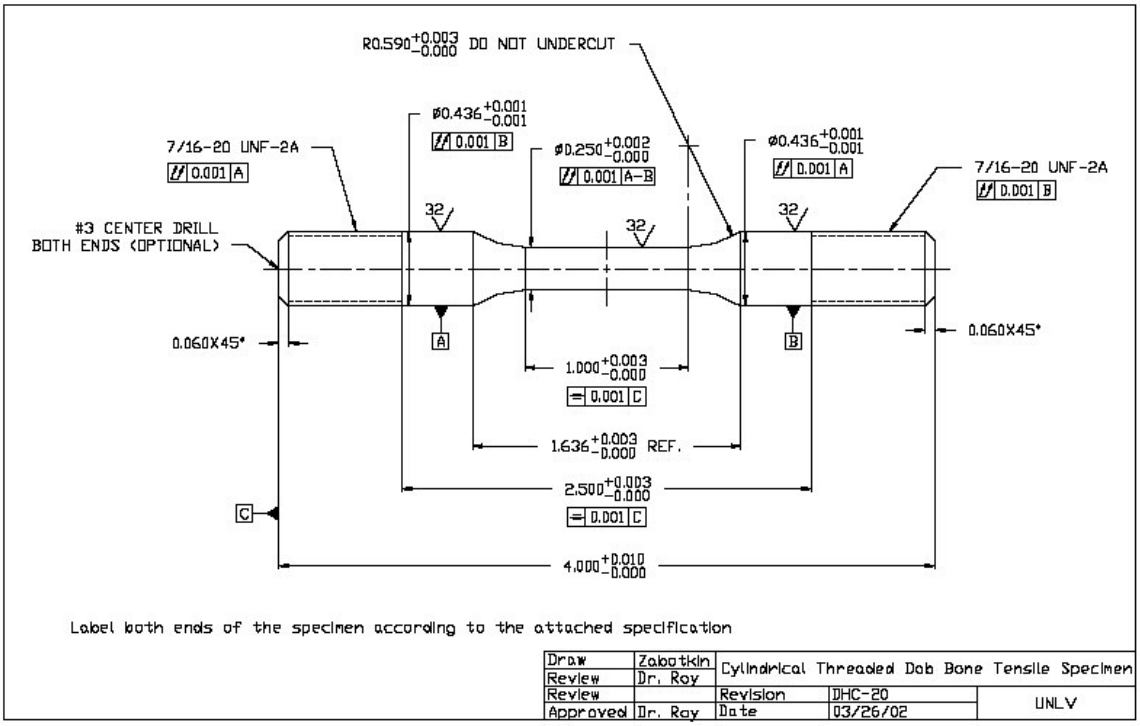

Figure 2.4: Dimensions of Smooth Cylindrical Specimen

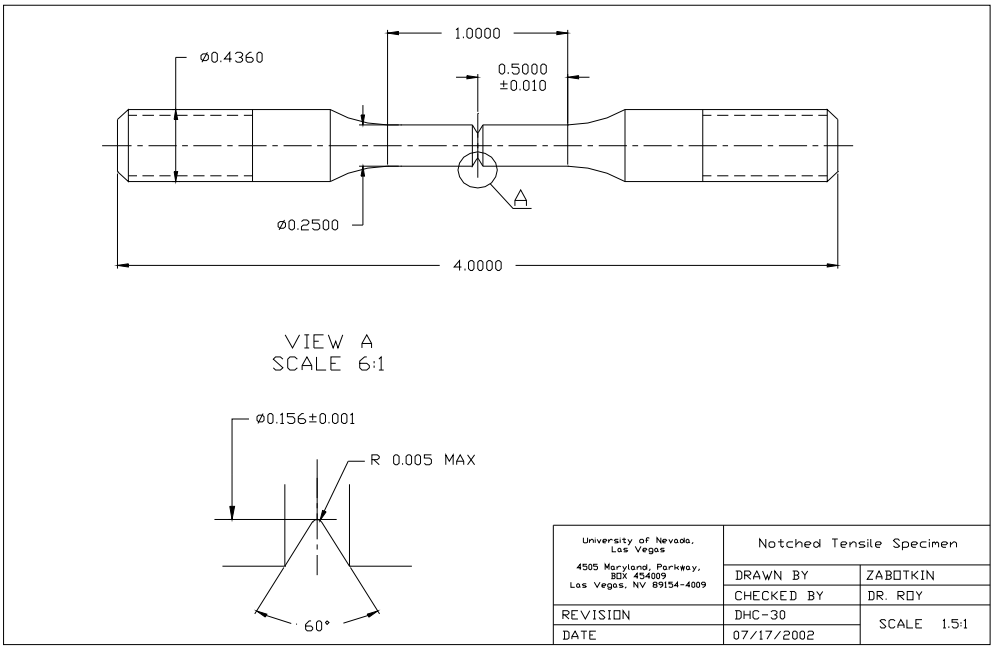

Figure 2.5: Dimensions of Notched Cylindrical Specimen

Based on the dimensions of the notched specimen, shown in Figure 2.4, the magnitude of the stress concentration factor (K_t) was determined, as shown by the following calculations. Using the D/d and r/d ratios of 1.60 and 0.032, respectively, the K_t value was computed from the plots, shown in Figure 2.6.[42] Based on these plots, an approximate K_t value of 2.9 was determined for the notched specimens.

$$\frac{D}{d} = \frac{0.250in}{0.156in} = 1.60$$

$$\frac{r}{d} = \frac{0.005}{0.156} = 0.032$$

Where,

D = Gage diameter of the specimen

d = Notch diameter of the specimen

r = Radius of curvature at the root of the notch

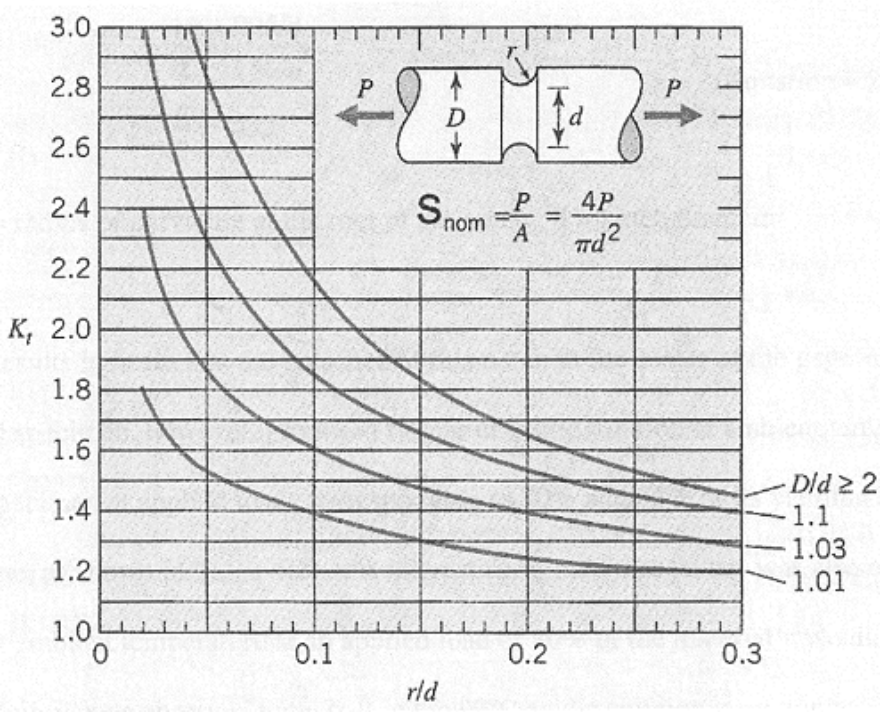

Figure 2.6: Geometric Stress Concentration Factor [42]

The smaller cylindrical specimens, used in the cyclic potentiodynamic polarization (CPP) experiments and their detailed dimensions, are shown in Figure 2.7.

(a)

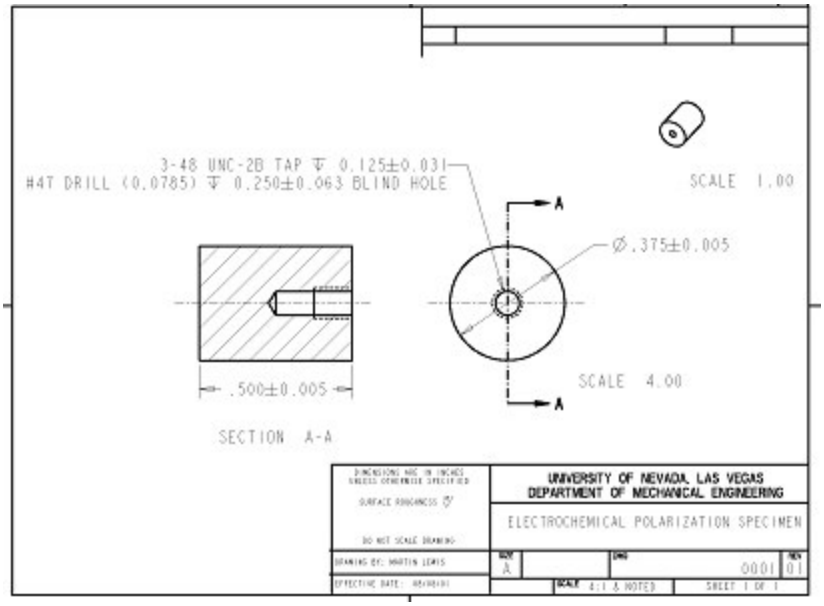

(b)

Figure 2.7: CPP Specimen (a) Schematic View and (b) Dimensions

2.3. Test Environments

Type 422 SS is a leading candidate structural material to contain the molten LBE, which acts as a target material during the transmutation process. The molten LBE has the tendency to corrode most engineering materials in the form of liquid-metal corrosion and embrittlement.[16] So far, very little work has been performed in the United States to identify and characterize the structural material that can sustain the hostile environments and temperature associated with the molten LBE. Therefore, it is appropriate to evaluate the performance of Type 422 SS in the molten LBE environment. Simultaneously, the

corrosion behavior of this alloy in aqueous environments of different pH is required to be evaluated to establish the baseline data that can be compared to those evaluated in the molten LBE, to achieve a thorough understanding of the corrosion behavior of Type 422 SS. Aqueous corrosion testing has been performed at the UNLV's Material Performance Laboratory (MPL) to study the susceptibility of Type 422 SS to environment-induced-embrittlement including SCC and HE. The localized corrosion behavior was also investigated. The effects of environmental and mechanical parameters on SCC, HE and localized corrosion behavior have been evaluated in this investigation. Both neutral and acidic solutions have been tested at ambient temperature, 60 and 90°C. The compositions of these environments, are shown in Table 2.5.

Table 2.5: Chemical Composition of Tested Solutions (gm/liter)

Environment (pH)	**$CaCl_2$**	**K_2SO_4**	**$MgSO_4$**	**NaCl**	**$NaNO_3$**	**Na_2SO_4**
Neutral (6.0-6.5)	2.77	7.58	4.95	39.97	31.53	56.74
Acidic (2.0-2.2)	Same as above except for an addition of HCl to adjust the pH to the desired range					

CHAPTER 3

EXPERIMENTAL PROCEDURES

The study of stress-corrosion-cracking (SCC) involves the consideration and evaluation of the inherent compatibility between a material and the environment under conditions of either applied or residual stress. The evaluation of SCC susceptibility of a material using laboratory testing methods can provide data that can increase the confidence level and at the same time allow proper selection of the structural materials.

Type 422 SS is a candidate structural material to contain the molten LBE during the transmutation process. During this process, significant amount of stress, heat, hydrogen and helium can be generated and hence, the structural material may be subjected to various environment-induced degradations such as SCC and HE in susceptible environments.[27] In addition, the molten LBE has a tendency to corrode most engineering materials in the form of the liquid-metal corrosion and liquid-embrittlement.[16, 27] Thus, it is appropriate to evaluate the susceptibility of Type 422 SS to SCC and HE in the molten LBE environment at elevated temperatures. In addition, it is necessary to establish baseline corrosion data in aqueous solution to correlate these data to those generated in molten LBE environment. Based on the overall data obtained in the aqueous environments and the molten LBE, the most viable structural material will eventually be selected for transmutation applications.

In view of this rationale, SCC testing in the molten LBE has just been initiated at the LANL. Simultaneously, SCC/HE tests have been performed at the UNLV's MPL in neutral and acidic aqueous solutions at ambient and elevated temperatures using the constant-load (CL) and slow-strain-rate (SSR) testing techniques. Both smooth and notched tensile specimens have been used to evaluate the SCC behavior of Type 422 SS. Prior to the SCC testing; the room-temperature mechanical properties of the test material were determined by using a mechanical testing system (MTS). The susceptibility of this alloy to localized corrosion has been determined in similar environments by CPP testing technique. The effect of hydrogen on the cracking behavior (HE) of Type 422 SS was also evaluated by performing SSR tests under controlled cathodic potential. The fractographic and metallographic evaluations of tested specimens were performed by scanning electron microscopy (SEM) and optical microscopy, respectively.

3.1. Mechanical Properties

A computer-controlled MTS unit, shown in Figure 3.1, was used to determine the ambient-temperature tensile properties of Type 422 SS according to the ASTM Designation E 8.[15] This system has a capability of tensile properties evaluation at temperatures up to 600°C.

Figure 3.1: High-Temperature MTS unit

3.2. Stress Corrosion Cracking

No single experimental technique exists for the SCC evaluation. However, the SCC evaluation of a material involves the use of a specimen type and technique that take both metallurgical and environmental factors into consideration. As mentioned earlier, the susceptibility of Type 422 SS to SCC was determined by both CL and SSR testing techniques. The experimental details for each type of testing are given below.

3.2.1. Constant-Load Testing

One of the most common and basic methods utilized in the SCC tests is the use of a constant applied tensile load that can act as a driving force for SCC to occur. Smooth and notched cylindrical specimens were employed to load them at various levels of applied stress/load according to the ASTM Designation G-49.[43, 44]

A loading device such as a calibrated proof ring was used for the CL testing. Proof rings fabricated from precision-machined alloy steel were designed to precisely determine the SCC susceptibility of the test material to meet the requirements of the National Association of Corrosion Engineers (NACE) Standards.[45] The basic CL testing unit consisted of a calibrated proof ring, proof ring base, specimen grips, environment chamber, microswitch, dial indicator, thermocouple, heating coil, temperature controller, elapsed timer controller and accessory support. Each proof ring was calibrated showing a load versus deflection curve, which was used to determine the applied load during the CL testing, as shown in Figure 3.2.

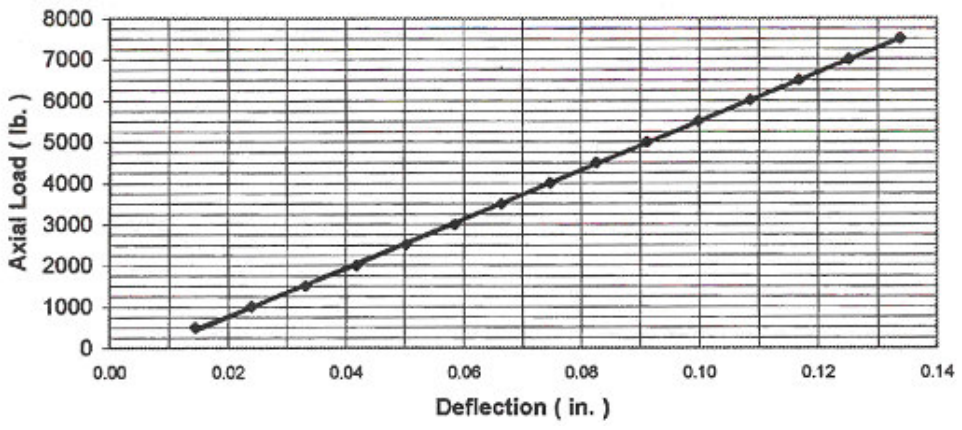

Figure 3.2: A Typical Calibration Curve for the Proof Ring

Micrometers with the supplied dial indicator were used to measure the ring deflection. The operation of the proof ring was based on the ability to transfer the load of a deflected proof ring to a tensile specimen to obtain a sustained loading. The entire test method was performed in accordance with the NACE Test Standard TM-01-77.[45] Load was applied on the proof ring by using a standard wrench on the tension-adjusting screw and lock nut. A thrust bearing was employed to distribute the load and prevent seizure. The experimental setup for CL testing is shown in Figure 3.3.

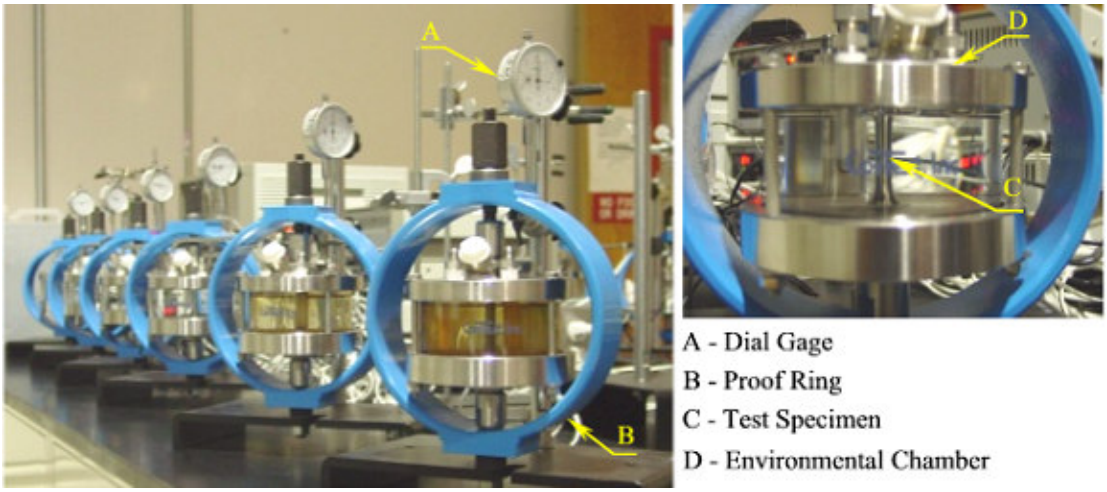

Figure 3.3: Constant-Load Test Setup

Specimen grips on the proof rings were made of stainless steel to be fully resistant to the test environment. A standard clear, durable acrylic/pyrex glass environment chamber was used for the ambient-temperature testing to permit the visual observation of the specimen. A Hastelloy C-276 vessel was used for the high-temperature testing. The environmental chamber was firmly secured by using O-ring seals to prevent any leakage. For high-temperature testing, the heating coil was connected to the bottom cover of the

environmental chamber and a thermocouple was added in the top cover to monitor the testing temperature by the use of a temperature controller. The test specimens were electrically isolated by means of nylon bushings and all tube fittings were wrapped with Teflon tapes to prevent any leakage. Elapsed time monitors were used to record and provide digital display of the time-to-failure (TTF).

The magnitude of the applied load was based on the ambient-temperature tensile yield strength (YS) of the test material. The applied load was calculated by using the following equation:

$$P = S \times A$$

Where,

P = Applied Load

A = Cross-sectional area at the gage section

S = YS of Type 422 SS

Cylindrical specimens with a notch at the center of the gage section were also used to study the effect of stress concentration. For the notched specimens, the magnitude of the applied load was based on the ambient-temperature tensile yielding load (YL), as opposed to the YS used for a smooth specimen.

The amount of deflection needed to apply the desired load on the smooth and notched specimens was obtained from the calibration curve of each proof ring. The specimens were loaded at values equivalent to the different percentages of the material's YS and YL

values for the smooth and notched tensile specimens, respectively. The corresponding TTF was recorded by a timer attached to the test specimen. During the CL testing, once cracking is initiated in the specimen, the cross-sectional area reduces and hence, the applied stress increases. Thus, the specimen often fails soon after the initiation of cracking in susceptible environments. The determination of the cracking tendency using this method was based on the TTF for the maximum test period of 30 days. The cracking tendency in the CL testing was expressed in terms of a threshold stress/load for a particular test condition, below which failure did not occur during the maximum test period of 30 days.

3.2.2. Slow-Strain-Rate Testing

The slow-strain-rate (SSR) testing, also known as the constant extension rate testing (CERT), is a dynamic SCC evaluation technique. During the SSR testing, the specimen was continuously strained in tension until fracture, according to the ASTM Designation G129,[46] in contrast to more conventional SCC testing conducted under a sustained load condition. The application of a dynamic plastic strain reduces the initiation time for the onset of cracking and causes an accelerated rupture of the surface films in the susceptible materials. Hence, it can cause failure that probably might not occur under a CL condition or might have taken a prohibitively longer duration to initiate cracks in producing failures in the tested specimens.[47]

The primary advantage of the SSR testing technique is that it allows the evaluation of the effect of metallurgical variables such as alloy composition, heat treatment, microstructure, and/or environmental parameters, in a relatively short duration. The SSR unit employed in this study has a load capacity of 7500 pounds with linear extension rates

ranging from 10^{-5} to 10^{-8} in/sec. This unit contained a heavy-duty load-frame to minimize the system compliance but at the same time maintained the precise axial alignment of the load train. An all-gear drive system provided the consistent extension rate.

The experimental setup for SCC testing by the SSR method is shown in Figure 3.4. This unit consisted of a load frame, top-loaded actuator, environmental chamber, load cell, linear variable displacement transducer (LVDT), specimen grips, stepper motor, motion controller, thermocouple, heating coil, temperature controller and accessory support. A top-loaded actuator was used to pull the specimen at a specified strain rate. The load cell was employed to apply the load through a front panel interface system. The LVDT was used to record the displacement of the gage section during straining.

Prior to the SCC testing by the SSR technique, the load-frame-compliance factor (LFCF), which is defined as the deflection in the frame per unit load, was determined by using ferritic Type 430 SS. The generated LFCF data are shown in Figure 3.5. The LFCF values were fed to the load frame acquisition system, prior to the SCC testing.

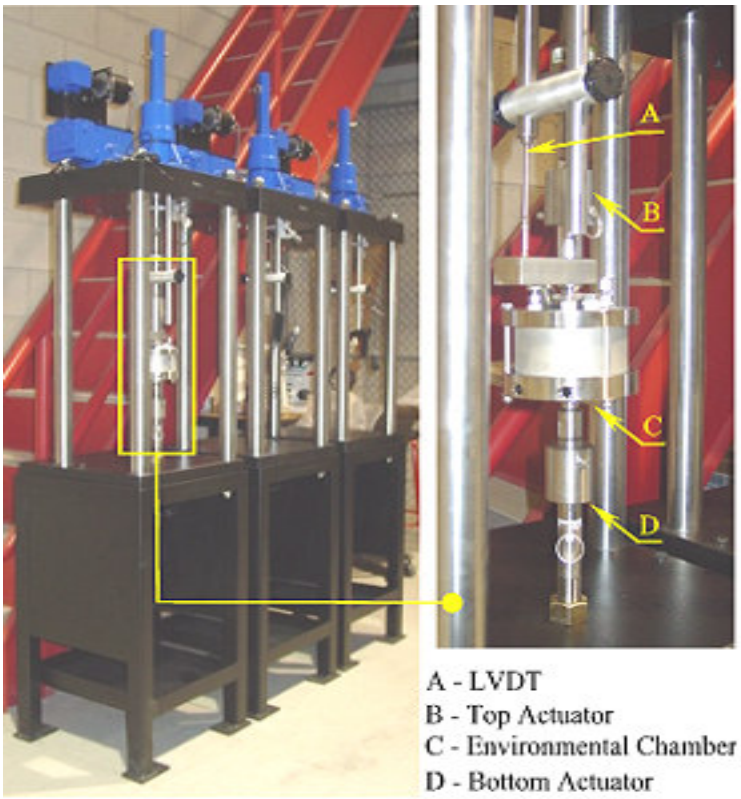

Figure 3.4: Slow-Strain-Rate Test Setup

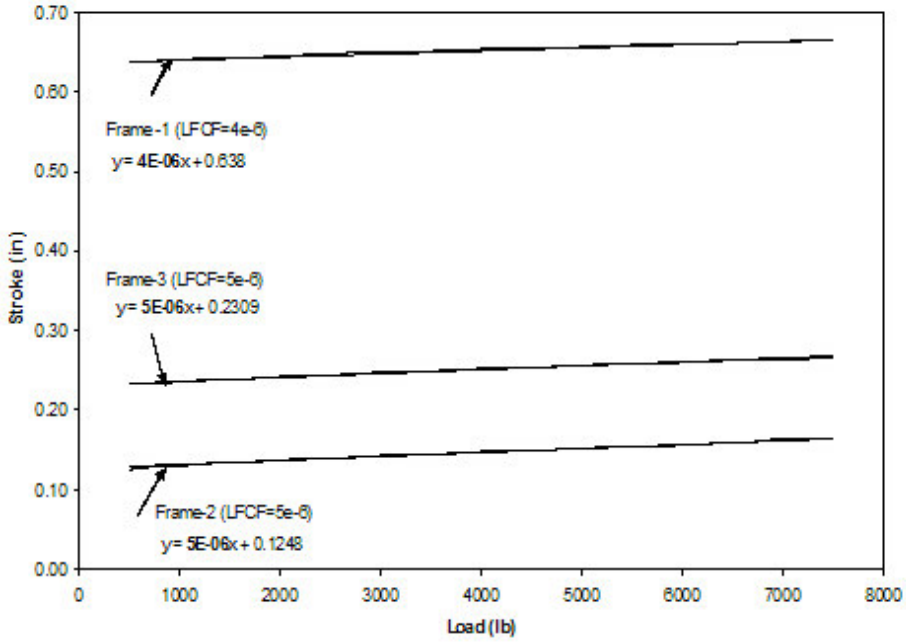

Figure 3.5: Load Frame Compliance Test Results

A strain rate of $3.3x10^{-6}$ s^{-1}, was used during the SSR testing. This strain rate was selected based upon the prior research work performed at the Lawrence Livermore National Laboratory (LLNL). It is well known that the SCC occurrence is an effect of two significant factors such as the applied/residual stress and a susceptible environment. If the stress is applied at a very fast rate to the test specimen, while it is exposed to the aqueous environment, the resultant failure may not be different from the conventional mechanical deformation produced without an environment. On the other hand, if the strain rate is too slow, the resultant failure may simply be attributed to the corrosive damage due to environmental interaction with the material, thus, causing breakdown of the protective surface film. In view of this rationale, the SSR testing at LLNL was initially conducted at strain rates ranging between 10^{-5} and 10^{-7} s^{-1}. Based upon this experimental work, it was determined that a strain rate of around 10^{-6} s^{-1} would provide the most effective contributions of both the mechanical and environmental variables in enhancing the environment-induced cracking susceptibility during the SSR testing.[48]

The susceptibility of Type 422 SS to SCC was evaluated by using both smooth and notched tensile specimens in neutral and acidic environments at ambient temperature, 60 and 90°C. The load versus displacement curves for this alloy were generated during these tests. The dimensions (length and gage diameter) of the test specimens before and after testing were measured. During the SSR testing, the test specimen was subjected to a continuously changing stress. Hence, the cracking tendencies of the test material were characterized by the TTF and ductility parameters such as the percent elongation (%El) and percent reduction in area (%RA). Further, the maximum load (P_m), failure load (P_f), maximum stress (σ_m) and true failure stress (σ_f) were also utilized to characterize the

cracking tendency. The values of P_m and P_f were obtained from load versus displacement curves and the values of %El, %RA, σ_m and σ_f were calculated by using the following equations.

$$\%El = \frac{L_o - L_f}{L_o} \times 100$$

$$\%RA = \frac{A_o - A_f}{A_o} \times 100$$

$$\sigma_f = \frac{P_f}{A_f}$$

$$\sigma_m = \frac{P_m}{A_o}$$

Where,

L_o = Initial length of the specimen

L_f = Final length of the specimen

A_0 = Initial cross sectional area of the gage section

A_f = Final cross sectional area of the gage section

3.3. Localized Corrosion

The localized corrosion is a type of corrosion where there is intense attack at localized sites on the surface of a component while the rest of the surface undergoes damage at a slower rate. The localized corrosion is a serious concern. The presence of

halide ions and concentration cells developed on the surface of the alloys tend to induce degradation due to localized corrosion. The resistance to localized corrosion varies greatly between materials, and is dependent upon the environmental factors. Hence, it is important to study the susceptibility of Type 422 SS to localized corrosion, as a function of environmental variables.

3.3.1. Cyclic Potentiodynamic Polarization Testing

Electrochemistry plays a significant role in understanding the corrosion mechanism of metallic materials. The polarization techniques can provide significant information on the corrosion mechanisms, corrosion rate and susceptibility of materials to corrosion in different environments. The metallic surfaces can be polarized by the application of an external potential to deviate from its equilibrium electrochemical corrosion potential. This deviation from the equilibrium potential is called the polarization. The magnitude of polarization is usually described as overvoltage (η), which is a measure of polarized potential with respect to the corrosion potential (E_{corr}) of an electrode.[49] The magnitude of η can be either positive or negative depending on the applied electrochemical potential during the polarization of a specimen of interest. The η is given by the following equation.

$$\text{Overvoltage, } \eta = E_{app} - E_{corr}$$

Where,

E_{app} = Applied electrochemical potential

E_{corr} = Corrosion/open-circuit potential

The magnitude of η is positive for an anodic polarization while a negative η indicates a cathodic polarization.

The CPP is a test technique, where both anodic and cathodic polarizations can be performed in a cyclic manner. It is often used to evaluate the susceptibility of a material to pitting corrosion, which is usually characterized by a change in slope during the forward potential scan at a potential known as critical pitting potential (E_{pit}). At this potential, the material undergoes localized breakdown of protective surface film causing initiation of pits. Materials, which are capable of repassivation by formation of protective film during the reverse potential scan, are characterized by the development of a repassivation/protection potential (E_{prot}). Larger the difference between E_{pit} and E_{prot}, the greater is the resistance of the material to localized attack, particularly, the pitting corrosion.

The susceptibility of Type 422 SS to localized corrosion was determined by CPP experiments in neutral and acidic environments at 30, 60 and 90°C using a potentiostat, as shown in Figure 3.6.

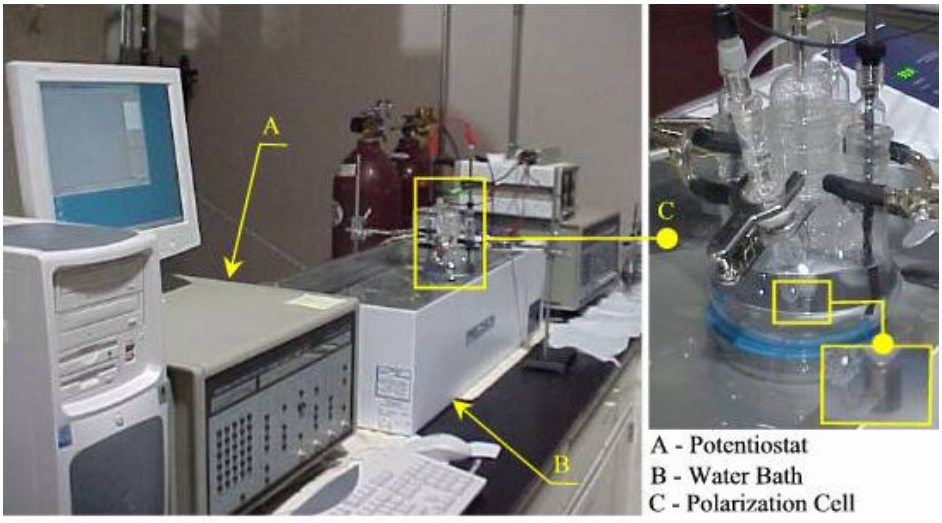

Figure 3.6: Cyclic Potentiodynamic Polarization Test Setup

A potentiostat is an electronic device that controls the potential between the working and reference electrode at a preset value. It allows the necessary current to flow between the working and counter electrode to maintain the desired potential, as long as the required cell potential and current do not exceed the compliance limits of the potentiostat.[50]

The potentiostat was calibrated according to the ASTM Designation G 5, prior to the CPP testing.[51] The potentiostat was calibrated to generate a characteristic polarization curve for a ferritic Type 430 SS specimen in 1 Normal (1N) sulfuric acid (H_2SO_4) solution at 30°C using a potential scan rate of 0.166 mV/sec, as shown in Figure 3.7.[51]

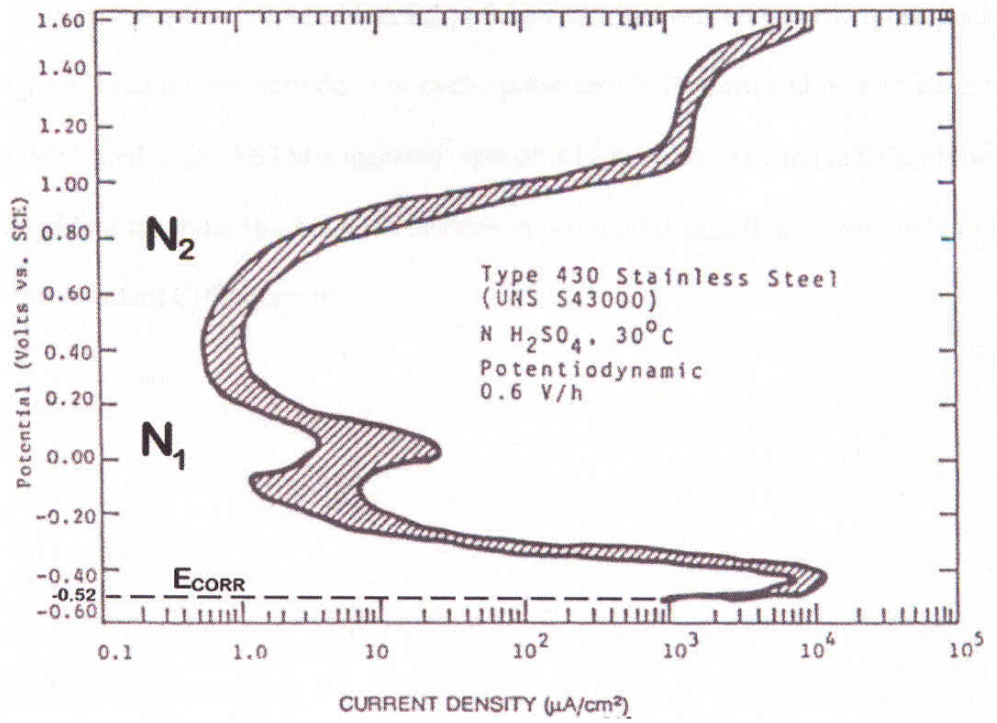

Figure 3.7: Standard ASTM G 5 Potentiodynamic Polarization Curve

The potentiostat used in the CPP tests involving the test material was considered to be functioning accurately, if the generated calibration curve showed similar E_{corr} value and shape, as shown in the standard ASTM G 5 polarization diagram.[51] A typical potentiodynamic polarization curve generated in this investigation, is shown in Figure 3.8. In order to get accurate results, calibration tests were performed once for every 20 CPP tests.

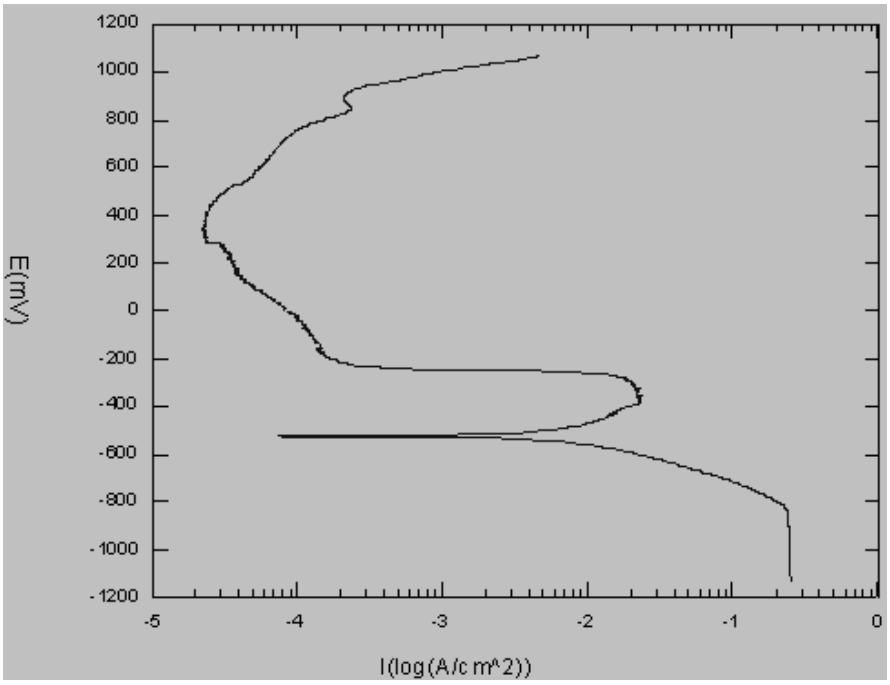

Figure 3.8: Generated ASTM G 5 Potentiodynamic Polarization Curve

The three-electrode polarization system used in this study consisted of the test specimen as an anode, two graphite rods as cathodes and silver/silver chloride (Ag/AgCl) as the reference electrode. This reference electrode was contained in a Luggin probe placed within 2-3 mm from the center of the specimen that also acted as a salt bridge, as shown in Figure 3.9.

An initial delay time of 50 minutes was given before performing the forward and reverse scans, to attain a stable E_{corr} value. The E_{corr} value of the test material in the desired test environment was determined with respect to the Ag/AgCl reference electrode, followed by the forward and reverse potential scans at the ASTM specified rate of 0.166 mV/sec.[51] The magnitudes of the E_{pit} and E_{prot}, if any, were obtained from the CPP diagram.

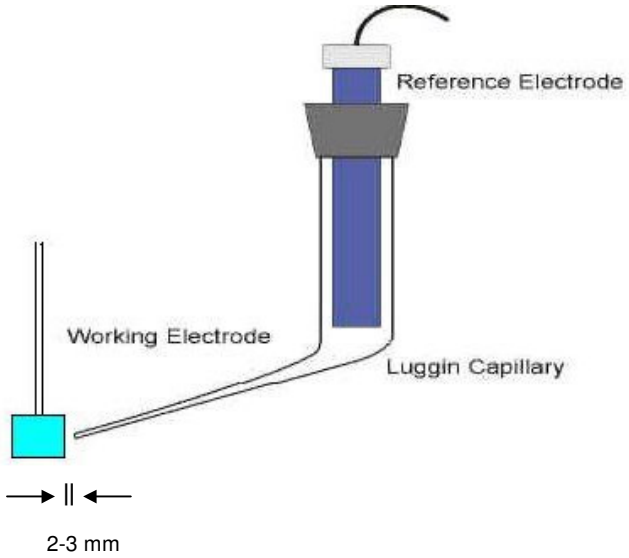

Figure 3.9: Luggin Probe Arrangement

3.4. Hydrogen Embrittlement

During the transmutation process, significant amount of hydrogen may be generated, causing hydrogen-induced embrittlement (HE) to the target structural material, such as Type 422 SS.[15, 52-57] HE is a delayed brittle failure resulting from the interaction of atomic hydrogen (H) embedded inside the metal lattice. Hydrogen can be produced from an external environment or during the melting of a material of interest. However, the role of hydrogen studied in this investigation is primarily due to the hydrogen produced during the potentiostatic polarization using cathodic potential. Electrochemically speaking, a metal is considered to be in equilibrium in an aqueous environment when the rate of oxidation reaction (metal dissolution) and the rate of reduction reaction (hydrogen reduction) become equal. However, this equilibrium can be disturbed by polarizing the test specimen that involves the application of an external potential or current, and subsequently, monitoring the resultant current and potential, respectively.

The potentiostatic polarization performed in this investigation involved the application of a negative applied potential to the gage section of the specimen, thereby, producing atomic hydrogen ($H^+ + e^- = H$) due to cathodic charging. The hydrogen generated by this process is nascent in nature, thus enabling its diffusion into the metal lattice in the form of atomic hydrogen. With time, the concentration of atomic hydrogen is increased inside the metal lattice, which then interacts at the weakest region, known as triaxial stress region, enhancing internal stresses with subsequent formation of cracks. This phenomenon, by which a metallic material undergoes failure in a hydrogen-containing environment, due to the combined effect of applied/internal stress and the presence of aggressive chemical species, such as H, is known as HE. The susceptibility of a material to HE becomes more pronounced in the acidic environment due to the increased concentration of hydrogen ion, compared to that in a neutral solution, generated during an electrochemical reaction.

3.4.1. Slow-Strain-Rate Testing under Controlled Cathodic Potential

The potentiostatic polarization under a cathodic applied potential is a common method of evaluating HE in susceptible materials. In this investigation, a constant potential, cathodic to the measured E_{corr} value, was applied to the test specimen, which was spot-welded (Figure 3.10) with a conductive metallic wire for electron flow. The spot-welded specimen was continuously strained in tension in the test environment using a similar strain rate (3.3×10^{-6} s^{-1}), while simultaneously applying the controlled cathodic potential (E_{cont}) to the same specimen, as shown in Figure 3.11.[58-61] The resultant current was plotted as a function of time during this potentiostatic polarization testing, as shown in Figure 3.12. Subsequently, an attempt was made to compare the load versus

displacement curves generated during cathodic charging of the spot-welded specimen to those obtained without the application of E_{cont} in a similar environment.

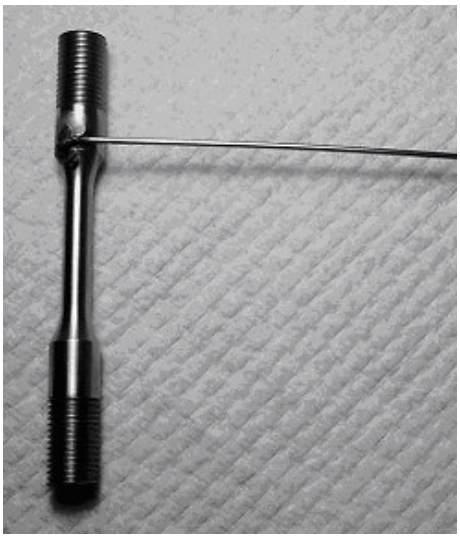

Figure 3.10: Spot-Welded Tensile Specimen

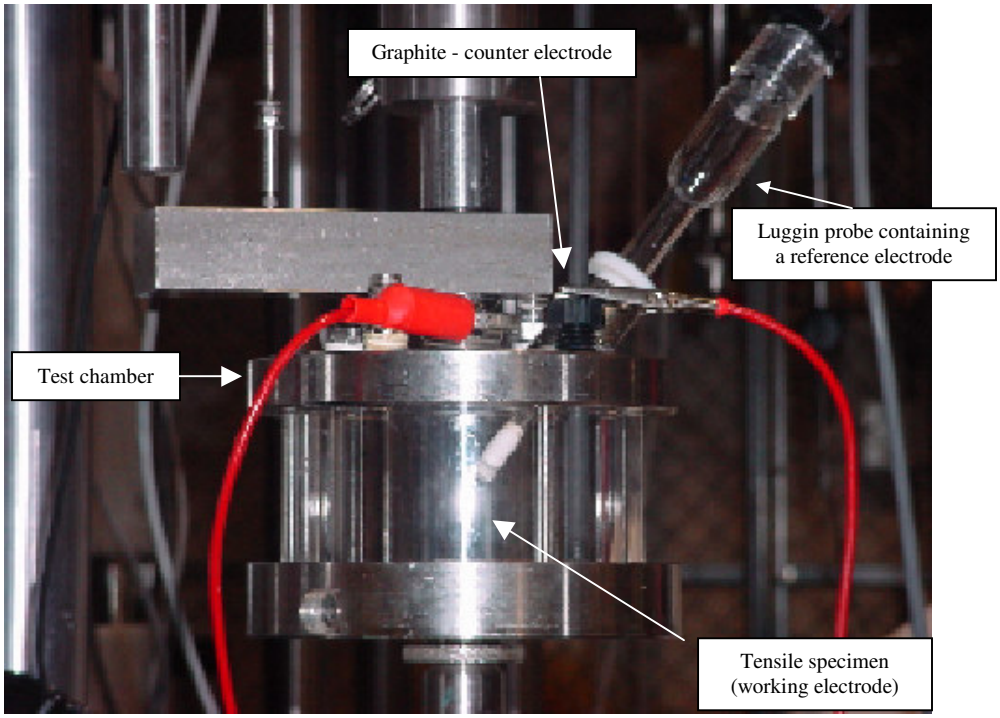

Figure 3.11: Controlled Cathodic Potential SCC Test Setup

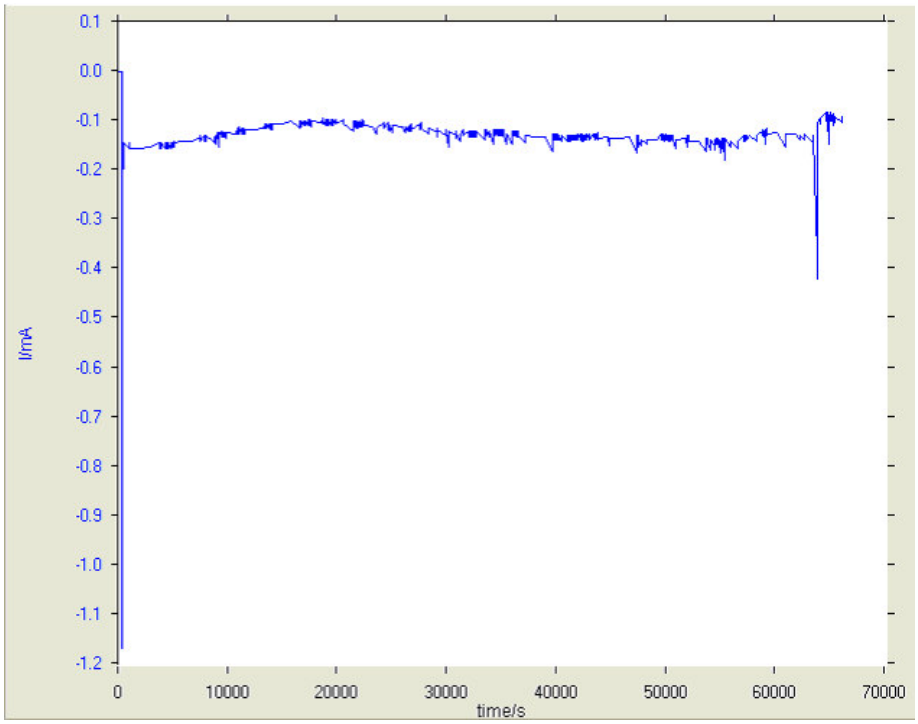

Figure 3.12: Current as a Function of Time

3.5. Surface Analyses

The metallurgical properties of an engineering alloy depend on its chemical composition, thermal treatment and their resultant microstructure. The microstructure places an important role in differentiating properties of one alloy versus another. Thus, the evaluation of metallurgical microstructure of a material of interest constitutes a significant step in characterizing the performance of this material, when exposed to a hostile environment under tensile stress. In view of this rationale, it is always customary to evaluate the metallurgical microstructure by optical microscopy at meaningful magnifications. Simultaneously, the characterization of failure, in particular, the extent and morphology of primary and secondary failure by optical microscopy and SEM, respectively, is critical to develop a fundamental understanding on the failure mechanism of a material under certain environmental condition.

Accordingly, significant emphasis has been placed in this project to characterize the metallurgical microstructure and fractography of Type 422 SS using optical microscopy and SEM, respectively. The detailed analytical procedures are discussed next in this section.

3.5.1. Optical Microscopy

It is very important to ensure that sample preparation was carried out with care to produce high quality and useful micrographs. During the sample preparation, care was taken to ensure that the material was sectioned at a proper location for characterization of a specific feature. The sample was mounted using the right ratio of epoxy and hardener. Steps were taken to ensure that the mounted specimen had the appropriate thickness to prevent rocking during grinding and polishing. The edges of the mounted specimen were

rounded to minimize the damage to the grinding and polishing discs. The mounted specimens were ground with rotating discs of abrasive paper. The grinding procedure involved several stages using a finer paper each time. This was done to remove scratches resulting from the previous coarser paper. This was achieved by orienting the sample perpendicular to the previous scratches. The polished sample was washed with deionized water to prevent contamination. Finally, etching was done by using Fry's reagent to reveal the microstructure of Type 422 SS using standard etching procedures. Care was taken to ensure that the specimen was not over-etched. The specimen was then immediately washed with deionized water and subsequently dried with alcohol.

The metallographic evaluations of the mounted specimens were performed by using a Leica optical microscope with a magnification up to 100X. The optical micrographs were obtained in both as-polished and etched conditions, to evaluate the metallurgical microstructure and secondary cracks along the gage length.

3.5.2. Scanning Electron Microscopy

Electron microscope uses a beam of highly energetic electrons to examine objects on a very fine scale. This examination can yield information on topography, morphology, composition and crystallographic information.

A sample of length 1 cm was cut from the tested specimen by using a precision cutter. The sample was then held on a sample holder by using a double-sided carbon tape. The mounted specimen was examined by SEM to determine the morphology of failure and cracking along the primary fracture face of the tested tensile specimens. Further, the appearance of the polarized specimens was also analyzed by this technique.

CHAPTER 4

RESULTS

4.1. Hardness Testing

The results of hardness testing of Type 422 SS using a Rockwell testing machine is shown in Table 4.1 both in the austenitized/quenched and tempered conditions. As expected, the hardness value in R_C scale was reduced in the quenched and tempered condition due to the homogenization of the metallurgical microstructure and relaxation of internal stresses resulting from the quenching operation.

Table 4.1: Results of Hardness Testing

	Austenitized/Quenched	**Quenched/Tempered**
Edge 1 (R_C)	44	29.5
Center (R_C)	46	30
Edge 2 (R_C)	48	30.5
Average (R_C)	46	30

4.2. Ambient-Temperature Mechanical Properties Testing

An MTS machine was used to determine the room-temperature tensile properties of quenched and tempered Type 422 SS. The resultant tensile properties, based on three measurements, are shown in Table 4.2.

Table 4.2: Ambient-Temperature Tensile Properties

Material/ Heat Treatment	Thermal Treatments	Yield Strength, ksi	Ultimate Tensile Strength, ksi	%El	%RA
Type 422 SS/ 2051	1850°F/1 hour/Oil Quenched 1150°F/1.25 hours/Air Cooled	122	145	19.92	59.68

4.3. Constant-Load Testing

The susceptibility of Type 422 SS to SCC was determined in neutral and acidic solutions at ambient temperature and 90°C using smooth and notched cylindrical specimens by CL testing technique. The determination of the cracking tendency using this method was based on the TTF for the maximum test period of 30 days. The cracking tendency in CL testing was expressed in terms of a threshold stress (σ_{th}) for a particular test condition, below which failure did not occur during the maximum test period of 30 days.

The results of the CL testing involving smooth cylindrical specimens indicate that no failures were observed in the neutral solution at any testing temperature, at stresses up to 95% of its YS value. Specimens tested in the acidic solution at ambient temperature also did not show any failure. However, failures were observed when tested in the 90°C acidic solution at applied stresses equivalent to 95, 90 and 85% of the material's YS value, as shown in Table 4.3. This cracking behavior may be attributed to the synergistic effect of lower pH and elevated temperature used in these tests. No failure was observed at 80% of the material's YS value in this environment, suggesting a σ_{th} value of 80% of its YS value, as shown in Figure 4.1. However, the presence of a notch reduced the threshold

load value to 25% of this material's YL, as shown in Table 4.3. These results were based on at least 2 tests conducted per experimental condition, as presented in Appendix A.

Table 4.3: Results of the CL SCC Tests

Specimen Geometry	Environment/Temperature (°C)	% YS/YL	Failure (hours)/No Failure
Smooth	Neutral/Ambient	95% YS	NF
	Neutral/90	95% YS	NF
	Acidic/Ambient	95% YS	NF
	Acidic/90	95% YS	212 hours
	Acidic/90	90% YS	250 hours
	Acidic/90	85% YS	383 hours
	Acidic/90	80% YS	NF
Notched	Acidic/90	35% YL	Failed while applying load
	Acidic/90	30% YL	Failed while applying load
	Acidic/90	25% YL	NF

NF: No Failure

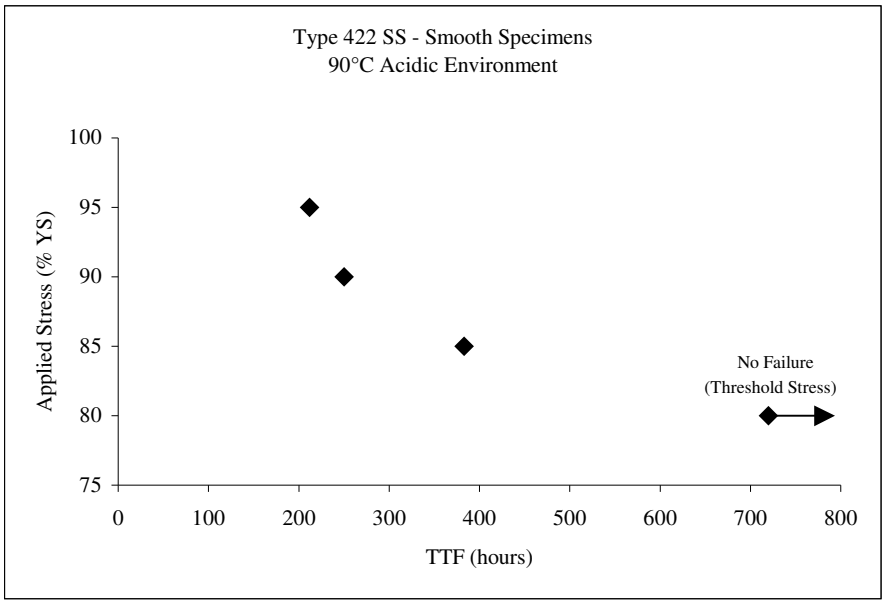

Figure 4.1: Applied Stress versus TTF in the CL SCC Tests

4.4. Slow-Strain-Rate Testing

The SSR testing was also performed to evaluate the susceptibility of Type 422 SS to SCC using smooth and notched cylindrical specimens in neutral and acidic solutions at ambient and elevated temperatures. During the SSR testing, the test specimen was subjected to a continuously changing stress at an applied strain rate of 3.3×10^{-6} s^{-1} until fracture. The cracking tendency was characterized by the TTF and ductility parameters such as the %El and %RA. Further, the σ_f, σ_m, P_m and P_f were also considered in determining the SCC susceptibility.

A comparison of load versus displacement curves using smooth cylindrical specimens, tested in neutral and acidic environments at different test temperatures, is shown in Figure 4.2. An analysis of these data clearly reveals that the displacement was reduced with increasing temperature in both environments, showing more pronounced effect in the acidic solution. The results, shown in Table 4.4, involving smooth specimens indicate, that the magnitude of %El, %RA, TTF, σ_f, σ_m and P_m, determined from Figure 4.2 and the specimen dimensions, were gradually reduced with increasing temperature in both tested environments, as expected. However, this effect was more pronounced in the acidic environment due to the combined effect of lower pH and higher testing temperature on the susceptibility of this material to cracking. These results were based on at least 2 tests conducted per experimental condition, as presented in Appendix B.

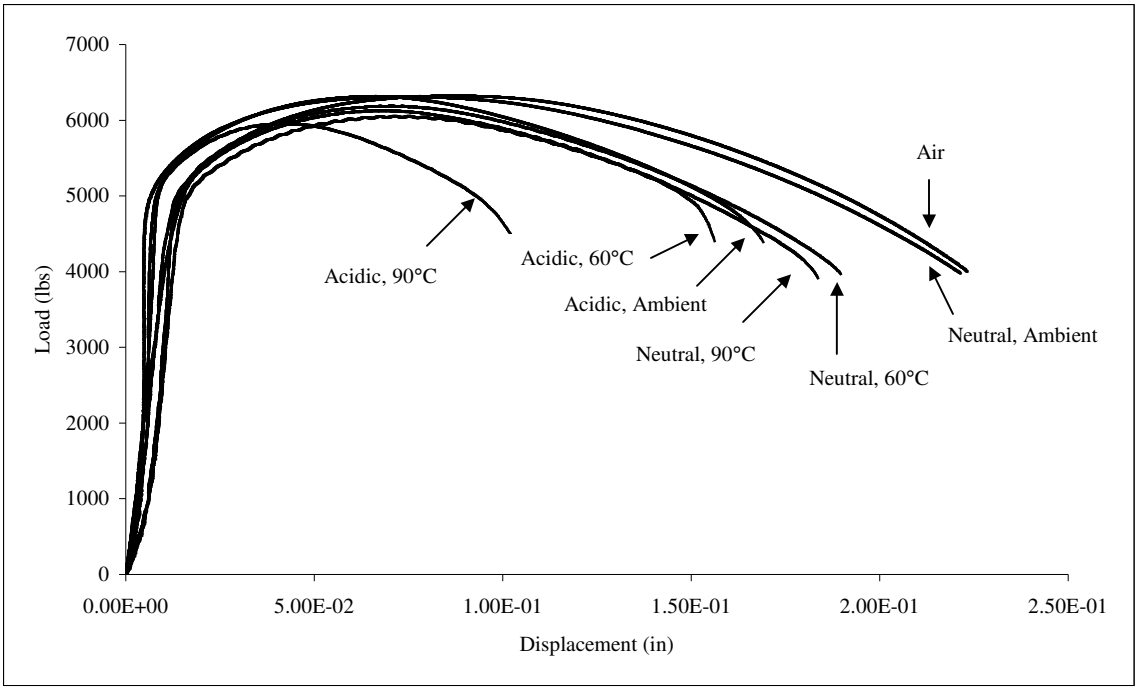

Figure 4.2: Load versus Displacement Curves for Smooth Specimens

Table 4.4: Results of the SSR SCC Testing using Smooth Specimens

Environment/ Temperature (°C)	**P_m (lbs)**	**σ_m (ksi)**	**P_f (lbs)**	**σ_f (ksi)**	**%EL**	**%RA**	**TTF (hours)**
None	6321	127	4001	195	21.95	58.93	21.17
Neutral/Ambient	6318	127	4014	177	21.20	55.16	20.59
Neutral/60	6203	124	3951	175	18.21	54.96	18.74
Neutral/90	6127	123	3913	172	18.13	54.33	18.12
Acidic/Ambient	6314	125	4128	160	18.34	49.06	19.21
Acidic/60	6002	120	4238	141	15.75	40.03	16.03
Acidic/90	5899	117	4332	117	10.52	26.63	11.90

Since, the mechanical constraint due to the presence of a notch is substantially higher compared to that in a smooth specimen, SSR testing using notched specimens were performed at ambient temperature and 90°C. It was thought that in the presence of a

notch, the test specimen would not show a significant effect, when tested at an intermediate temperature of 60°C. The load versus displacement curves, obtained in the SSR testing performed in similar environments using notched specimens, are shown in Figure 4.3. These data indicate that the displacement was reduced as the temperature was increased in either environment. However, the extent of reduction in displacement was more pronounced in the acidic solution.

The results of SSR testing using notched specimens, shown in Table 4.5, indicate that the magnitude of %El, %RA, TTF, P_m, P_f, σ_m and σ_f, determined from Figure 4.3 and the specimen dimensions, were gradually reduced with increasing temperature in the tested environments, as expected. This effect was more pronounced in the acidic environment due to the combined effect of lower pH and higher testing temperature, as seen earlier with the smooth specimens. These results were based on at least 2 tests conducted per experimental condition, as presented in Appendix B.

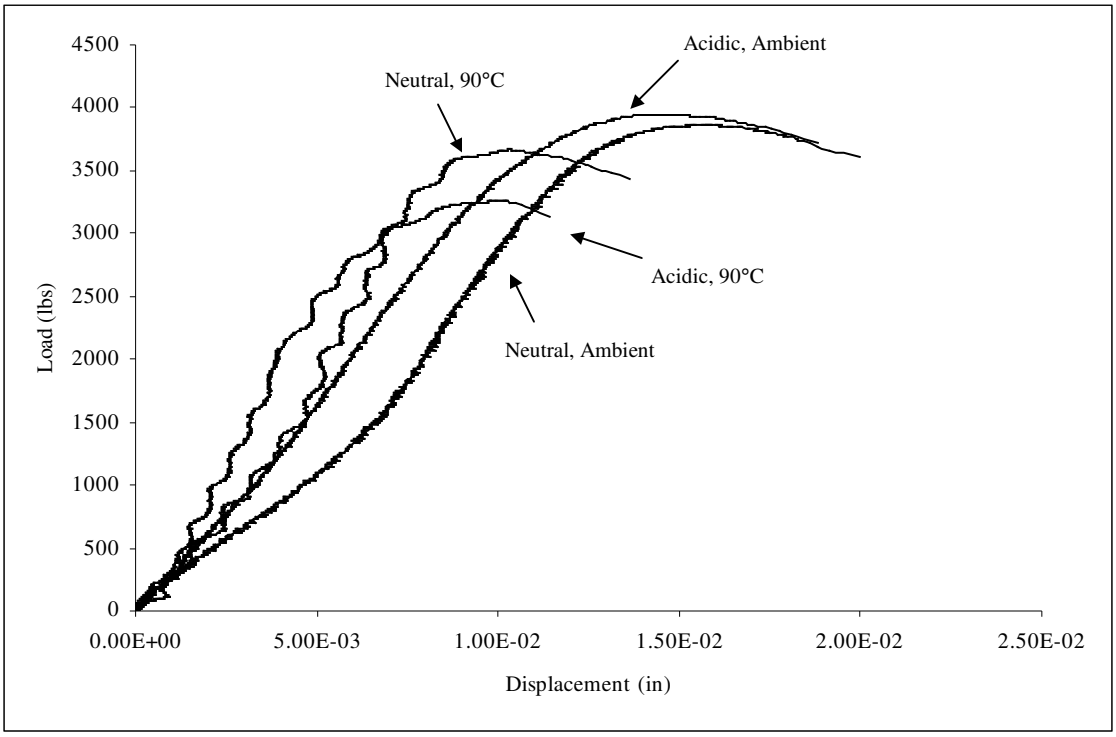

Figure 4.3: Load versus Displacement Curves for Notched Specimens

Table 4.5: Results of the SSR SCC Testing using Notched Specimens

Environment/ Temperature (°C)	**P_m (lbs)**	**σ_m (ksi)**	**P_f (lbs)**	**σ_f (ksi)**	**%EL**	**%RA**	**TTF (hours)**
Neutral/Ambient	3975	208	3687	203	2.05	9.87	4.13
Neutral/90	3748	196	3493	191	1.58	6.27	3.90
Acidic/Ambient	3974	208	3753	205	1.49	4.13	4.13
Acidic/90	3314	173	3181	169	1.25	2.54	3.69

The SSR testing data, presented in Tables 4.4 and 4.5 for smooth and notched cylindrical specimens, respectively, are graphically reproduced in Figures 4.4 through 4.10, showing the effect of pH, temperature and specimen geometry on %El, %RA, TTF, P_m, P_f, σ_m and σ_f. Examination of these figures clearly indicates that all these parameters

were reduced in both environments at elevated temperatures, showing more pronounced effect in the acidic solution. The presence of a notch significantly reduced the %El, %RA, TTF, P_m and P_f, as shown in these figures. However, the magnitude of σ_m and σ_f was increased with the notched specimens, due to its relatively smaller cross-sectional area at the root of the notch.

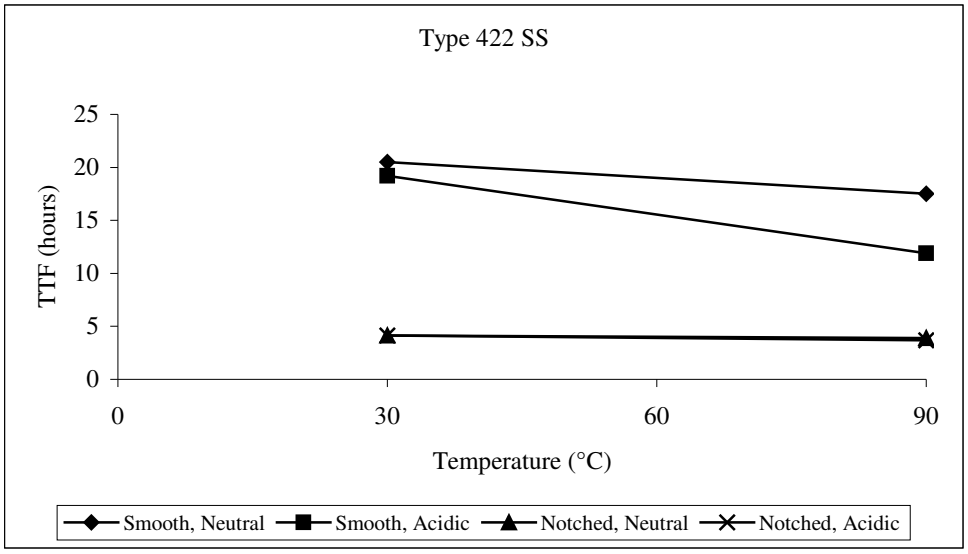

Figure 4.4: Effect of pH, Temperature and Specimen Geometry on TTF

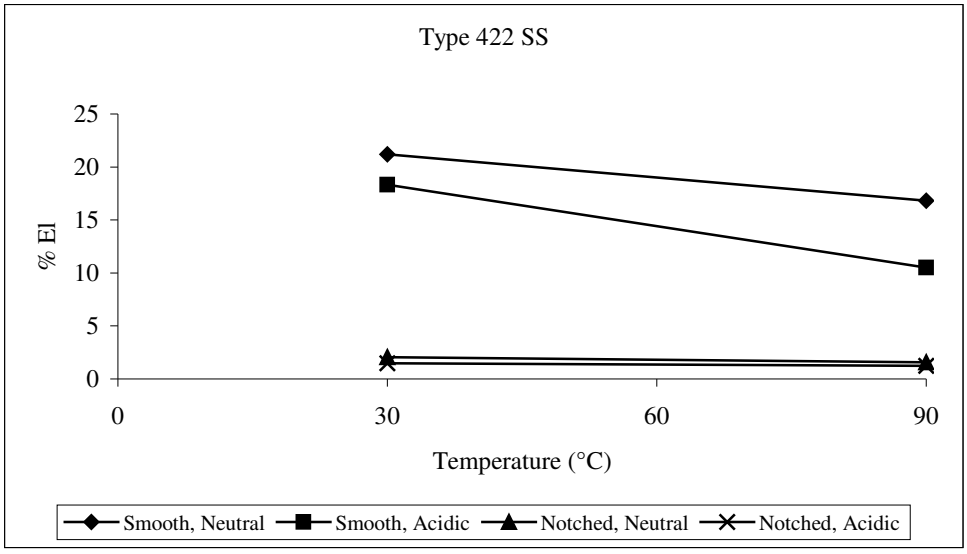

Figure 4.5: Effect of pH, Temperature and Specimen Geometry on %El

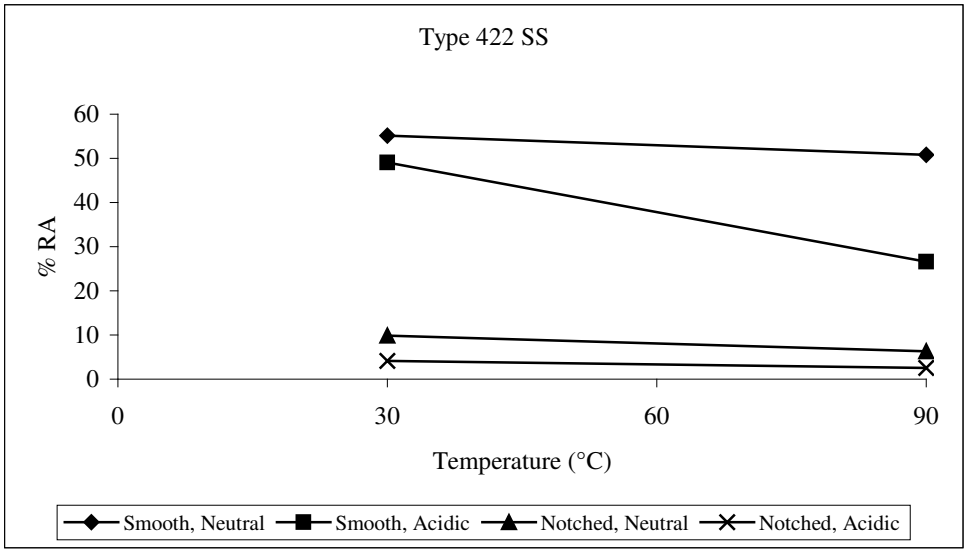

Figure 4.6: Effect of pH, Temperature and Specimen Geometry on %RA

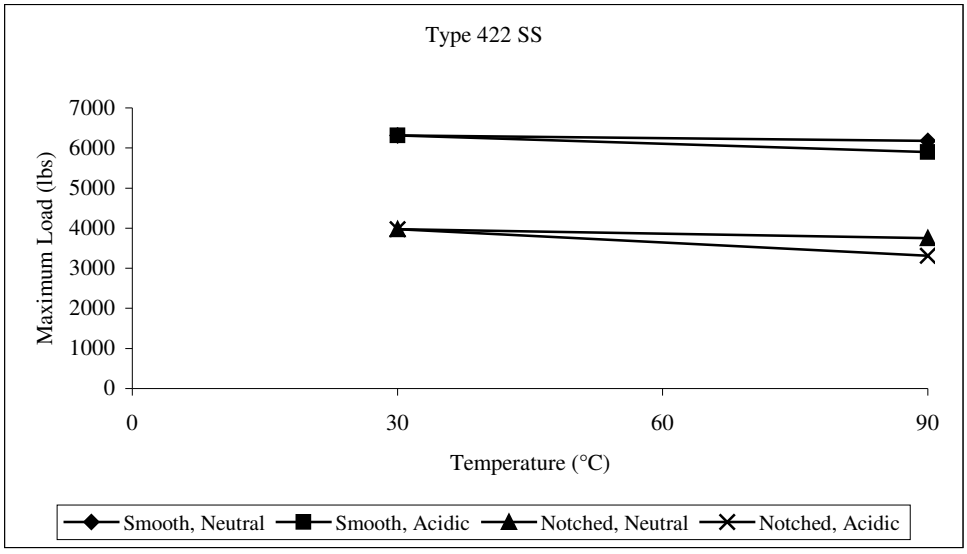

Figure 4.7: Effect of pH, Temperature and Specimen Geometry on Maximum Load

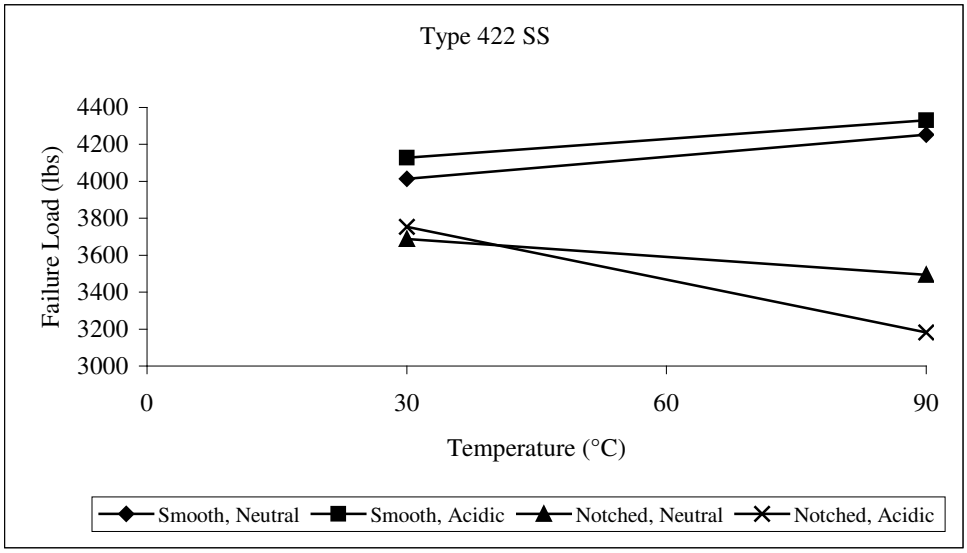

Figure 4.8: Effect of pH, Temperature and Specimen Geometry on Failure Load

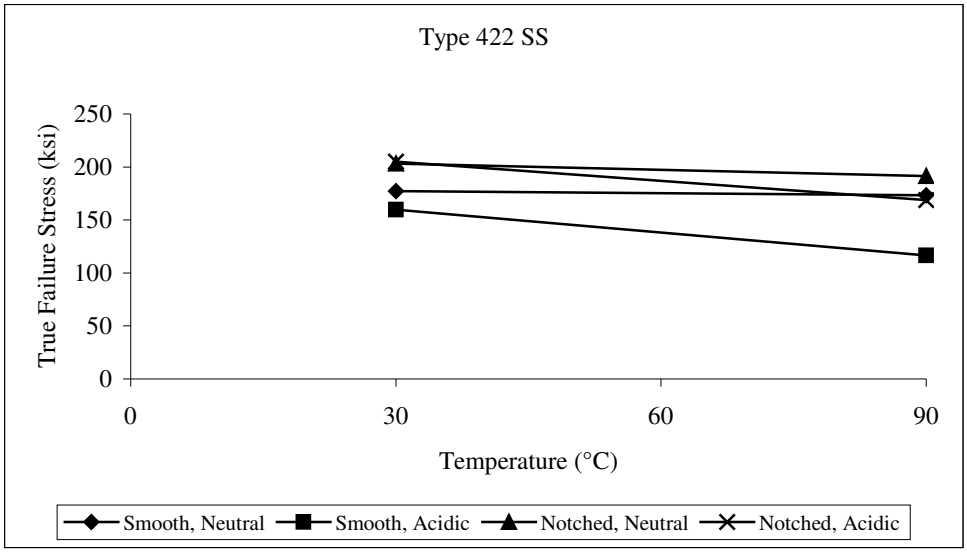

Figure 4.9: Effect of pH, Temperature and Specimen Geometry on True Failure Stress

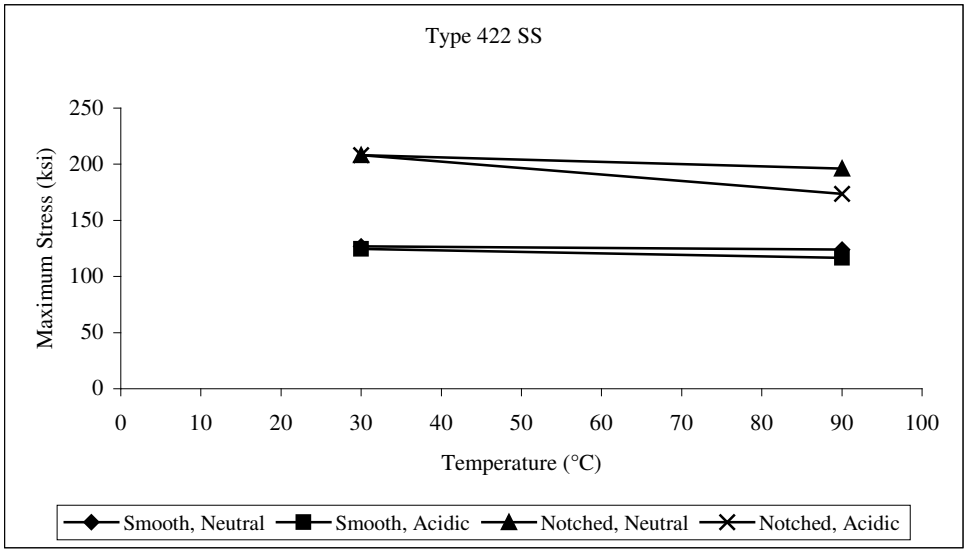

Figure 4.10: Effect of pH, Temperature and Specimen Geometry on Maximum Stress

Comparisons of load versus displacements curves for Type 422 SS tested in neutral and acidic solution are shown in Figures 4.11 and 4.12, respectively, as a function of specimen geometry and temperature. It is obvious from these plots that the presence of a

notch in the cylindrical specimen resulted in a significant reduction in the failure load, irrespective of the testing environments. It should however be noted that the reduction in the failure load was higher in the acidic solution at comparable testing temperatures. With respect to the strain value obtained with smooth and notched cylindrical specimens, a general observation was that the strain value was significantly reduced in the presence of a notch indicating substantially reduced ductility parameters, as compared in Tables 4.4 and 4.5.

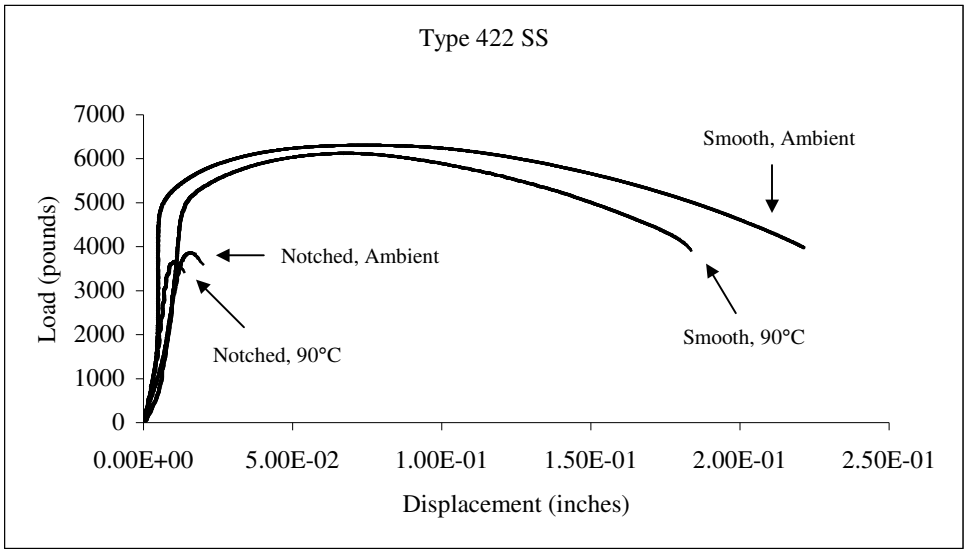

Figure 4.11: Load versus Displacement Curves in Neutral Environment

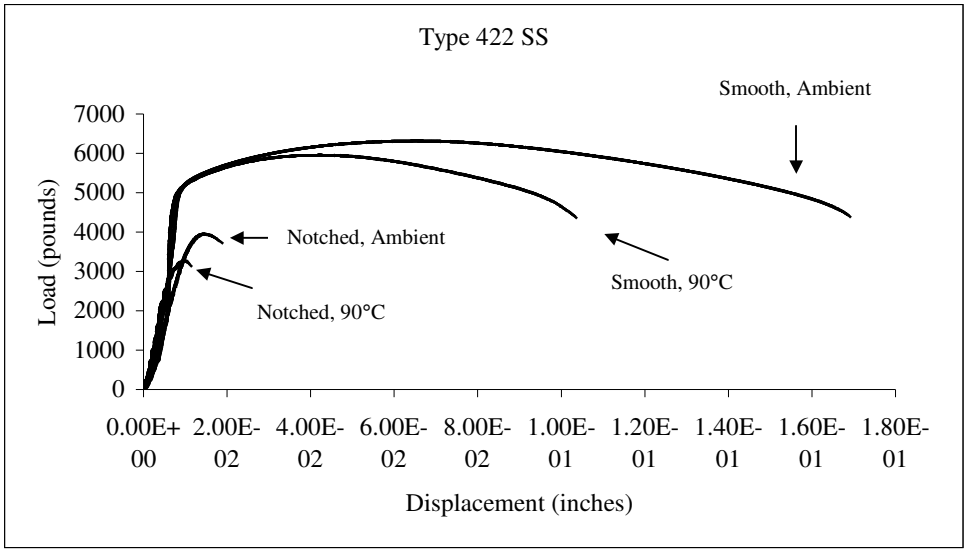

Figure 4.12: Load versus Displacement Curves in Acidic Environment

4.5. Cyclic Potentiodynamic Polarization Testing

The susceptibility of Type 422 SS to localized corrosion was evaluated by performing CPP experiments in neutral and acidic environments at 30, 60 and 90°C by using a potentiostat. The effects of testing temperature and pH on critical potentials were evaluated by this technique. Typical CPP diagrams obtained in the acidic solution are illustrated in Figures 4.13 through 4.15, showing E_{corr}, E_{pit} and E_{prot} as a function of the testing temperature. The resultant CPP data, shown in Table 4.6, indicate that the E_{corr} value became more active (negative) in either environment, as the temperature was increased from 30 to 60°C. However, the E_{corr} value became relatively more noble in the 90°C testing, showing less negative potential. Other investigators, who tested different materials, observed similar phenomenon.[62] Nevertheless, more severe localized attack was observed in th 90°C environment, as expected.

It is interesting to note that the E_{pit} value was gradually reduced with increasing temperature in either environment, showing more pronounced effect in the acidic environment due to the synergistic effect of pH and temperature. Usually, initiation of pitting occurs at a critical potential known as E_{pit} obtained during the forward potential scan, due to the localized breakdown of protective surface film beyond the passive region. This phenomenon is associated with a change in slope as the current density is increased. A repassivation behavior was also noticed in the acidic solution at 30 and 60°C, during the reverse potential scanning. The potential at which repassivation of the specimen surface occurred was identified with a protective potential (E_{prot}). The results given in Table 4.6 are graphically reproduced in Figures 4.16 and 4.17, showing the effect of pH and temperature on E_{corr} and E_{pit}, respectively. These results were based on at least 2 tests conducted per experimental condition, as presented in Appendix C.

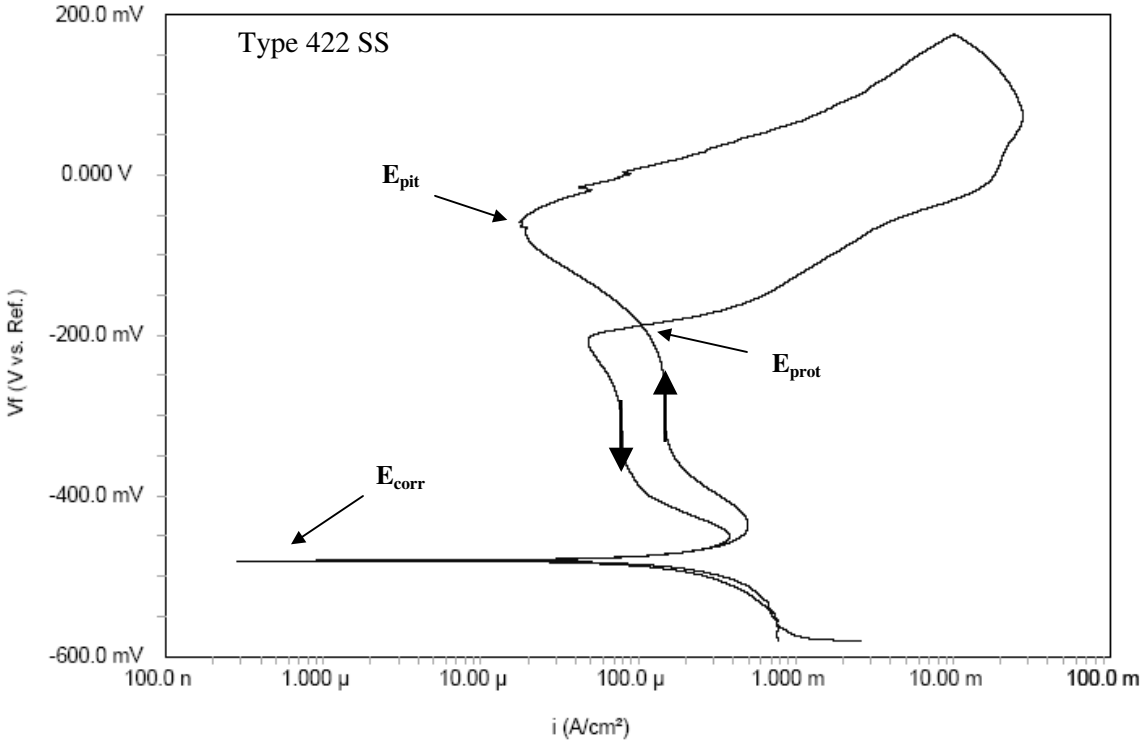

Figure 4.13: CPP Curve in 30°C Acidic Environment

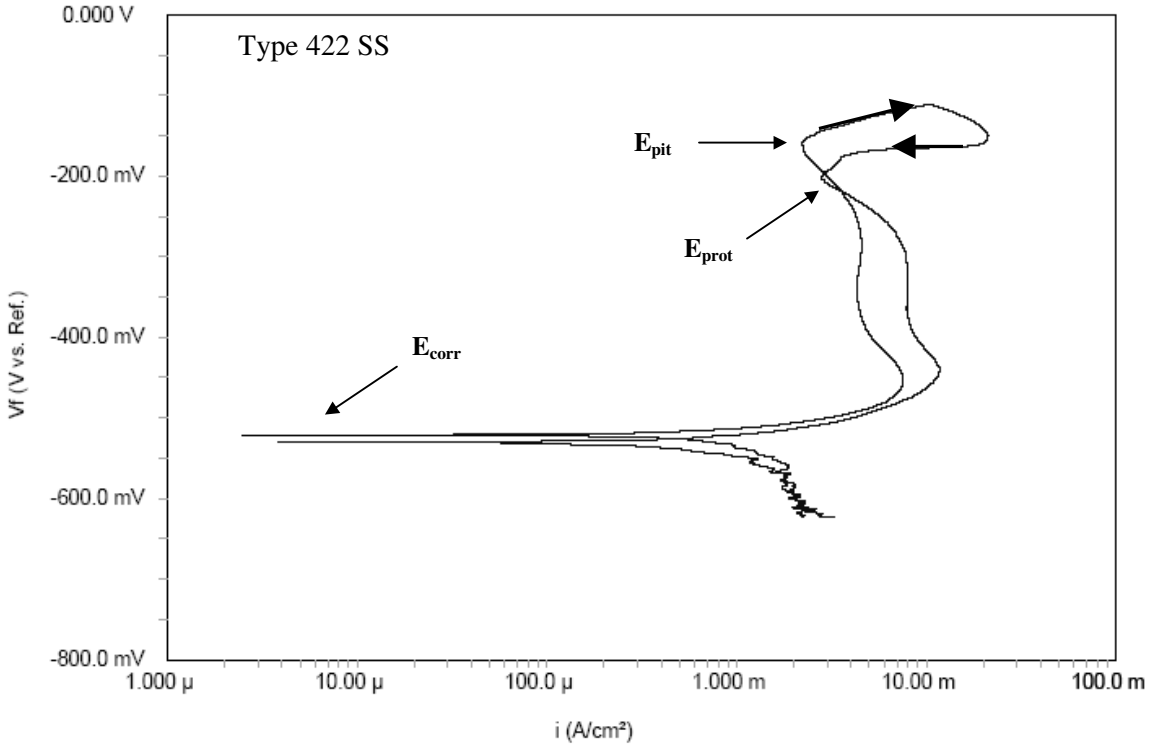

Figure 4.14: CPP Curve in 60°C Acidic Environment

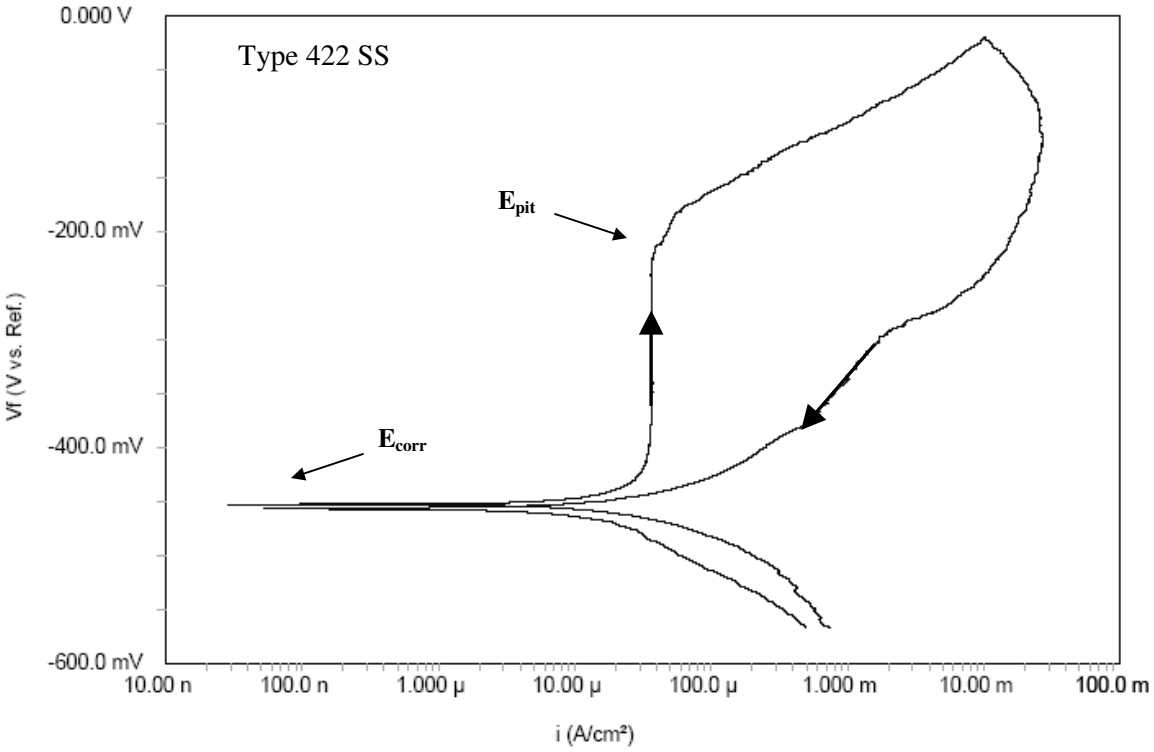

Figure 4.15: CPP Curve in 90°C Acidic Environment

Table 4.6: Results of the CPP Testing

Environment	**Temperature (°C)**	**Critical Potentials (mV)**		
		E_{corr}	**E_{pit}**	**E_{prot}**
Neutral	30	- 205	+ 85	None
Neutral	60	- 334	- 19	None
Neutral	90	- 245	- 100	None
Acidic	30	- 499	- 109	- 189
Acidic	60	- 532	- 192	- 212
Acidic	90	- 479	- 200	None

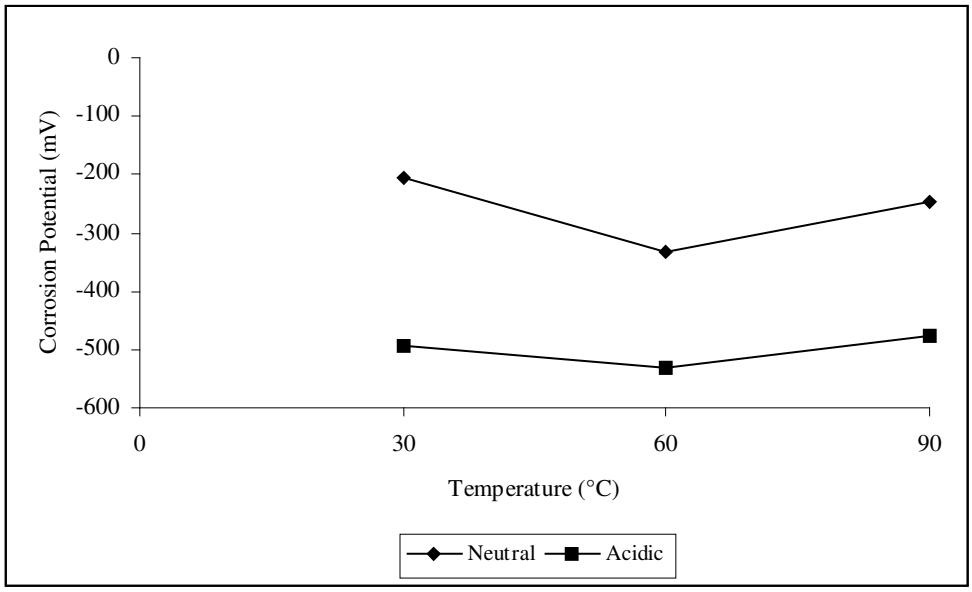

Figure 4.16: Effect of pH and Temperature on Corrosion Potential

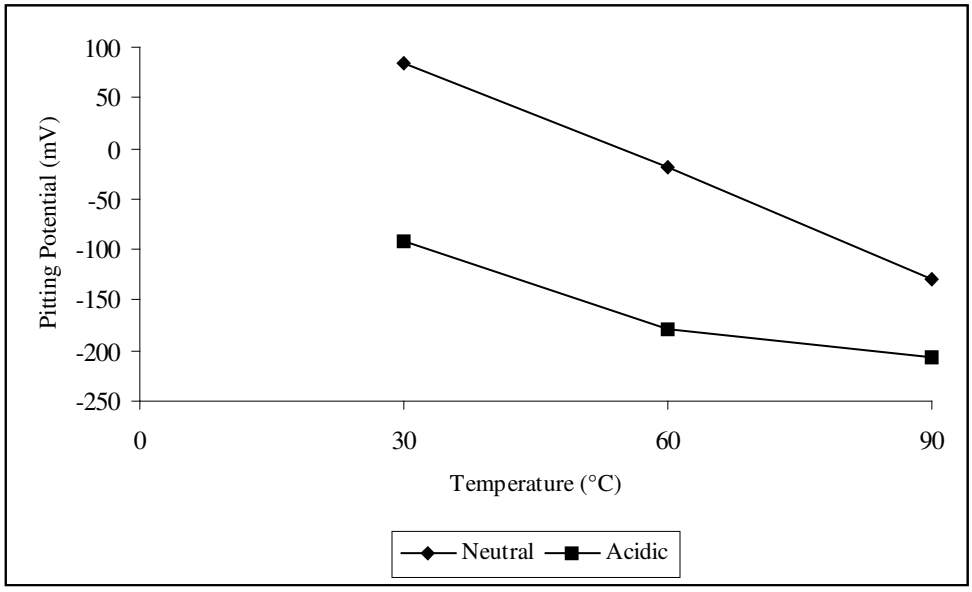

Figure 4.17: Effect of pH and Temperature on Pitting Potential

The visual examination of the polarized specimens indicate that Type 422 SS exhibited both pitting and crevice corrosion, showing more pronounced pitting susceptibility in the 90°C acidic solution. An evaluation of Figures 4.18 and 4.19 indicates that the extent of crevice corrosion was less pronounced in the neutral solution at either testing temperature. An interesting observation was that the pits forming in the neutral solution were very much aligned in the vertical direction, which may be the direction of deformation, during the rolling operation. These figures also indicate that the susceptibility of this alloy to crevice corrosion was higher in the 90°C acidic solution. Further, the pits were larger and deeper in this environment, showing more detrimental effect of the acidic pH at 90°C.

(a) 30°C

(b) 90°C

Figure 4.18: Polarization Specimens Before and After Testing in Neutral Environment

(a) 30°C

(b) 90°C

Figure 4.19: Polarization Specimens Before and After Testing in Acidic Environment

4.6. Slow-Strain-Rate Testing under Controlled Cathodic Potential

Potentiostatic polarization experiments were performed under a controlled cathodic potential (E_{cont}) using the SSR testing technique to evaluate the effect of hydrogen, generated by cathodic polarization in the acidic solution, on the cracking tendency of Type 422 SS while the specimen was continuously strained in tension. An E_{cont} value of -1000 mV with respect to the Ag/AgCl reference electrode was used during cathodic charging.

The load versus displacement curves for this alloy, with and without the application of E_{cont}, are shown in Figure 4.20. These data clearly indicate that the magnitude of displacement was reduced due to the application of E_{cont}. The TTF, ductility parameters

(%El and %RA) and σ_f, obtained from these tests, are shown in Table 4.8. An examination of these data indicates that all these parameters were reduced due to the application of an external electrochemical cathodic potential to the test specimen during straining, as expected. The variations of TTF, %El, %RA and σ_f, due to the application of E_{cont}, are shown in Figures 4.21 through 4.24, respectively.

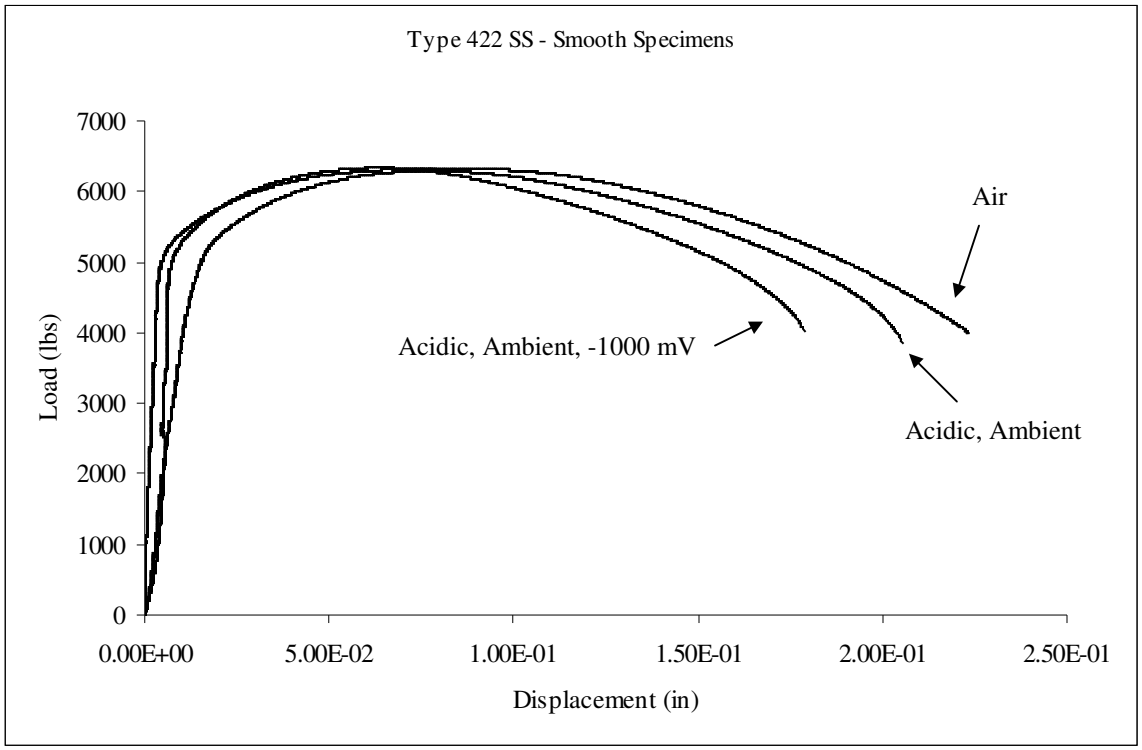

Figure 4.20: Comparison of Load versus Displacement Curves

Table 4.7: Results of the SSR Testing with and without E_{cont}

Environment/ Temperature/E_{cont}	P_m (lbs)	σ_m (ksi)	P_f (lbs)	σ_f (ksi)	%EL	%RA	TTF (hours)
None	6321.19	126.80	4001.11	195.42	21.95	58.93	21.17
Acidic/Ambient/0 mV	6314.30	126.66	3862.41	159.68	18.34	49.15	20.67
Acidic/Ambient/-1000mV	6325.17	126.13	4007.49	138.63	16.22	42.36	18.57

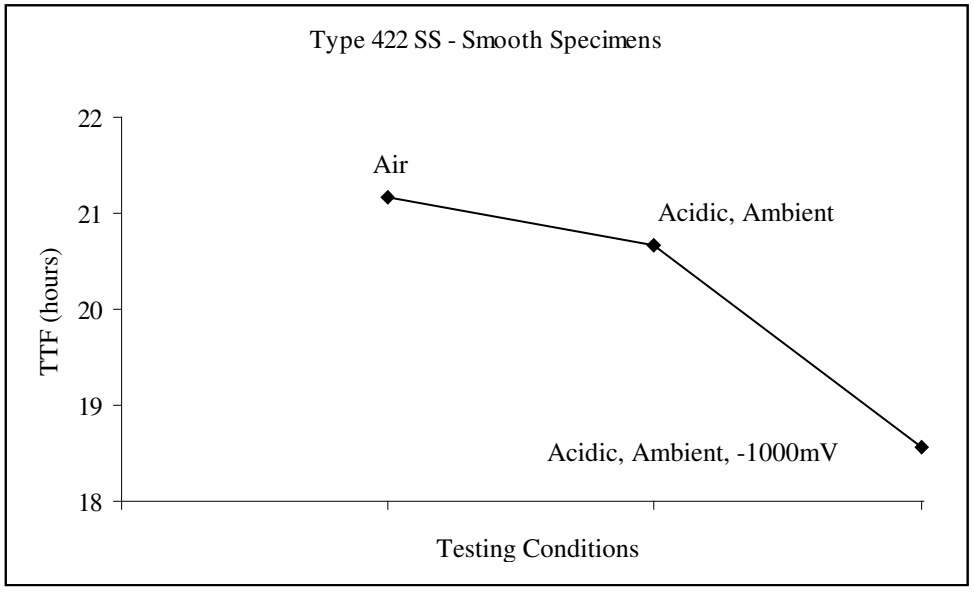

Figure 4.21: Effect of E_{cont} on TTF

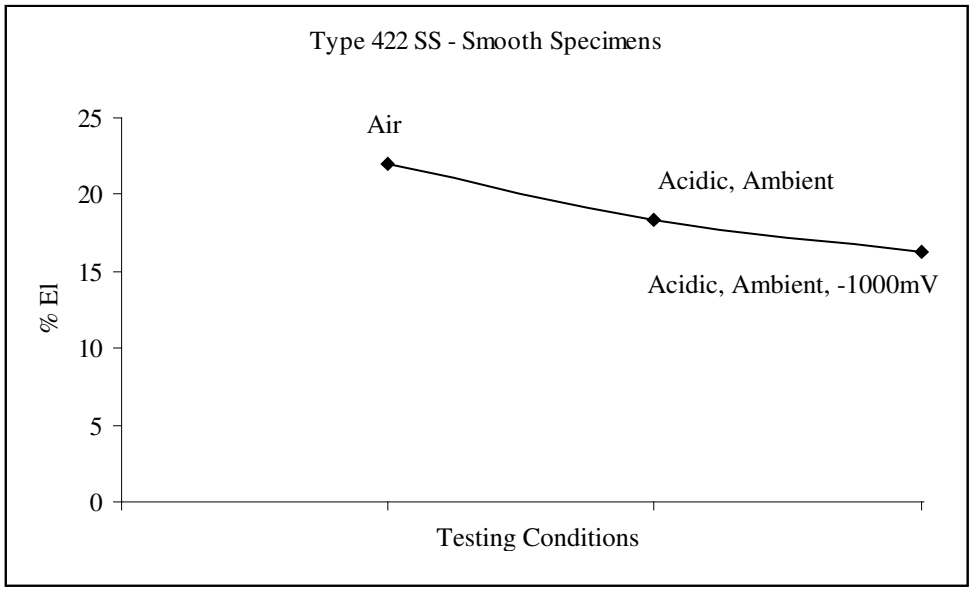

Figure 4.22: Effect of E_{cont} on %El

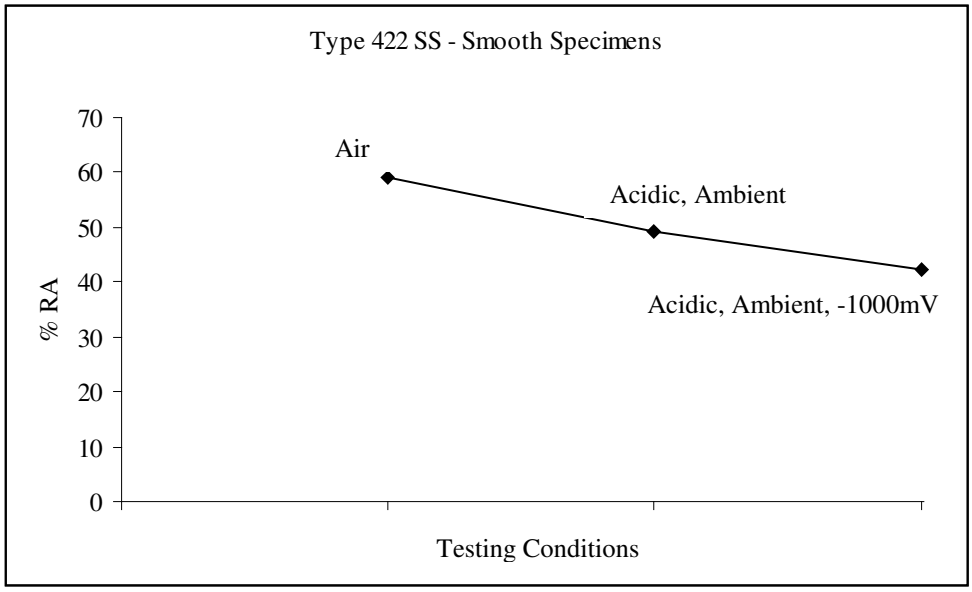

Figure 4.23: Effect of E_{cont} on %RA

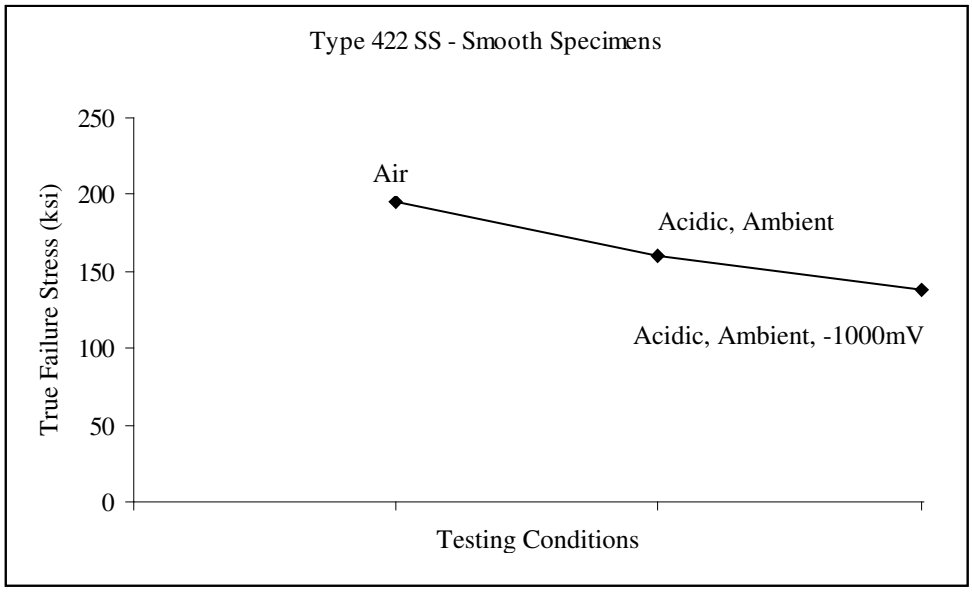

Figure 4.24: Effect of E_{cont} on True Failure Stress

4.7. Optical Microscopy

Optical microscopy was used to examine the surface characteristics and evaluate basic metallurgical information including the microstructure and the presence of secondary cracking along the gage length of the tested specimens. Both polished and etched specimens were examined for microstructural and secondary cracking evaluation.

The results of optical microscopy, shown in Figure 4.25a, indicated fine-grained martensitic microstructure, characteristic of a quenched and tempered (Q & T) stainless steel. Optical microscopic evaluation of the gage section, upon completion of testing, exhibited secondary cracks with branches. The optical micrographs of these secondary cracks in the polished and etched conditions are shown in Figures 4.25b and 4.25c.

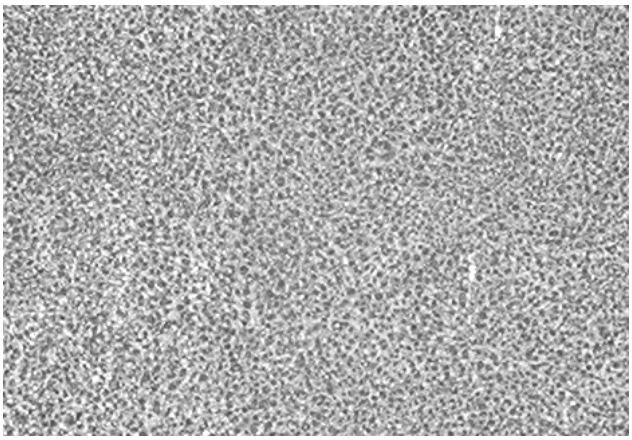

(a) Microstructure of Q & T Type 422 SS, Etched (Fry's Reagent), 40X

(b) Secondary Cracks, As-Polished, 40X

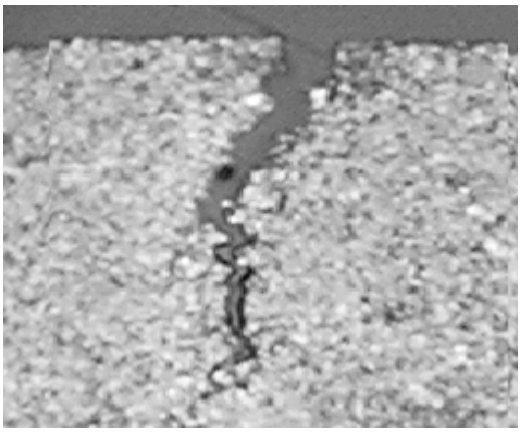

(c) Secondary Cracks, Etched (Fry's Reagent), 40X

Figure 4.25: Optical Micrographs of Tested Specimens in 90°C Acidic Environment

4.8. Scanning Electron Microscopy

SEM was primarily used to study the extent and morphology of failure at the primary fracture face of the tested cylindrical specimens to develop a basic understanding on the failure mechanism, as a function of the testing environment. In addition, SEM was used to characterize the nature of localized attack in the polarized specimens.

Based on the fractographic evaluations, it appears that the failure mode at the primary fracture face of the broken specimens tested in the neutral solution at ambient temperature was ductile, showing dimpled microstructure (Figure 4.26). However, transgranular brittle failure was observed in the similar environment at 90°C, as shown in Figure 4.27. The specimens, tested in the acidic solution at ambient temperature, showed a combination of intergranular and transgranular brittle failure (Figure 4.28). However, transgranular brittle failure only was observed in the 90°C acidic solution, as shown in Figure 4.29. Examinations of these SEM micrographs suggest that the extent of cracking was more pronounced in the 90°C acidic environment.

The examination of polarized specimens by SEM showed larger and deeper pits in Type 422 SS when polarized in the 90°C acidic environment, compared to those seen in the other environment, as shown in Figures 4.30 and 4.31.

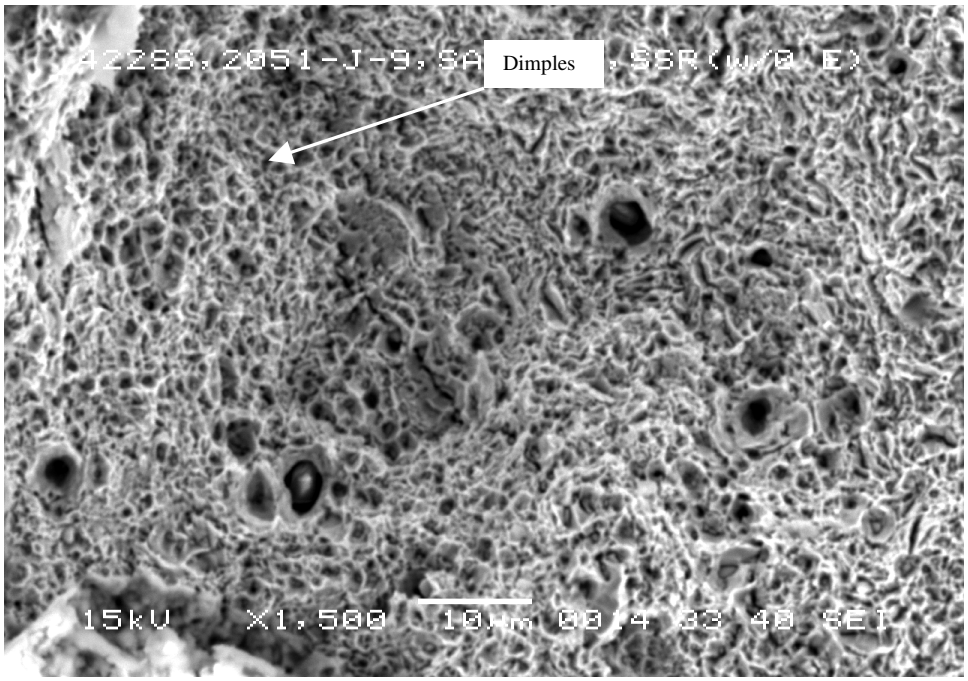

Figure 4.26: Ductile Failure in Tensile Specimens, Ambient Temperature, Neutral Solution, 1500X

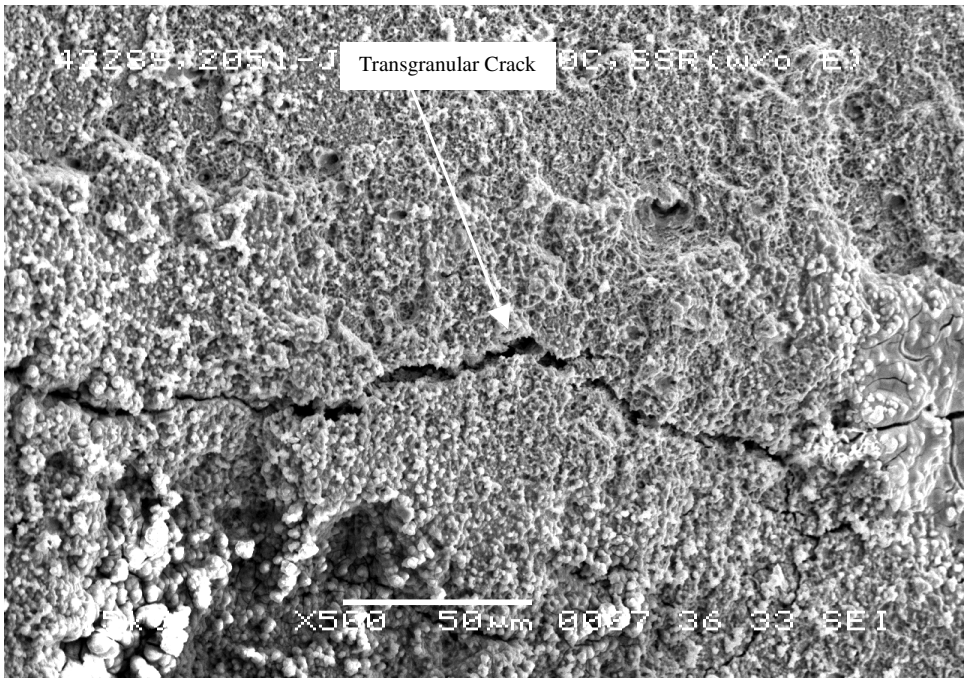

Figure 4.27: Transgranular Brittle Failure in Tensile Specimens, 90°C, Neutral Solution, 500X

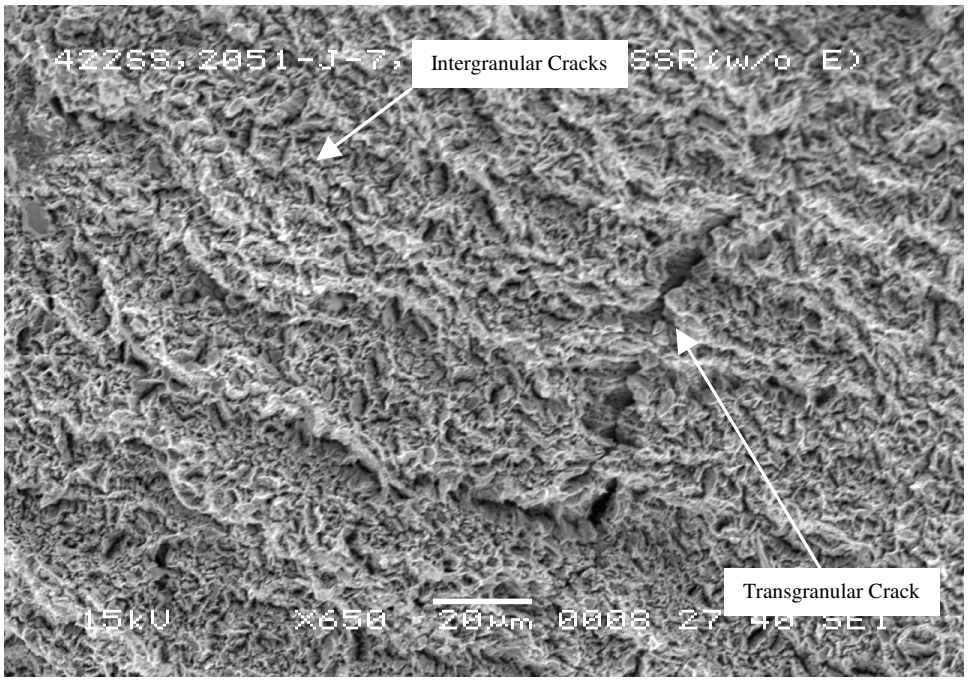

Figure 4.28: Intergranular and Transgranular Brittle Failure in Tensile Specimens, Ambient Temperature, Acidic Solution, 650X

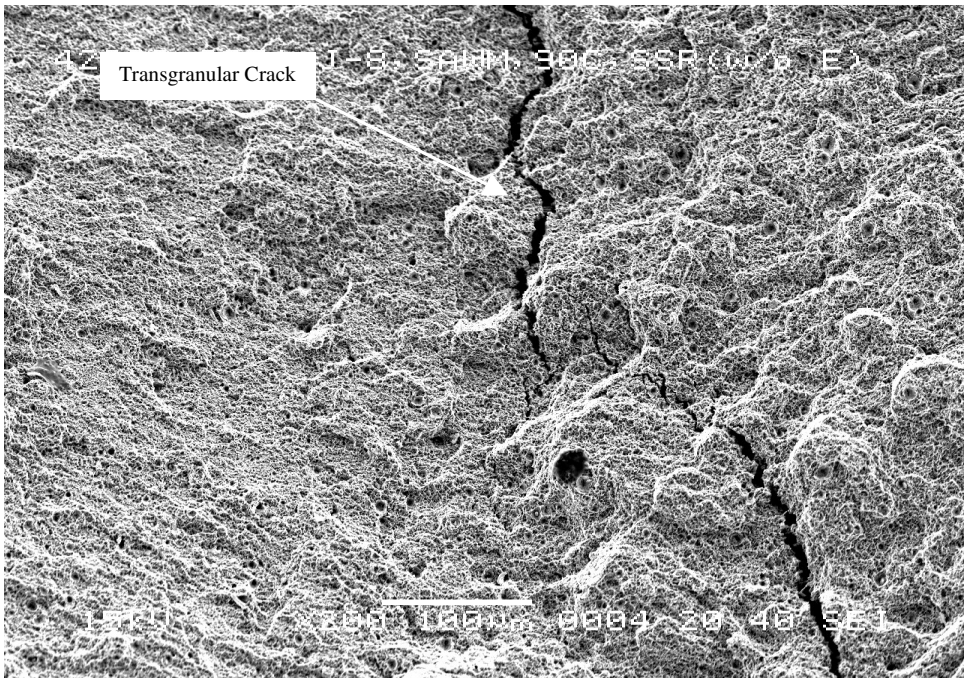

Figure 4.29: Transgranular Brittle Failure in Tensile Specimens, 90°C, Acidic Solution, 200X

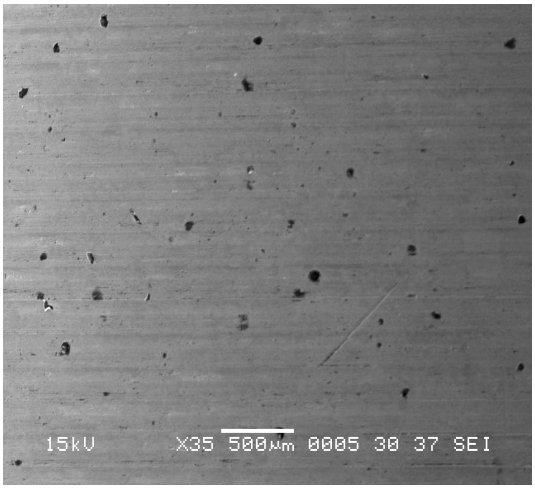

(a) 30°C

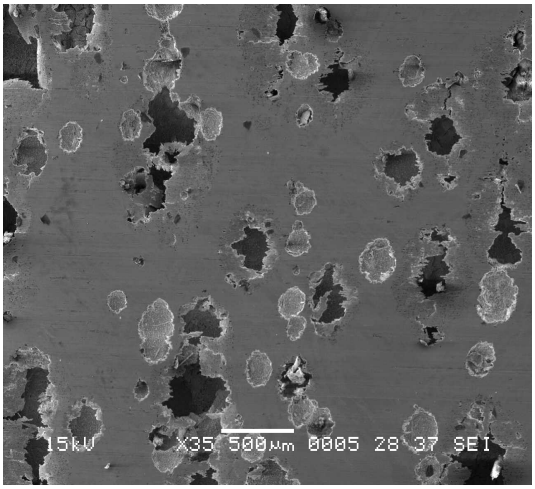

(b) 90°C

Figure 4.30: Pits in Polarized Specimens Tested in Neutral Environment, 35X

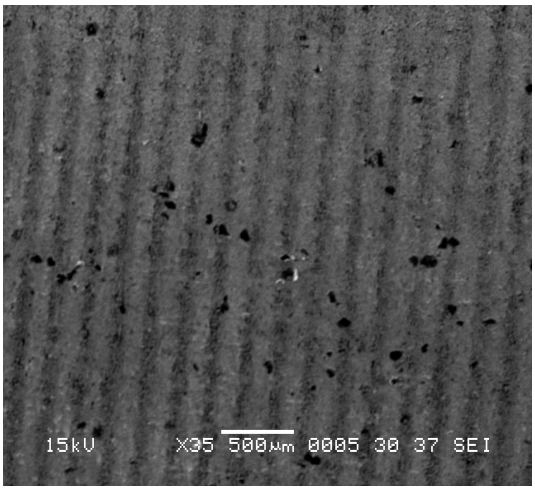

(a) 30°C

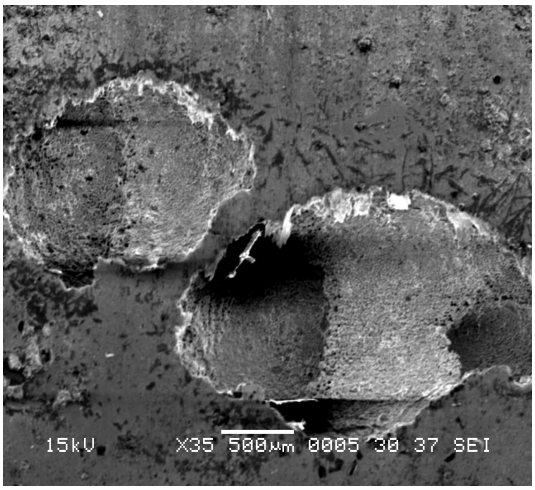

(b) 90°C

Figure 4.31: Pits in Polarized Specimens Tested in Acidic Environment, 35X

CHAPTER 5

DISCUSSION

As indicated in the previous section, martensitic Type 422 SS, a candidate structural material has been evaluated for its resistance to SCC, HE and localized corrosion in neutral and acidic aqueous environments at ambient and elevated temperatures. For SCC testing, CL and SSR techniques have been used. The effect of hydrogen on the cracking susceptibility has been evaluated by applying cathodic electrochemical potential in a potentiostatic mode. The localized corrosion behavior has been evaluated by CPP tests in similar environments. Microstructural evaluations and characterization of secondary cracks observed in the tested tensile specimens have been performed by optical microscopy. Fractographic evaluations have been conducted by SEM, to determine the extent and morphology of failures at the primary fracture face of the tested tensile specimens. Discussions on different topics related to this investigation are presented below.

5.1. Thermal Treatment and Resultant Properties

As described earlier, the objective of thermal treatment involving quenching and tempering of the test material was to develop a fine-grained and fully-tempered microstructure leading to the development of appreciable amount of ductility.[35, 41, 63] It is well known that the hardening produced by austenitizing and quenching can result in the

formation of hard but brittle martensite that can cause difficulty during the fabrication processes.[35] In view of this drawback associated with the hardened material, it is always customary to temper the brittle martensite, enhancing the resultant ductility in a material such as Type 422 SS. An evaluation of the hardness data before and after tempering clearly demonstrates this expected behavior of quenched and tempered material.

It is also well known that higher the carbon content, stronger is the material. As seen in the results, shown earlier, the hardness and YS values were substantially higher, compared to other martensitic steels such as Alloy EP-823 and HT-9.[64-66] The carbon content in the tested material was roughly 0.2 wt % and the very high yield and tensile strengths are due to the presence of relatively higher carbon content.[15, 32-39, 67] The presence of carbide forming elements such as molybdenum, vanadium and tungsten might have contributed to the relatively higher strength in this material.[35]

5.2. Constant-Load Testing

The results of CL testing using smooth specimens of Type 422 SS revealed no failure in neutral and acidic solutions at ambient temperature. Even though no failures were observed in the 90°C neutral solution, failures were observed in the acidic solution at similar temperature, at applied stresses corresponding to 95, 90 and 85% of its YS value. These results clearly indicate that the cracking susceptibility may be enhanced in the presence of acidic environment at elevated temperature, indicating a synergistic effect of pH and temperature on failures of this alloy.

The enhanced cracking susceptibility in the acidic environment may be the result of increased rate of cathodic reaction due to high concentration of hydrogen ions.[68] The

temperature dependence of cracking may be the result of temperature-induced change in the protective properties of passive films on the surface of the test material leading to the enhanced breakdown of these films as temperature was increased from ambient temperature to 90°C.[69] This change can be rationalized either by an increase in porosity or by an intrinsic modification of the chemical composition and/or physical structure of the passive film at higher test temperature.[70, 71] This detrimental effect of temperature and pH on environment-assisted cracking of metallic materials has been reported by other investigators.[72, 73]

Since failures were observed at applied stresses up to 85% of the material's YS value, CL testing was performed at 80% of its YS value. No failures were observed at this applied stress level, suggesting a σ_{th} value of approximately 0.80YS (97 ksi). It should however be noted that the presence of a notch in the test specimen reduced the magnitude of threshold value due to the smaller cross-sectional area at the root of the notch. The effect of stress concentration on the cracking susceptibility has been demonstrated by other investigators.[74, 75]

5.3. Slow-Strain-Rate Testing

The load versus displacement curves generated during the SSR testing in both test environments at ambient temperature, 60 and 90°C, using smooth specimens reduced displacement due to a change in temperature from ambient temperature to 90°C. This effect was more pronounced in the acidic environment. The reduction in these parameters in the acidic solution may be due to the increased hydrogen ion (H^+) concentration that may accelerate the breakdown of surface film.[76] The magnitude of %El, %RA, TTF, P_m,

σ_m and σ_f determined from the load versus displacement curves and specimen dimensions, were gradually reduced with increasing temperature, showing more pronounced effect in the acidic solution. This effect, which may be due to the combined effect of acidic pH and higher testing temperature, has been reported other investigators.[73] The presence of a notch further reduced %El, %RA, TTF and P_m values, as expected. However, the magnitude of σ_m and σ_f was enhanced due to the reduced cross-sectional area at the root of notch.

5.4. Localized Corrosion Testing

The results of localized corrosion presented earlier have clearly shown that Type 422 SS may undergo localized attack, including pitting and crevice corrosion, irrespective of the testing environment and temperature. A similar observation has been made by other investigators.[77, 78]

It is well known that the initiation of crevice corrosion in metallic materials immersed in chloride-containing aqueous solution environments may involve the dissolution of metal and maintenance of a high degree of acidity within the crevice solution by the hydrolysis of the dissolved metal ions.[79]

The initiation of pitting in susceptible active-passive metals and alloys is the result of the breakdown of the passive films on their surface in the presence of aggressive anions, such as chloride ions (Cl^-) and the subsequent establishment of an electrochemical cell in which the damaged site acts an anode and the surrounding passive surface acts as a cathode.[62]

However, as expected, the nature of localized attack was more severe in the acidic environment at elevated temperature.[68-71] The detrimental effect of lower pH and higher temperature on the breakdown of surface film, has also been reported by other researchers.[72, 73]

It is well known that more noble critical potentials (E_{corr} and E_{pit}) can be developed in a neutral solution compared to those in an acidic solution, irrespective of temperature. It is also known that the magnitude of these critical potentials may become more anodic (negative) with an increase in temperature.[77, 78, 80] A similar phenomenon was also observed in this investigation showing more anodic E_{pit} value due to change in temperature from 30 to 60 to 90°C, irrespective of the test environment and this effect was more pronounced in the acidic solution.

A repassivation behavior was also noticed in the acidic solution at 30 and 60°C, during the reverse potential scanning. The difference in the magnitude of E_{pit} and E_{prot} of a material of interest can influence its susceptibility to localized attack. Larger this difference better is the resistance of the material to localized attack. An examination of the resultant data indicate that the difference between E_{pit} and E_{prot} in the acidic environment was reduced as the temperature was increased from 30 to 60°C. By virtue of these results, it can be concluded that the 60°C acidic environment produced higher localized corrosion susceptibility that was also substantiated by the appearance of the polarized specimens at this temperature.

5.5. Slow-Strain-Rate Testing under Controlled Cathodic Potential

The results of SCC testing under cathodic charging using the SSR technique clearly showed that the ductility parameters, TTF and σ_f were reduced to some extent. This phenomenon may be attributed to the generation of more hydrogen ions (H^+) in the acidic solution, due to cathodic polarization. As discussed in the earlier section, the presence of hydrogen, due to cathodic polarizing can produce brittle failure, thus, reducing the magnitude of ductility parameters. A similar observation has been made by other investigators.[53-61, 81-83]

5.6. Metallography

Metallographic evaluations by optical microscopy showed conventional fine-grained and fully-tempered martensitic microstructures, as expected. Branched secondary cracks were noticed along the gage section. A similar observation has been made by other investigator.[61]

5.7. Fractography

Fractographic evaluations by SEM revealed ductile failure in specimens tested in the neutral solution at ambient temperature. However, a combined intergranular and transgranular brittle failure was observed in the acidic solution at similar test temperature. Transgranular brittle failures were observed at 90°C, irrespective of the test environment. Similar types of failure have been reported elsewhere.[61, 84-86] The evaluation of the polarized specimens by SEM revealed larger and deeper pits in the acidic solution, showing more pronounced effect at 90°C.

CHAPTER 6

SUMMARY AND CONCLUSIONS

Martensitic Type 422 SS has been suggested to be a candidate structural material to contain the target material during the transmutation process. This investigation is aimed at elucidating the susceptibility of Type 422 SS to environment-induced degradations including SCC, HE and pitting/crevice corrosion in neutral and acidic aqueous environments at ambient and elevated temperatures. The susceptibility to SCC behavior was determined by SSR and CL testing techniques, using smooth and notched specimens. The localized corrosion behavior was determined by CPP method. The effect of hydrogen on the cracking behavior was evaluated under controlled cathodic potential. Fractographic and metallographic evaluations of the tested specimens were performed by SEM and optical microscopy, respectively. The significant conclusions drawn from this investigation are summarized below.

- Type 422 SS showed higher hardness and yield strength values, due to the presence of higher carbon content, as expected.
- The results of the CL SCC testing involving smooth specimens showed no failures in the neutral solution at any tested temperature, irrespective of the applied stress. Similarly, no failures were observed in the acidic solution at ambient temperature.

- The results of CL SCC testing in the 90°C acidic solution showed failures in Type 422 SS at applied stresses corresponding to 95, 90 and 85% of this material's YS value. Since, no failure was observed at an applied stress corresponding to 0.80YS, a σ_{th} value of 97 ksi was noted. However, the presence of a notch reduced the threshold load to 25 percent of its yielding load.

- The results of SSR SCC testing involving smooth and notched specimens showed reduction in %El, %RA, TTF and P_m values in the acidic solution at elevated temperatures, showing a synergistic effect of acidic pH and higher test temperature on the cracking susceptibility of Type 422 SS. However, the presence of a notch enhanced the magnitude of $\sigma_{m,}$ and σ_f values, due to the reduced cross-sectional area at the root of the notch.

- The CPP testing showed more active (negative) E_{corr} values in both test environments, due to a change in temperature from 30 to 60°C. However, the magnitude of E_{pit} became more active with gradual increment in temperature up to 90°C. A repassivation behavior was also noticed in the acidic solution at 30 and 60°C, during the reverse potential scanning.

- The application of a -1000 mV controlled potential to the test specimen during SSR testing further reduced the magnitude of TTF, %El, %RA and σ_f, indicating a detrimental effect of hydrogen produced during cathodic charging on the cracking tendency.

- Both pitting and crevice corrosion were observed in specimens polarized in either environment at different temperatures. The extent of localized damage was more pronounced in the 90°C acidic environment.
- Optical microscopy revealed fine-grained martensitic microstructure, which is a characteristic of a Q & T stainless steel. Secondary cracks with branches were also observed in optical micrographs of tensile specimens along the gage length.
- The SEM micrographs of specimens tested in the neutral solution at ambient temperature were characterized by dimpled microstructure indicating ductile failure. On the contrary, combined intergranular and transgranular brittle failures were observed in the acidic solution. However, transgranular brittle failures were observed in both environments at 90°C.
- The examination of polarized specimens by SEM showed larger and deeper pits in the 90°C acidic environment, compared to those seen in other environment.

CHAPTER 7

SUGGESTED FUTURE WORK

The following additional work for further evaluations is suggested.

- Assuming that a research facility to accommodate molten LBE testing is established at UNLV, SCC testing needs to be performed in this environment at temperatures ranging between 400-550°C, using self-loaded (C-ring and U-bent) specimens. Efforts may also be made to see if localized dissolution of the surface film may occur in this temperature regime.
- Characterize the surface film in specimens tested in aqueous and molten LBE environments at comparable temperatures using relevant techniques.

APPENDIX A

CONSTANT-LOAD DATA

A1. SMOOTH SPECIMENS

Environment/Temperature (°C)/Applied Stress (%YS)	Failure (hours)/No Failure
Neutral/Ambient/0.95YS	No Failure
Neutral/Ambient/0.95YS	No Failure
Neutral/Ambient/0.95YS (Mean)	**No Failure**
Neutral/90/0.95YS	No Failure
Neutral/90/0.95YS	No Failure
Neutral/90/0.95YS (Mean)	**No Failure**
Acidic/Ambient/0.95YS	No Failure
Acidic/Ambient/0.95YS	No Failure
Acidic/Ambient/0.95YS (Mean)	**No Failure**
Acidic/90/0.95YS	139.5
Acidic/90/0.95YS	317.2
Acidic/90/0.95YS	179.7
Acidic/90/0.95YS (Mean)	**212**
Acidic/90/0.90YS	124.7
Acidic/90/0.90YS	375.3
Acidic/90/0.90YS (Mean)	**250**
Acidic/90/0.85YS	441.4
Acidic/90/0.85YS	311
Acidic/90/0.85YS	395.6
Acidic/90/0.85YS (Mean)	**383**
Acidic/90/0.80YS	No Failure
Acidic/90/0.80YS	No Failure
Acidic/90/0.80YS	No Failure
Acidic/90/0.80YS	No Failure
Acidic/90/0.80YS (Mean)	**No Failure**

A2. NOTCHED SPECIMENS

Environment/Temperature (°C)/Applied Stress (%YL)	Failure/No Failure
Acidic/90/0.35YL	Failed while applying load
Acidic/90/0.30YL	Failed while applying load
Acidic/90/0.25YL	No Failure
Acidic/90/0.25YL	No Failure
Acidic/90/0.25YL (Mean)	**No Failure**

APPENDIX B

SLOW-STRAIN-RATE DATA

B1. Load Versus Displacement Curves (Smooth Specimens)

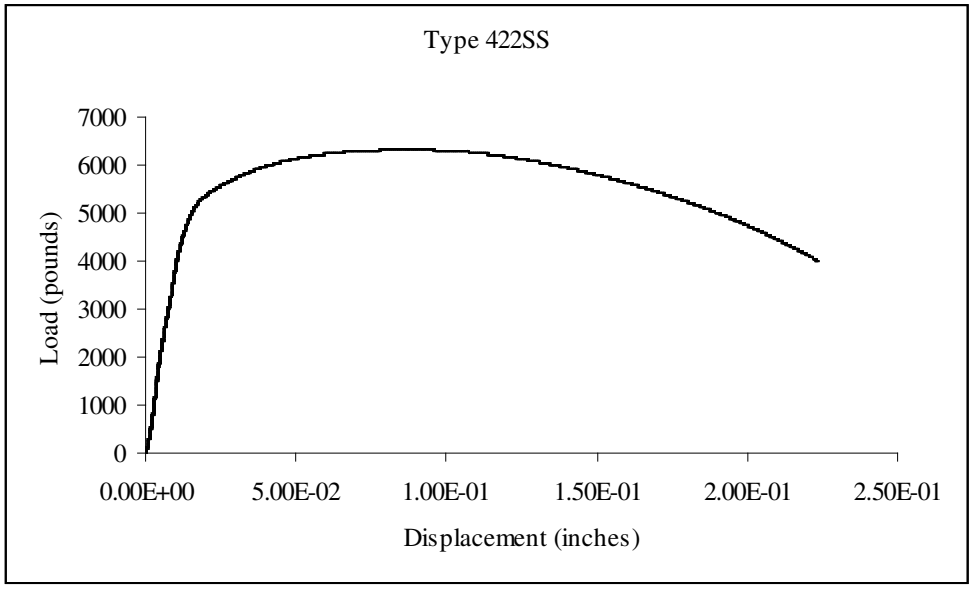

Air

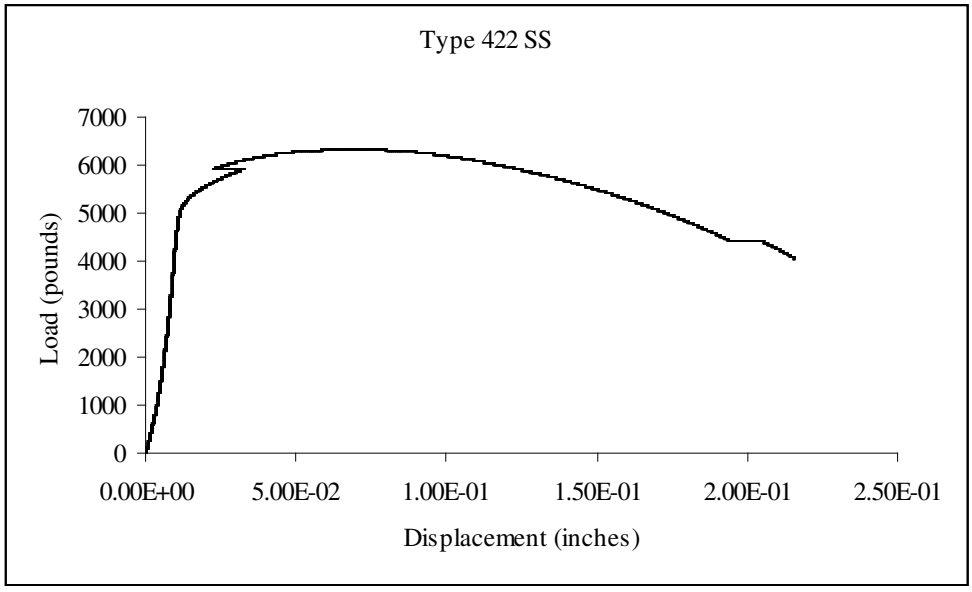

Neutral Environment, Ambient Temperature (Smooth Sample 1)

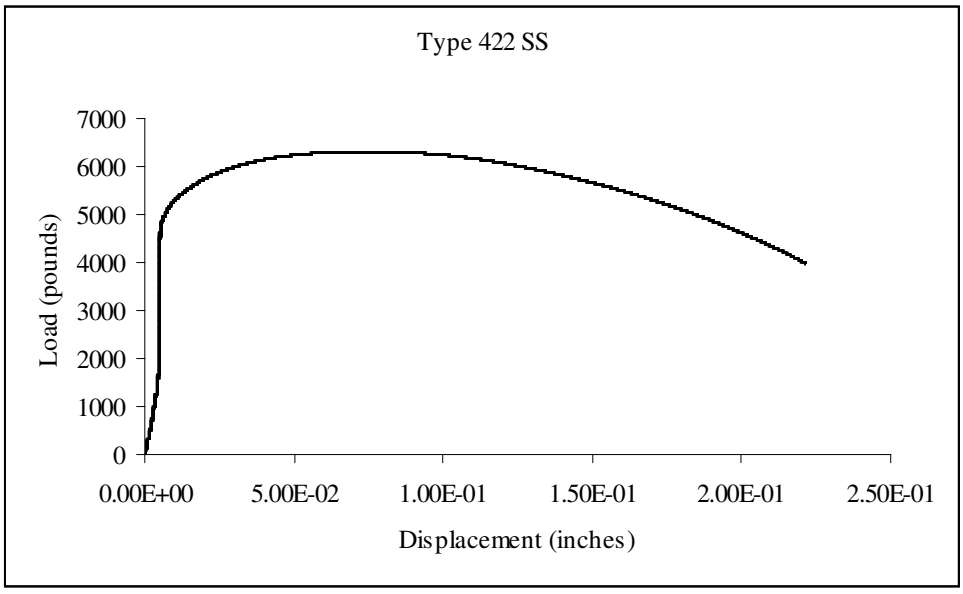

Neutral Environment, Ambient Temperature (Smooth Sample 2)

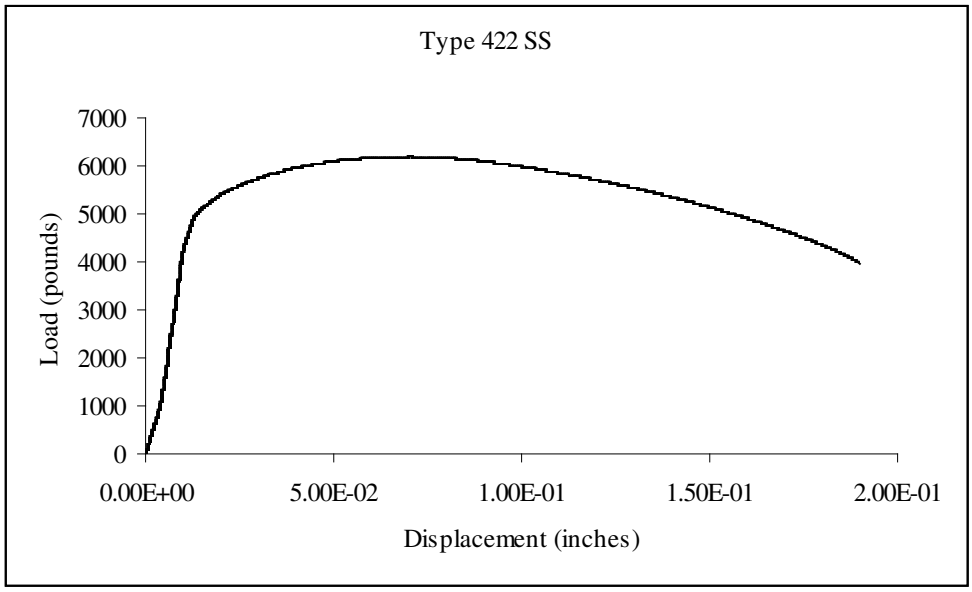

Neutral Environment, 60°C (Smooth Sample 1)

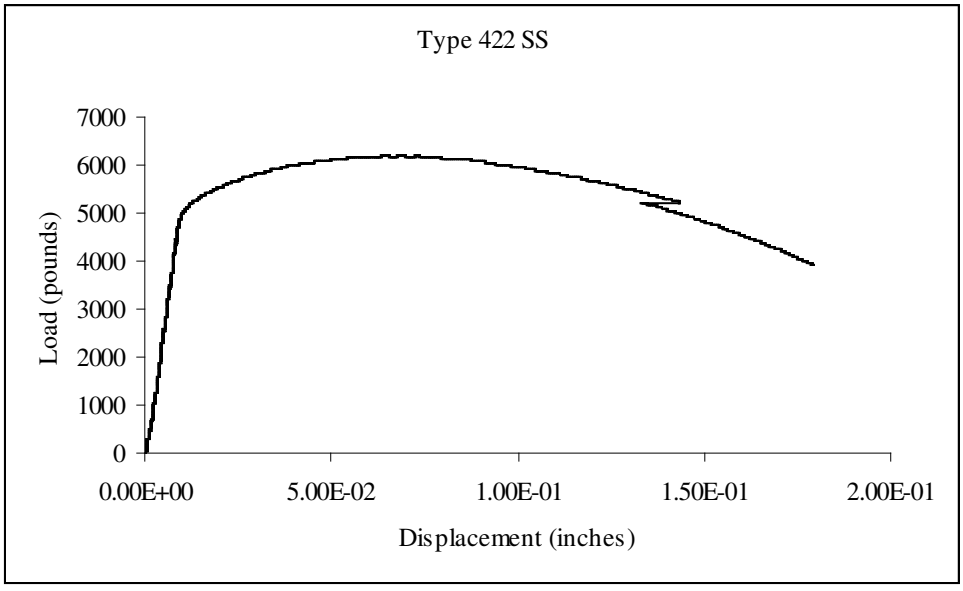

Neutral Environment, 60°C (Smooth Sample 2)

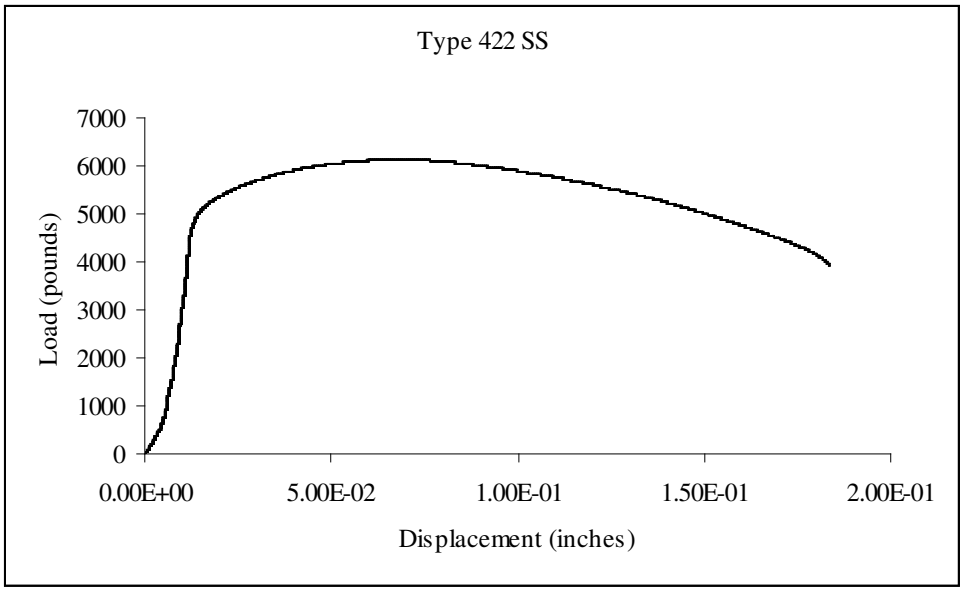

Neutral Environment, 90°C (Smooth Sample 1)

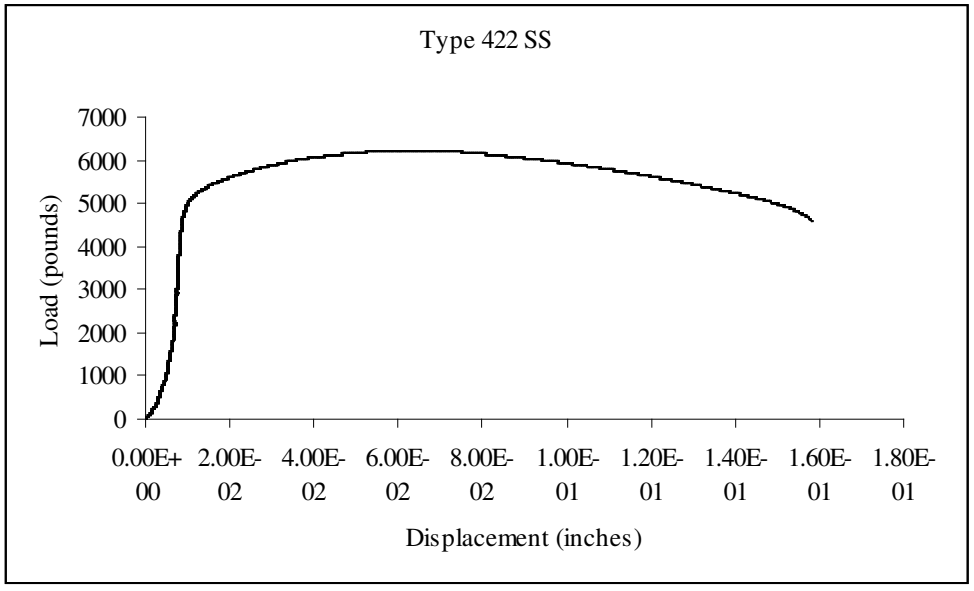

Neutral Environment, 90°C (Smooth Sample 2)

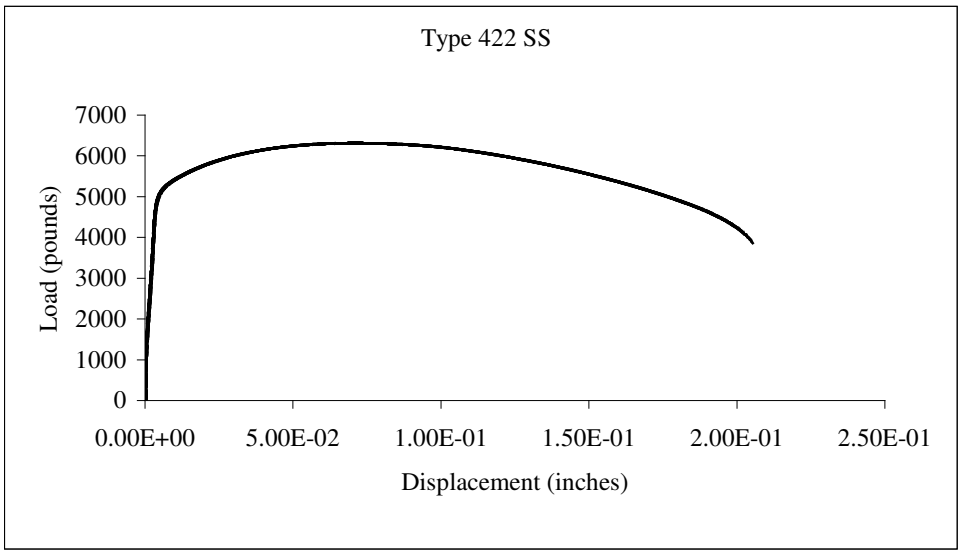

Acidic Environment, Ambient Temperature (Smooth Sample 1)

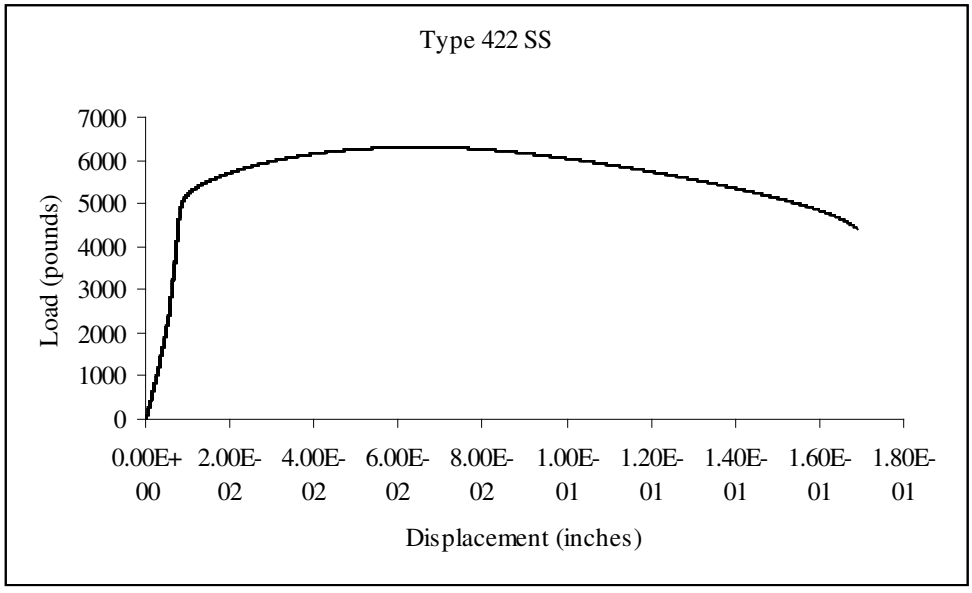

Acidic Environment, Ambient Temperature (Smooth Sample 2)

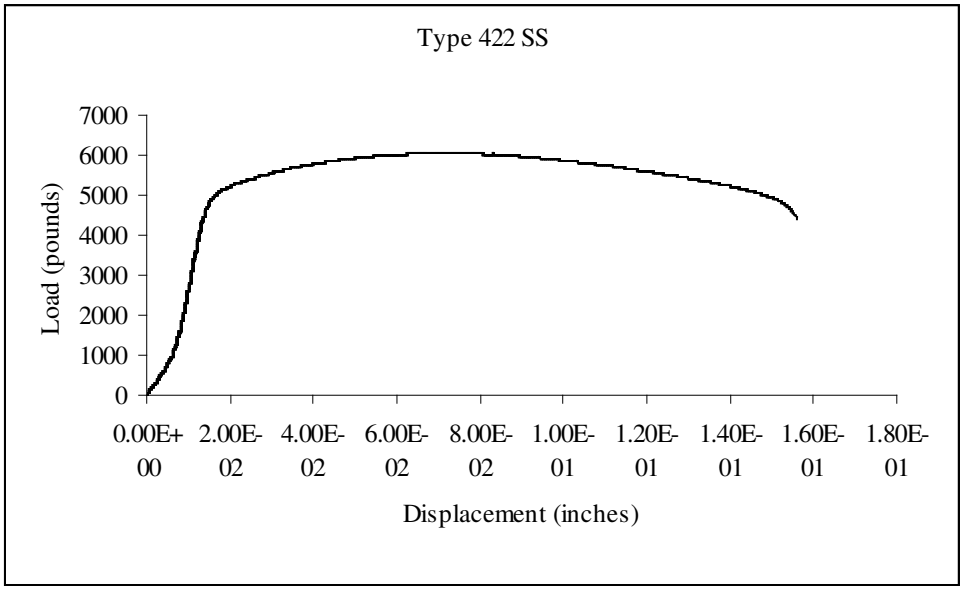

Acidic Environment, 60°C (Smooth Sample 1)

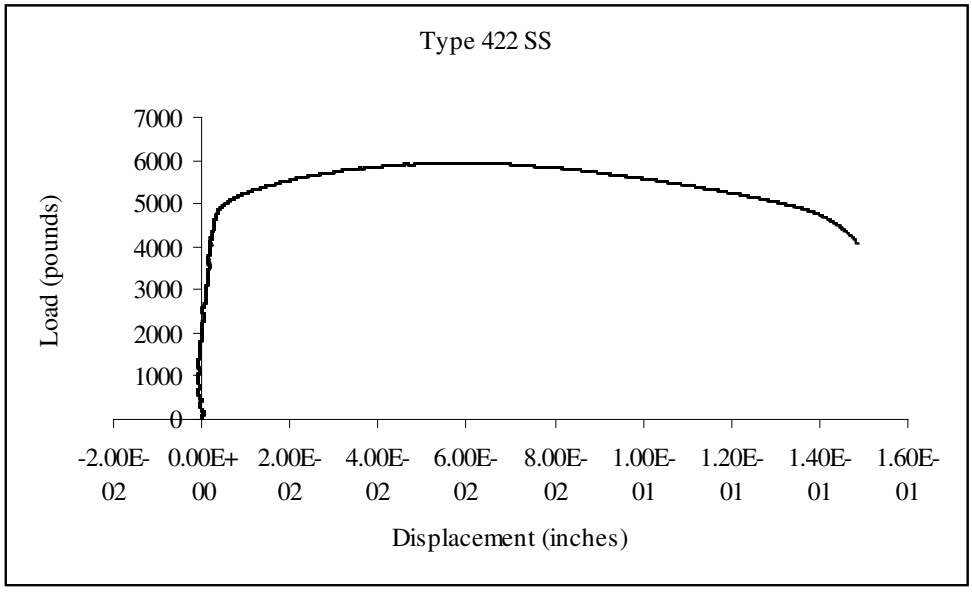

Acidic Environment, 60°C (Smooth Sample 2)

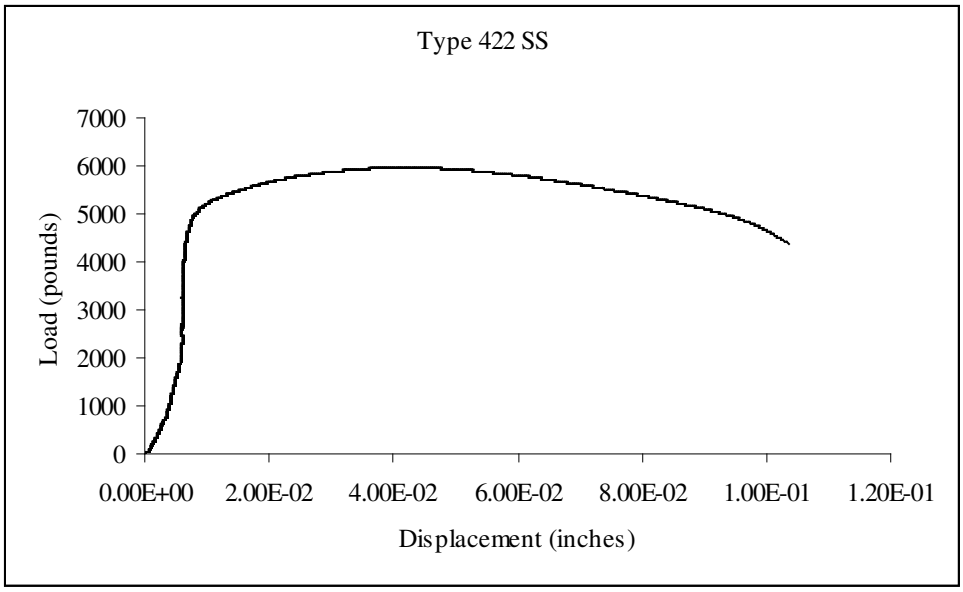

Acidic Environment, 90°C (Smooth Sample 1)

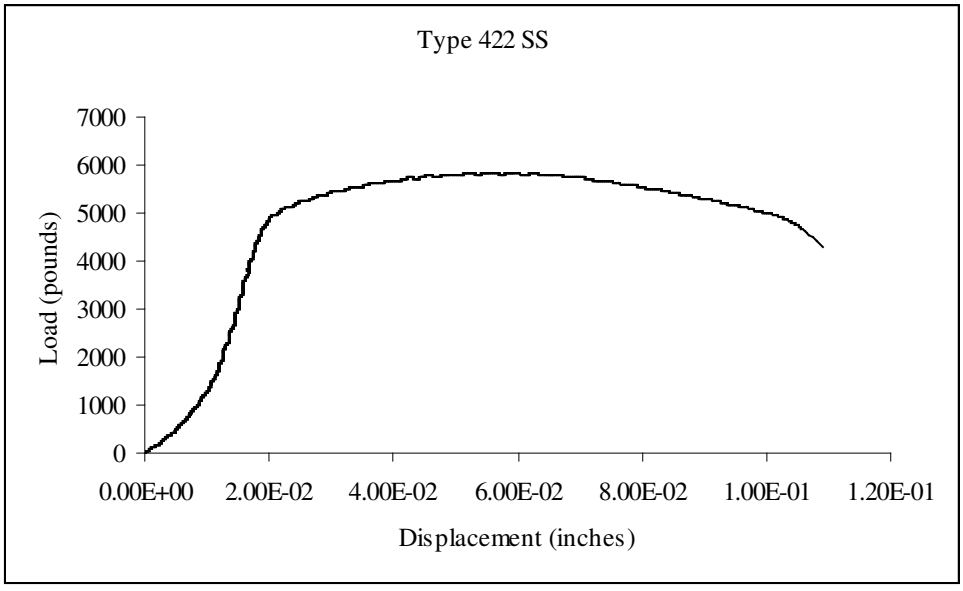

Acidic Environment, 90°C (Smooth Sample 2)

B2. SSR Data (Smooth Specimens)

Environment/ Temperature (°C)	P_m (lbs)	σ_m (ksi)	P_f (lbs)	σ_f (ksi)	%EL	%RA	TTF (hours)
None	**6321.19**	**126.80**	**4001.11**	**195.42**	**21.95**	**58.93**	**21.17**
Neutral/Ambient	6308.53	126.55	3975.71	180.52	21.77	55.82	20.02
Neutral/Ambient	6326.57	126.91	4052.06	173.81	20.63	54.49	21.00
Neutral/Ambient (Mean)	**6317.55**	**126.73**	**4013.89**	**177.17**	**21.20**	**55.16**	**20.51**
Neutral/60	6208.02	124.53	3988.72	175.82	18.00	54.89	18.45
Neutral/60	6197.77	124.33	3912.99	173.21	18.42	55.03	19.03
Neutral/60 (Mean)	**6202.90**	**124.43**	**3950.86**	**174.52**	**18.21**	**54.96**	**18.74**
Neutral/90	6127.16	122.91	3912.98	171.87	18.13	54.33	18.12
Neutral/90	6225.30	124.88	4592.17	174.68	15.48	47.26	16.88
Neutral/90 (Mean)	**6176.23**	**123.90**	**4252.58**	**173.28**	**16.81**	**50.80**	**17.50**
Acidic/Ambient	6313.80	122.44	4393.55	166.94	16.33	48.96	17.75
Acidic/Ambient	6314.30	126.66	3862.41	152.42	20.35	49.15	20.67
Acidic/Ambient (Mean)	**6314.05**	**124.55**	**4127.98**	**159.68**	**18.34**	**49.06**	**19.21**
Acidic/60	6054.69	121.46	4406.38	142.46	15.55	38.25	15.75
Acidic/60	5948.54	120.05	4069.64	138.75	15.95	41.81	16.30
Acidic/60 (Mean)	**6001.62**	**120.39**	**4238.01**	**140.61**	**15.75**	**40.03**	**16.03**
Acidic/90	5957.62	116.62	4366.03	116.39	10.21	26.57	12.27
Acidic/90	5840.53	116.60	4296.99	116.99	10.82	26.68	11.52
Acidic/90 (Mean)	**5899.08**	**116.61**	**4331.51**	**116.69**	**10.52**	**26.63**	**11.90**

B3. Load Versus Displacement Curves (Notched Specimens)

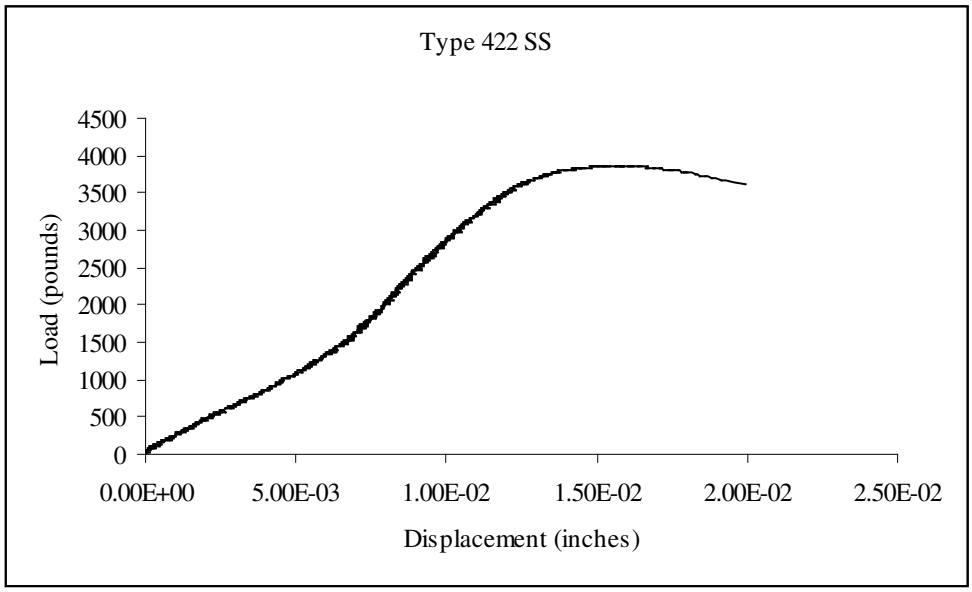

Neutral Environment, Ambient Temperature (Notched Sample 1)

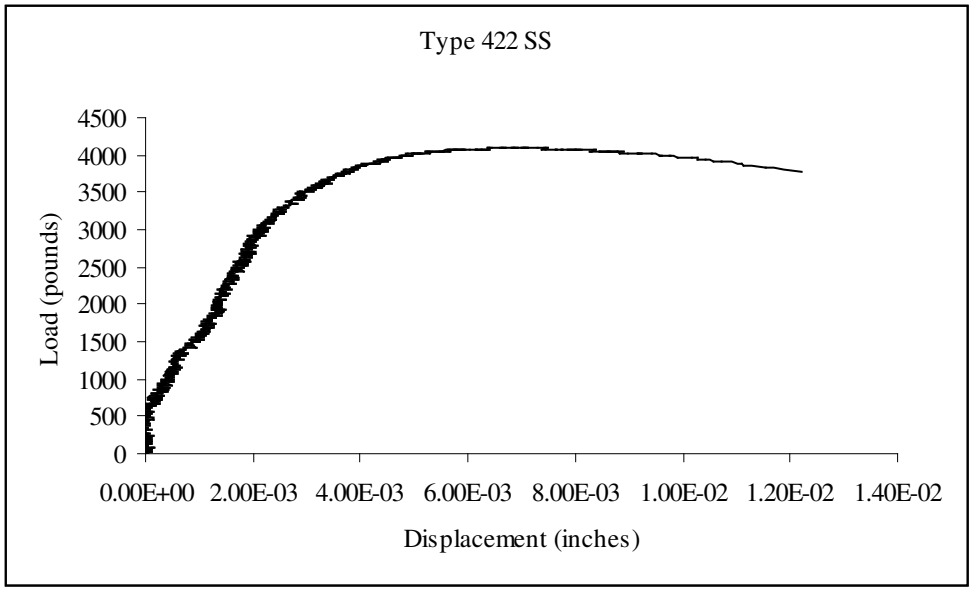

Neutral Environment, Ambient Temperature (Notched Sample 2)

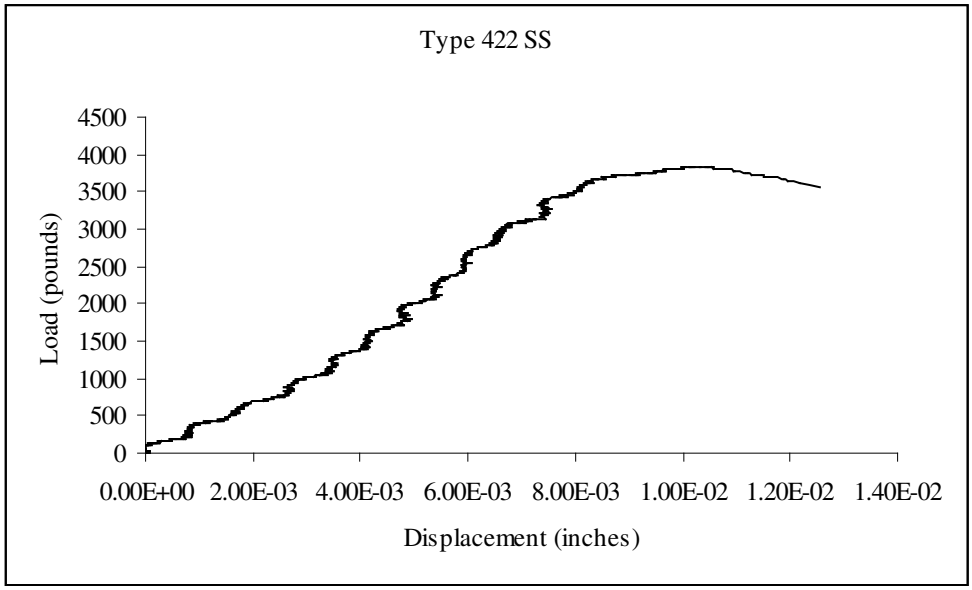

Neutral Environment, 90°C (Notched Sample 1)

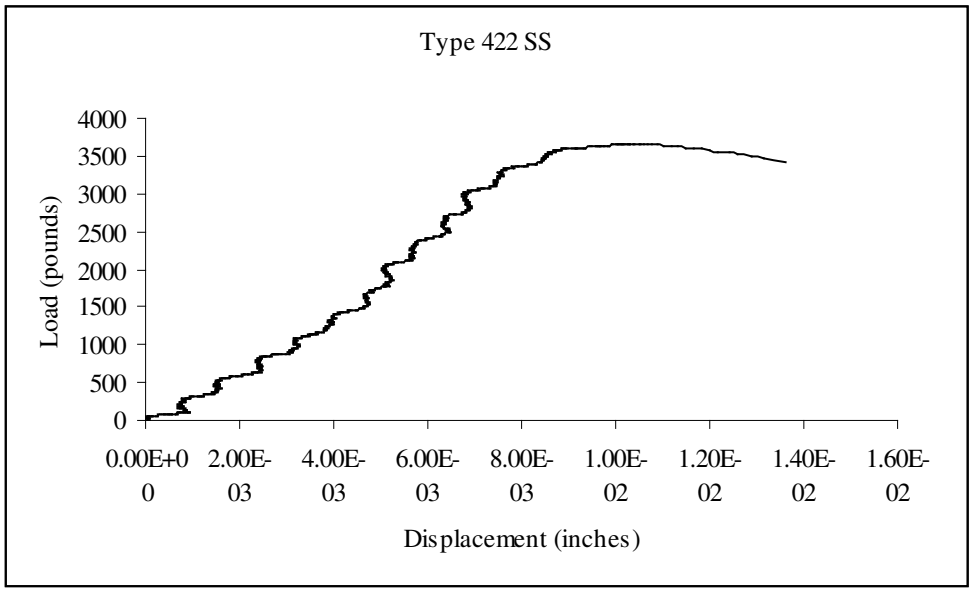

Neutral Environment, 90°C (Notched Sample 2)

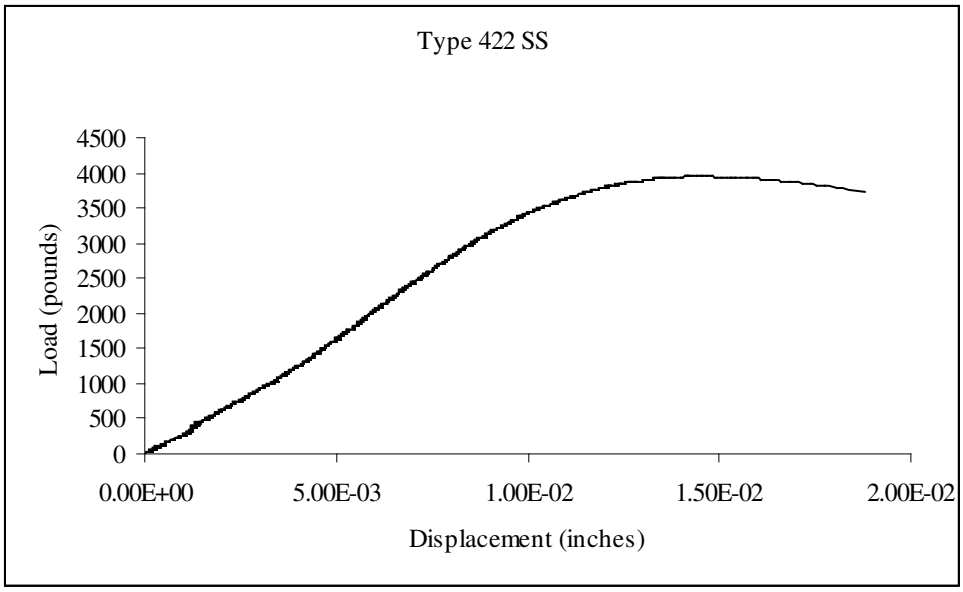

Acidic Environment, Ambient Temperature (Notched Sample 1)

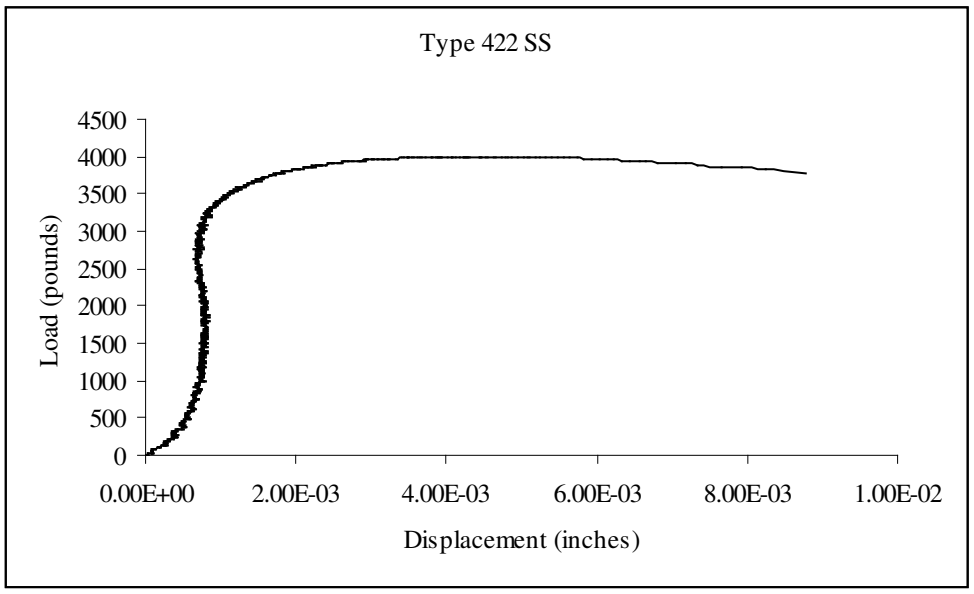

Acidic Environment, Ambient Temperature (Notched Sample 2)

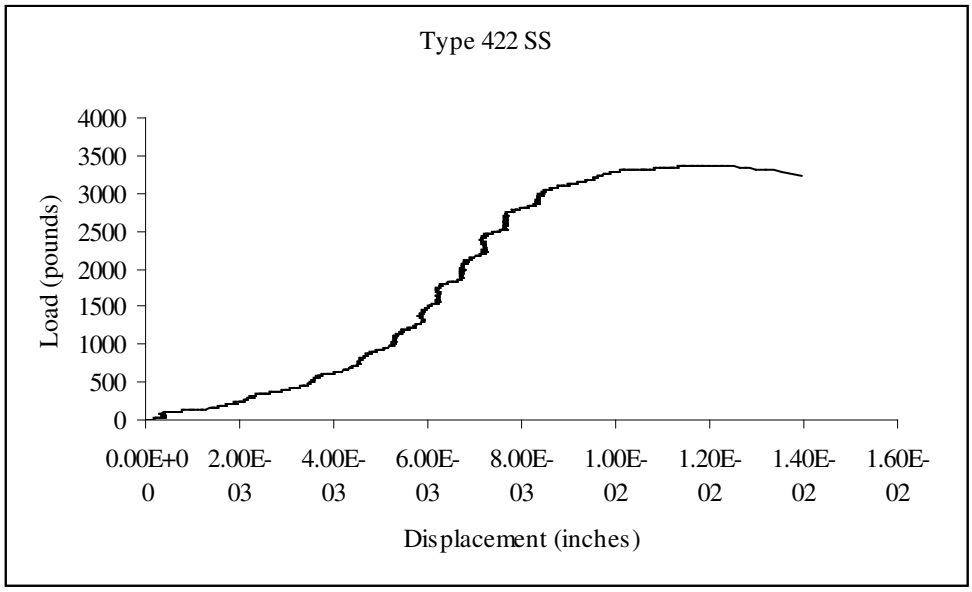

Acidic Environment, 90°C (Notched Sample 1)

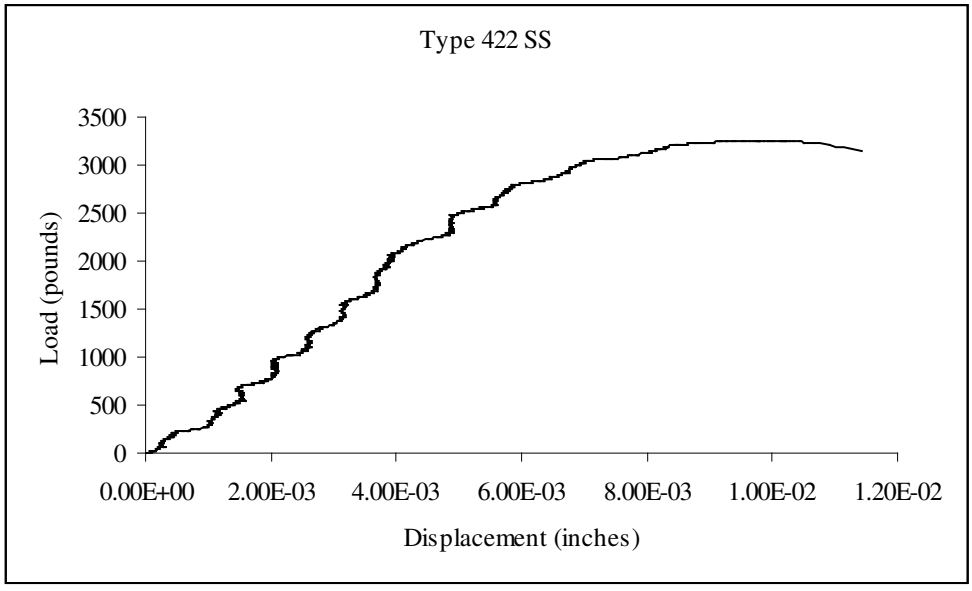

Acidic Environment, 90°C (Notched Sample 2)

B4. SSR Data (Notched Specimens)

Environment/ Temperature (°C)	P_m (lbs)	σ_m (ksi)	P_f (lbs)	σ_f (ksi)	%EL	%RA	TTF (hours)
Neutral/Ambient	3860.91	202.10	3604.42	198.74	1.80	9.87	4.03
Neutral/Ambient	4088.99	214.04	3769.65	207.85	2.30	9.87	4.23
Neutral/Ambient (Mean)	**3974.95**	**208.07**	**3687.04**	**203.30**	**2.05**	**9.87**	**4.13**
Neutral/90	3829.61	200.48	3556.60	196.10	1.50	5.06	3.97
Neutral/90	3665.38	191.86	3430.04	186.66	1.65	7.47	3.82
Neutral/90 (Mean)	**3747.50**	**196.17**	**3493.32**	**191.38**	**1.58**	**6.27**	**3.90**
Acidic/Ambient	3948.54	206.71	3725.85	202.76	1.48	3.81	4.13
Acidic/Ambient	3999.73	209.39	3780.35	207.07	1.49	4.44	4.13
Acidic/Ambient (Mean)	**3974.14**	**208.05**	**3753.10**	**204.92**	**1.49**	**4.13**	**4.13**
Acidic/90	3369.46	176.38	3224.75	170.99	1.50	2.54	3.62
Acidic/90	3258.88	170.58	3138.11	166.39	1.20	2.54	3.75
Acidic/90 (Mean)	**3314.17**	**173.48**	**3181.43**	**168.69**	**1.25**	**2.54**	**3.69**

B5. Load Versus Displacement Curves (Smooth Specimens - Applied Potential)

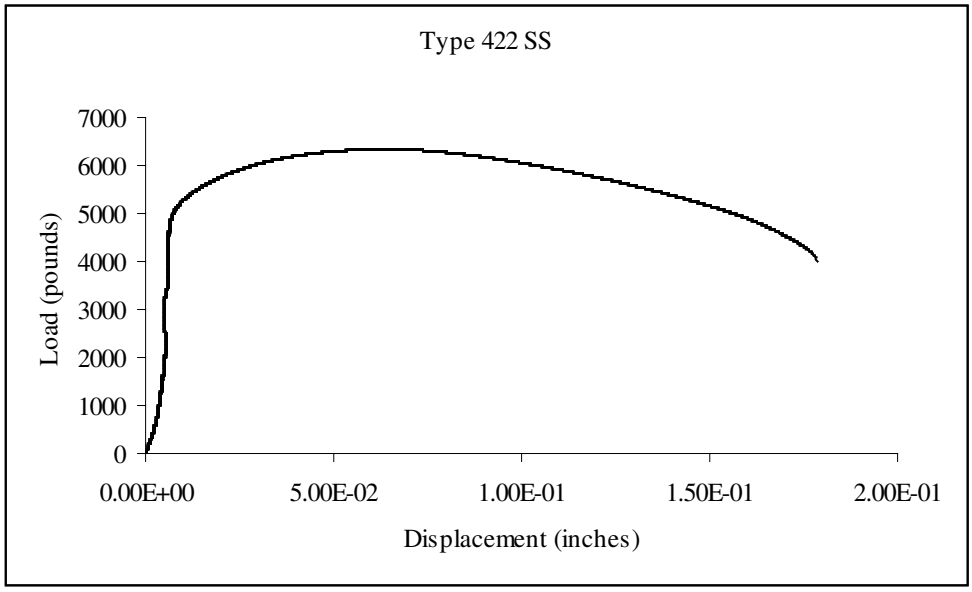

Acidic Environment, Ambient Temperature, E_{cont} = -1000mV (Smooth Sample 1)

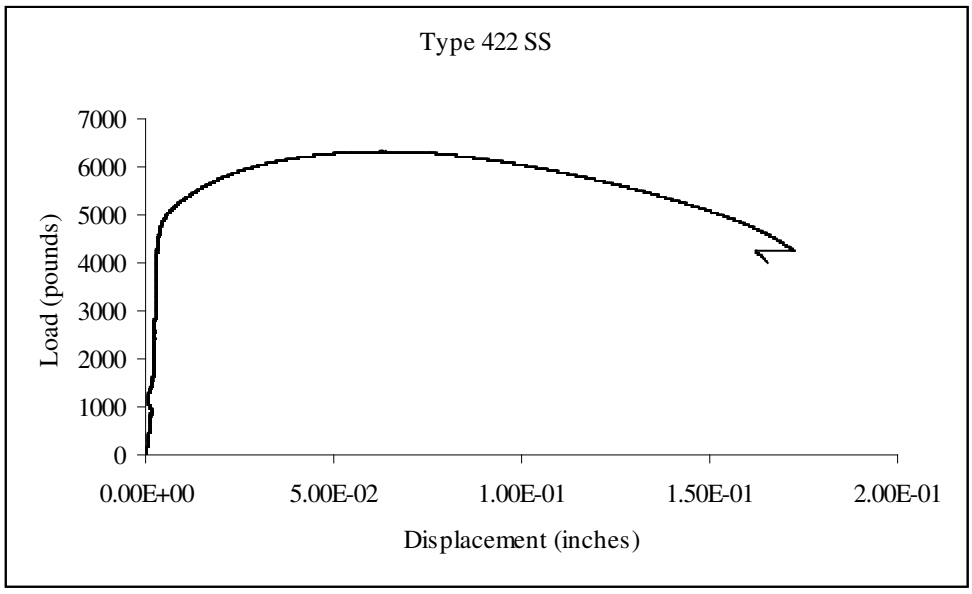

Acidic Environment, Ambient Temperature, E_{cont} = -1000mV (Smooth Sample 2)

B6. SSR Data (Smooth Specimens - Applied Potential)

Environment/ Temperature/E_{cont} (mV)	P_m (lbs)	σ_m (ksi)	P_f (lbs)	σ_f (ksi)	%EL	%RA	TTF (hours)
Neutral/Ambient/-1000	6337.55	126.13	4016.13	138.06	16.67	42.11	18.48
Neutral/Ambient/-1000	6312.78	126.13	3998.84	139.20	15.77	42.60	18.65
Neutral/Ambient/-1000 (Mean)	6325.17	126.13	4007.49	138.63	16.22	42.36	18.57

APPENDIX C

CYCLIC POTENTIODYNAMIC POLARIZATION DATA

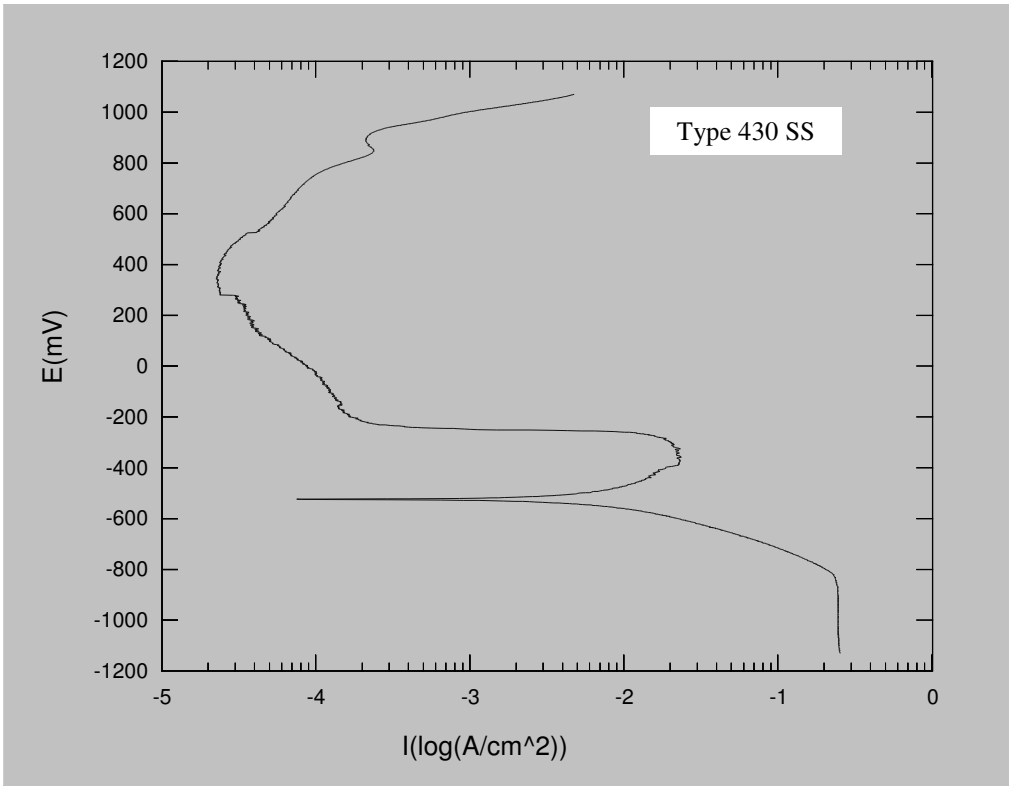

Generated ASTM G 5 Calibration Curve, 1N H_2SO_4, 30°C

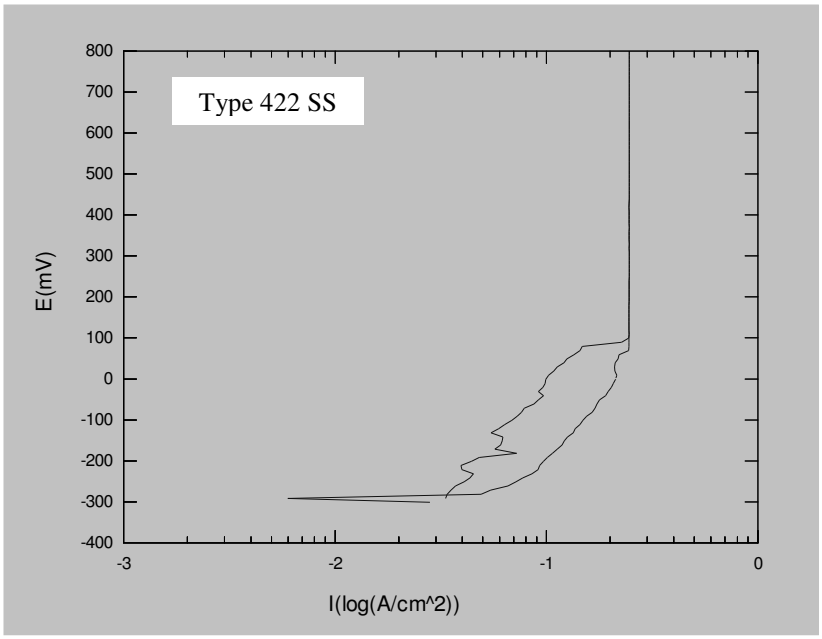

CPP Curve, Neutral Environment, 30°C (Sample 1)

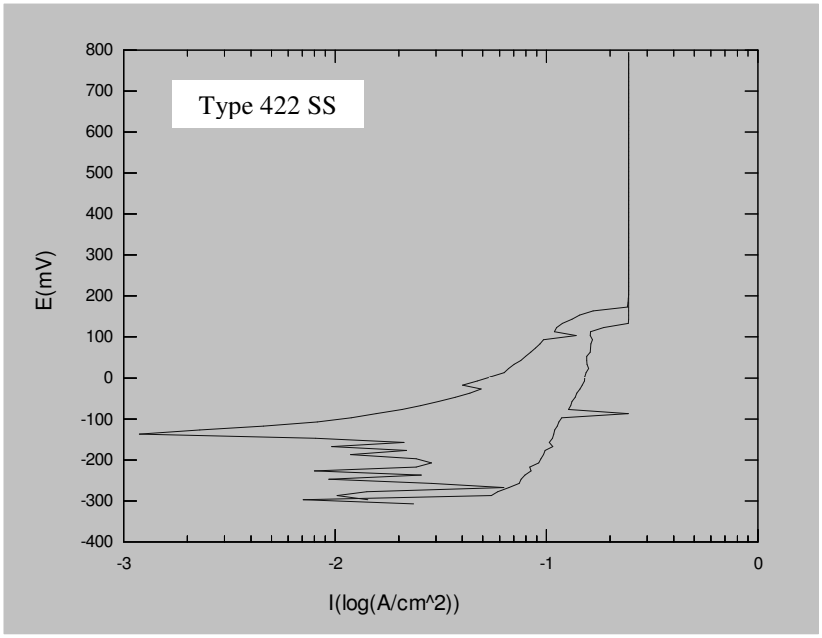

CPP Curve, Neutral Environment, 30°C (Sample 2)

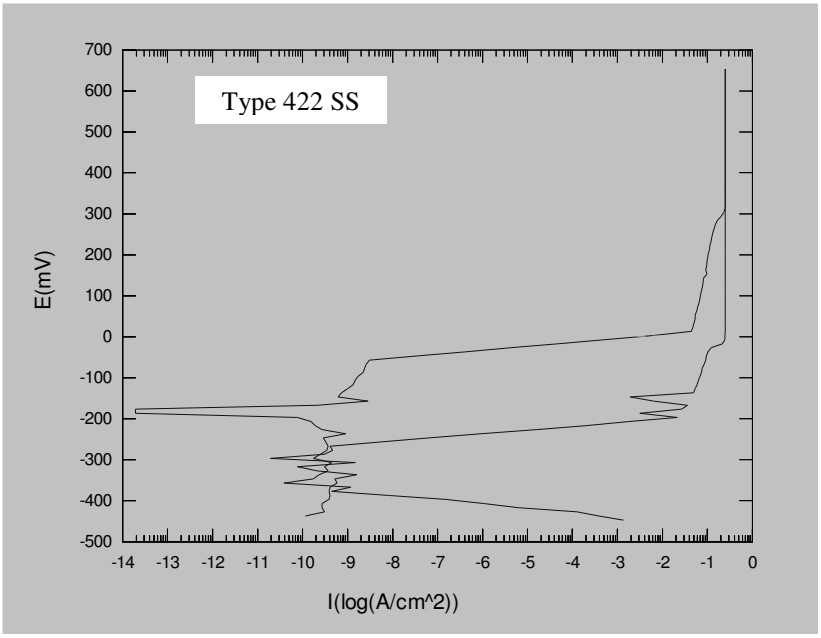

CPP Curve, Neutral Environment, 60°C (Sample 1)

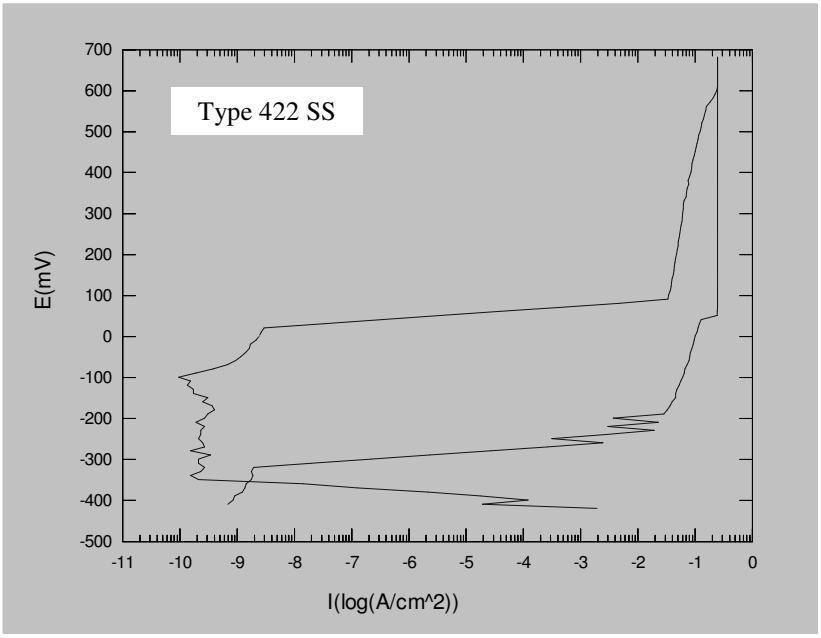

CPP Curve, Neutral Environment, 60°C (Sample 2)

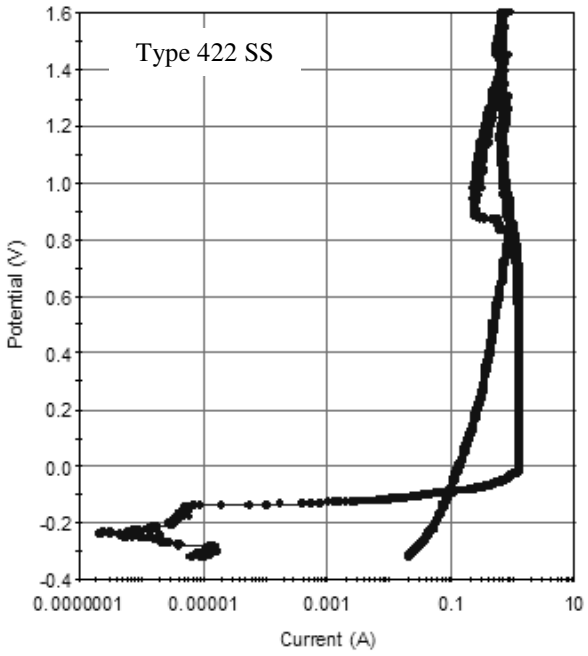

CPP Curve, Neutral Environment, 90°C (Sample 1)

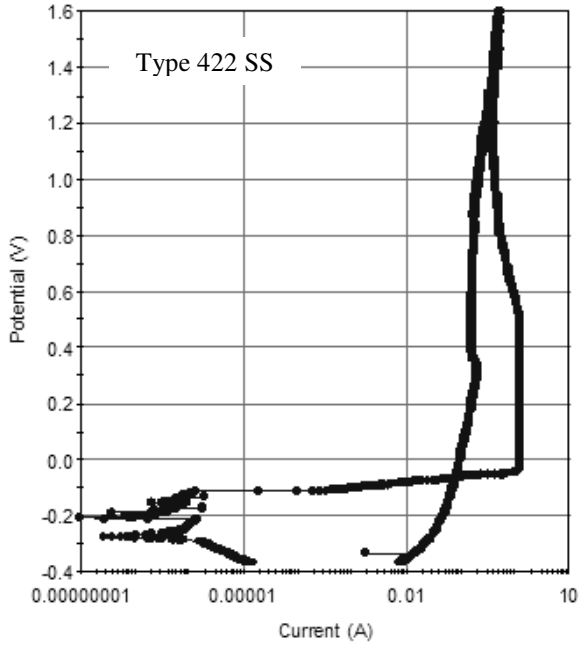

CPP Curve, Neutral Environment, 90°C (Sample 2)

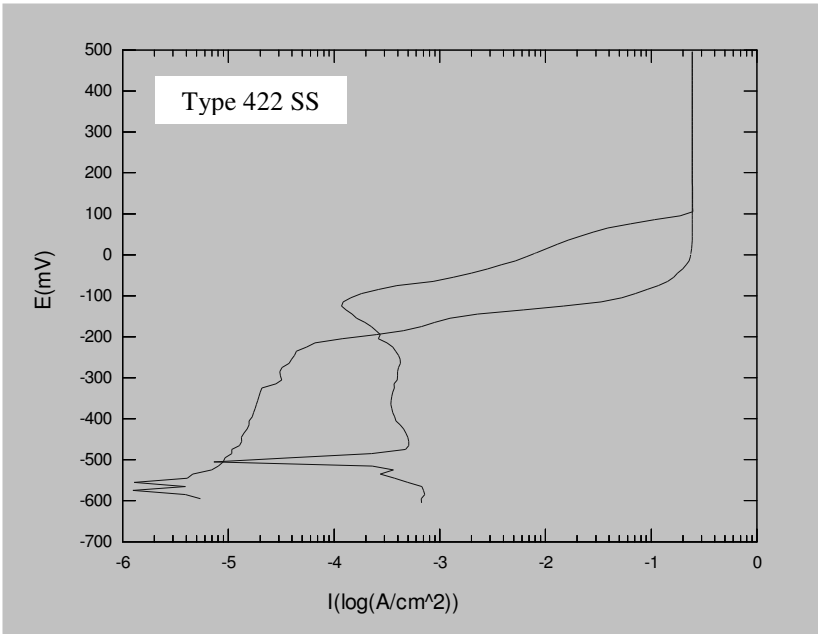

CPP Curve, Acidic Environment, 30°C (Sample 1)

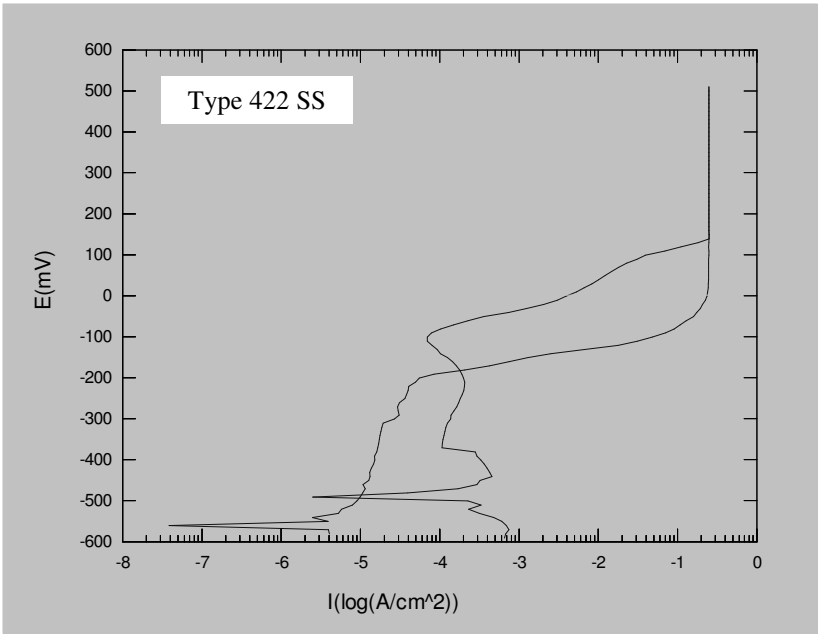

CPP Curve, Acidic Environment, 30°C (Sample 2)

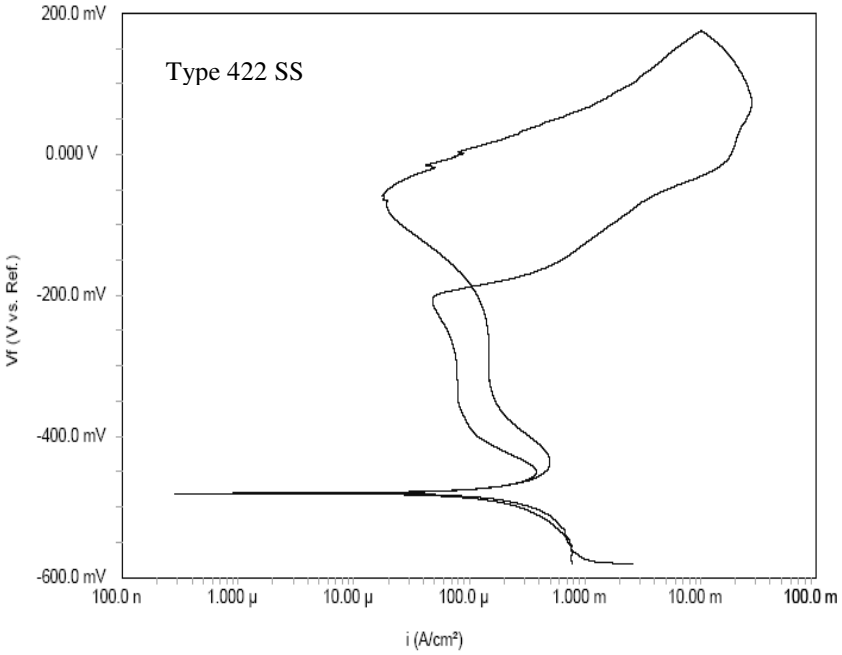

CPP Curve, Acidic Environment, 30°C (Sample 3)

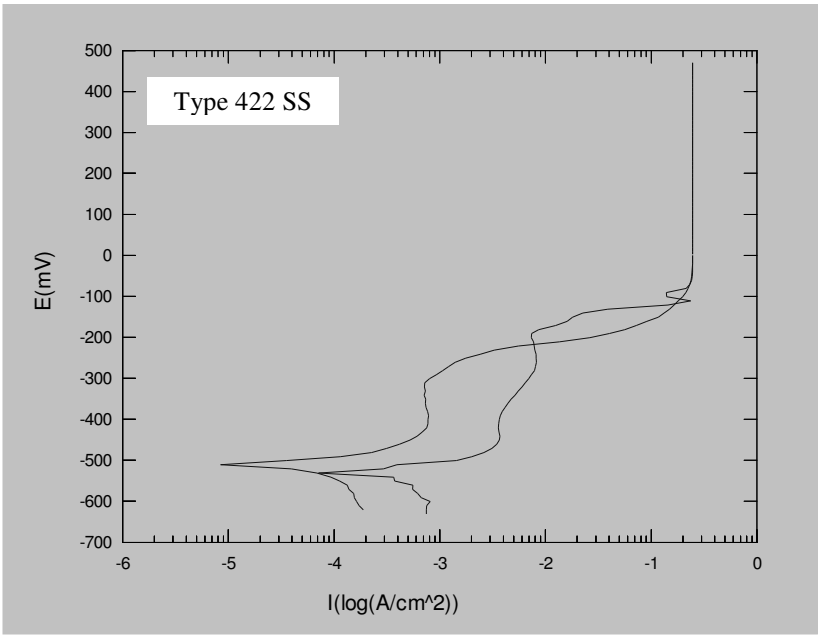

CPP Curve, Acidic Environment, 60°C (Sample 1)

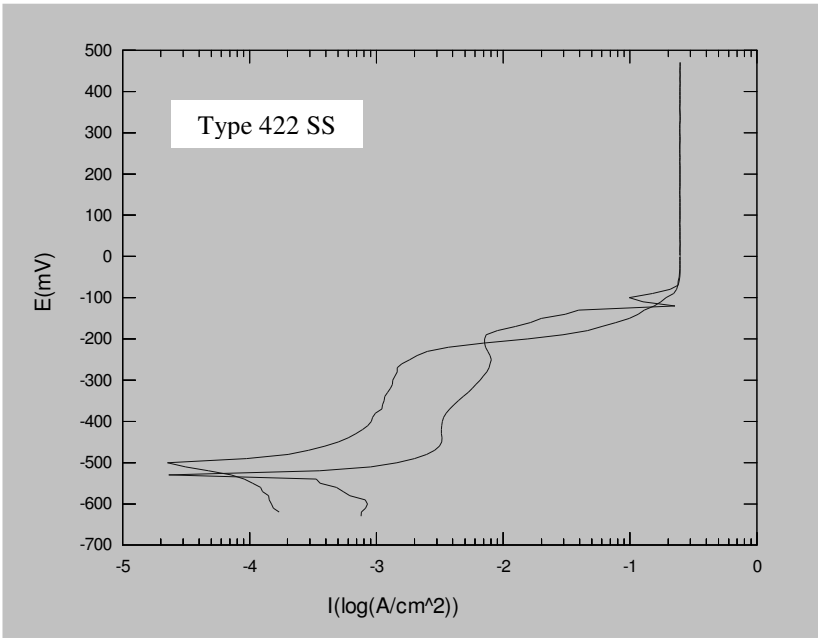

CPP Curve, Acidic Environment, 60°C (Sample 2)

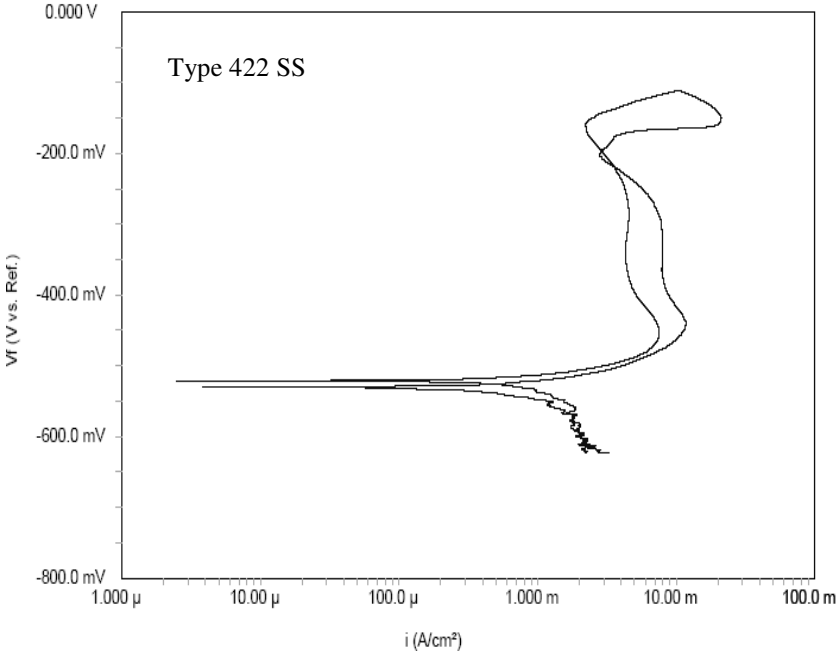

CPP Curve, Acidic Environment, 60°C (Sample 3)

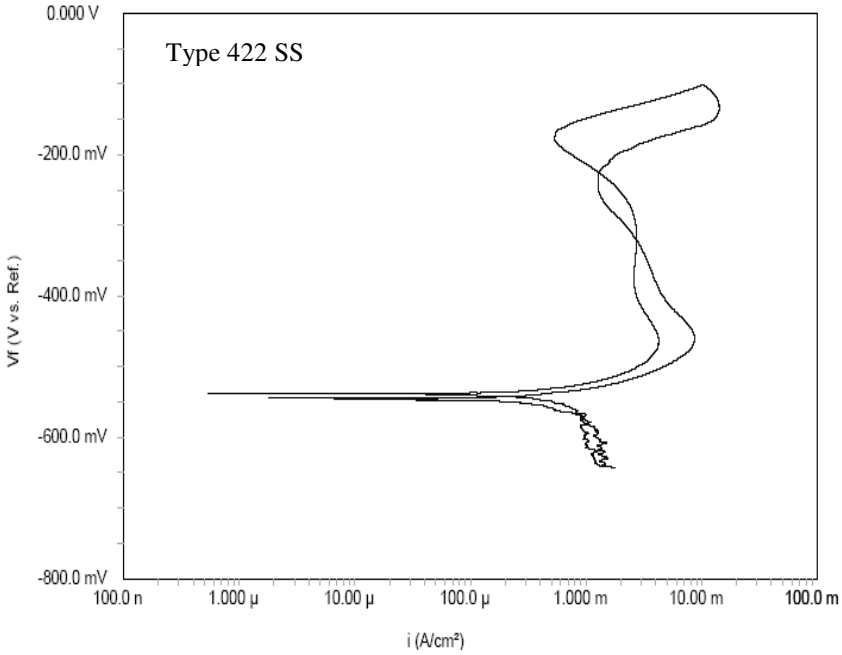

CPP Curve, Acidic Environment, 60°C (Sample 4)

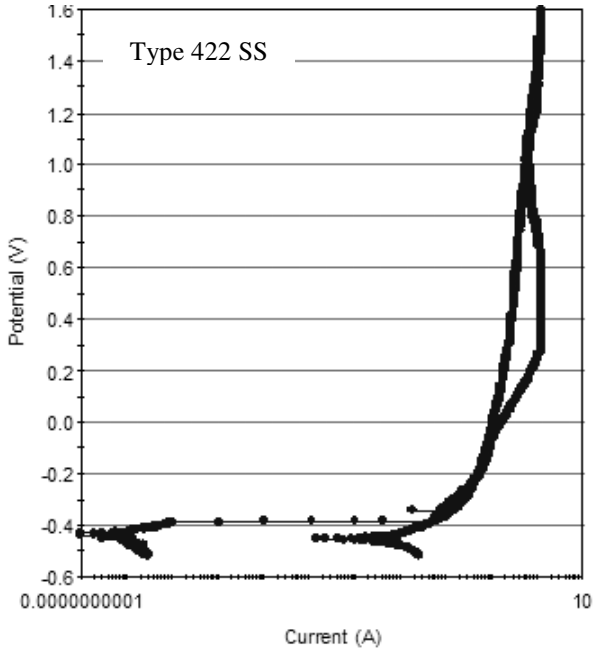

CPP Curve, Acidic Environment, 90°C (Sample 1)

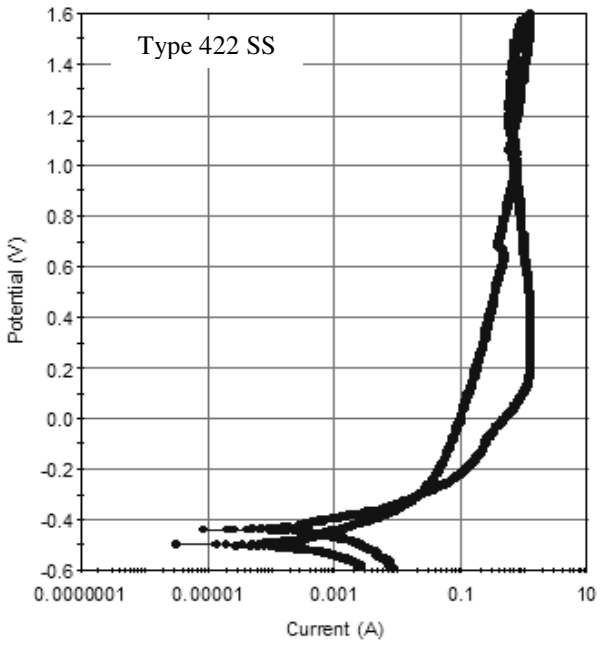

CPP Curve, Acidic Environment, 90°C (Sample 2)

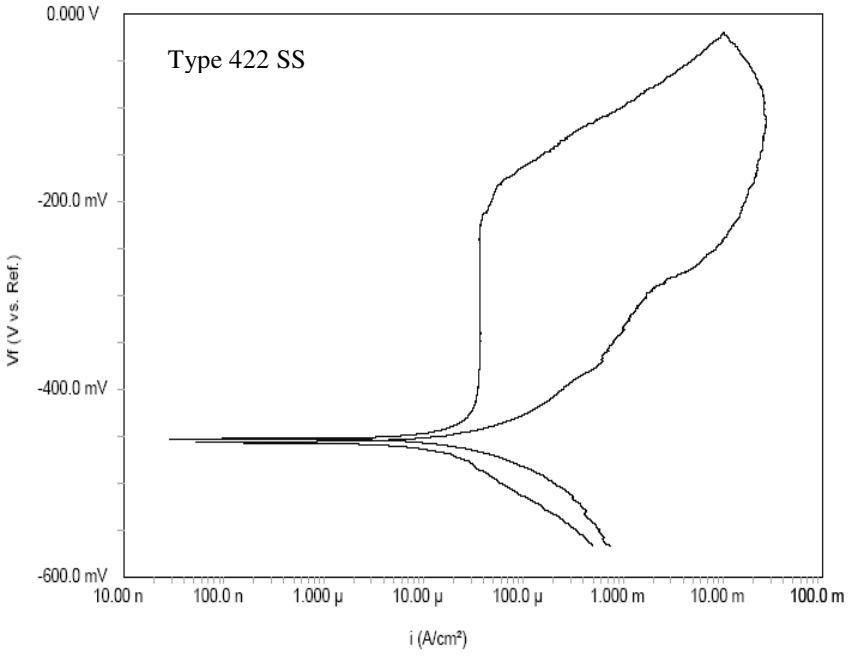

CPP Curve, Acidic Environment, 90°C (Sample 3)

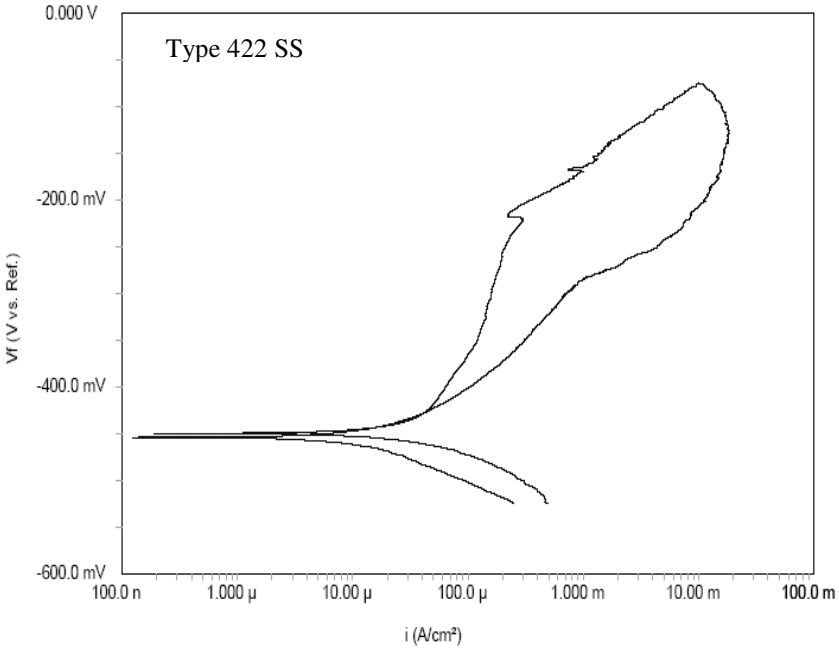

CPP Curve, Acidic Environment, 90°C (Sample 4)

CPP Data

Environment/Temperature (°C)	Critical Potential (mV)		
	E_{corr}	E_{pit}	E_{prot}
Neutral/30	- 202	58	None
Neutral/30	- 208	112	None
Neutral/30 (Mean)	**- 205**	**85**	**None**
Neutral/60	- 348	- 58	None
Neutral/60	- 320	20	None
Neutral/60 (Mean)	**- 334**	**- 19**	**None**
Neutral/90	- 221	- 142	None
Neutral/90	- 270	- 117	None
Neutral/90 (Mean)	**- 246**	**- 130**	**None**
Acidic/30	- 506	- 116	- 196
Acidic/30	- 492	- 102	- 182
Acidic/30	- 481	- 58	- 189
Acidic/30 (Mean)	**- 493**	**- 92**	**- 189**
Acidic/60	- 532	- 192	- 212
Acidic/60	- 524	- 157	- 198
Acidic/60	- 542	- 171	- 226
Acidic/60 (Mean)	**- 532**	**- 178**	**- 212**
Acidic/90	- 471	- 200	None
Acidic/90	- 486	- 200	None
Acidic/90	- 475	- 215	None
Acidic/90	- 467	- 214	None
Acidic/90 (Mean)	**- 475**	**- 207**	**None**

BIBLIOGRAPHY

1. National Research Council, Nuclear Wastes - Technologies for Separations and Transmutation, Washington, D.C., National Academy Press (1996)
2. Yucca Mountain Project, Office of Civilian Radioactive Waste Management FAQ's
3. S. Leray, "Nuclear Waste Transmutation," *Nuclear Instruments and Methods in Physics Research B*, Elsevier Science, **113**, pp. 495-500 (1996)
4. Yucca Mountain Project, Office of Civilian Radioactive Waste Management
5. Addressing the Nuclear Waste Issue, Advanced Fuel Cycle Initiative (AFCI) Website (http://afci.lanl.gov/pdf/AAApamphlet.pdf)
6. C. Rubbia, et al., European Organization for Nuclear Research, CERN Report AT/95-44 ET (1995)
7. L. Cinotti, Doc. ANSALDO, code nr. CRCE 1, SIEX 00001 (1999)
8. M. Salvatores, et al., PSI Bericht Nr. 00-05, ISSN 1019-0643 (2000)
9. F. Venneri, et al., "Disposition of Nuclear Waste using Subcritical Accelerator-Driven Systems: Technology Choices and Implementation Scenarios," *Nuclear Technology*, Vol. **132**, No. 1, pp. 15 (2000)
10. Y. Kurata, et al., "Excellent corrosion resistance of 18Cr-20Ni-5Si steel in liquid Pb-Bi," *Journal of Nuclear Materials*, **325**, pp. 217-222 (2004)
11. X. Jia, et al., "Microstructure in martensitic steels T91 and F82H after irradiation in SINQ Target-3, *Journal of Nuclear Materials*, **318**, pp. 207-214 (2003)
12. Y. Dai, et al., Mechanical properties of modified9Cr–1Mo (T91) irradiated at 6300C in SINQ Target-3, *Journal of Nuclear Materials*, 318, pp. 192-199 (2003)
13. Y. Dai, *Proceedings of ICANS-XIII and ESS-PM4*, PSI, pp. 604 (1995)
14. R.L. Klueh, *Proceedings of 1st International Workshop on Spallation Materials Technology*, Oak Ridge, pp. 3.3-19 (1996)
15. P. Jung, C. Liu, J. Chen, "Retention of Implanted Hydrogen and Helium in Martensitic Stainless Steels and their Effects on Mechanical Properties." *Journal of Nuclear Materials*, **296**, pp. 165-173 (2001)
16. A.L. Johnson, et al., "Spectroscopic and Microscopic Investigation of the Corrosion of 316/316L Stainless Steel by Lead-Bismuth Eutectic (LBE) at Elevated Temperatures: Importance of Surface Preparation," Accepted for *Journal of Nuclear Materials*

17. F. Barbier, et al., "Corrosion Behavior of Steels in Flowing Lead-Bismuth", *Journal of Nuclear Materials,* **296**, pp. 231-236 (2001)

18. V. Ghetta, et al., *Journal of Nuclear Materials,* **296**, pp. 295 (2001)

19. H. Glasbrenner, et al., *Journal of Nuclear Materials*, **296**, pp. 237 (2001)

20. G. Muller, et al., *Journal of Nuclear Materials*, **301**, pp. 40 (2002)

21. G. Nicaise, et al., *Journal of Nuclear Materials*, **296**, pp. 256 (2001)

22. M. Broc, et al., *Proceedings of the BNES International Conference: Liquid Metal Engineering and Technology*, London, pp. 361 (1984)

23. J. Sannier, et al., Fusion Technology, **1**, pp. 901 (1991)

24. J. Sannier, et al., Fusion Eng. Des., **14**, pp. 299 (1991)

25. T. Flament, et al., *Journal of Nuclear Materials*, **191-194**, pp. 132 (1992)

26. G. Benamati, et al., "Temperature Effect on the Corrosion Mechanism of Austenitic and Martensitic Steels in Lead-Bismuth", *Journal of Nuclear Materials*, **301,** pp. 23-27 (2002)

27. H. Rauh and H. Ullmaier, "Hydrogen Concentrations near Cracks in Target Materials for High-Power Spallation Neutron Sources," *Journal of Nuclear Materials*, Elsevier Science, **295**, pp. 109 (2001)

28. A. Kohyama, et al., *Journal of Nuclear Materials*, **138**, pp. 233-237 (1996)

29. F.A. Garner, et al., *Journal of Nuclear Materials*, **276**, 123 (2000)

30. R.L. Klueh, et al., "High chromium ferritic and martensitic steels for nuclear applications," ASTM stock number: MONO3 (2001)

31. Mechanical Properties of Stainless Steel, Outokumpu Stainless Website (http://www.outokumpu.com/pages/Page____5832.aspx)

32. R. L. Klueh, et al., "Ferritic/Martensitic Steels: Promises and Problems," *Journal of Nuclear Materials*, **191-94**, pp. 116-124 (1992)

33. S. N. Roseowasser, et al., *Journal of Nuclear Materials*, **85 & 86**, pp. 177 (1979)

34. D. R. Harries, *Proceedings of Tropical Conference on Ferritic Steels for Use in Nuclear Energy Technology*, The Metallographic Society of AIME, Warrendale, PA, pp. 141 (1984)

35. Heat Treater's Guide - Standard Practices and Procedures for Steel, American Society of Metals, 1982

36. J.G. Gonzalez-Rodriguez, et al., "Effect of Heat Treatment on the Stress Corrosion Cracking Behavior of 403 Stainless Steel in NaCl at 95°C," *Materials Letters*, **43**, 208-214 (2000)

37. H. Spachn, "Stress Corrosion Cracking and Corrosion Fatigue of Martensitic, ferritic and Ferritic-Austenitic Duplex Stainless Steels, in: R.P. Gangloff, et al., *Environment-Induced Cracking of Metals*, pp. 449-487, NACE-10 (1988)

38. Properties of Type 422 SS, efunda (Engineering Fundamentals) Website (http://www.efunda.com/materials/alloys/stainless_steels/show_stainless.cfm?ID=AISI_Type_422&prop=all&Page_Title=AISI%20Type%20422)

39. Welding Stainless Steel, Welding Engineer Website (http://www.weldingengineer.com/Stainless%20Steel.htm)

40. Stainless - Heat Treatment, The A to Z of Materials (AZoM) Website (http://www.azom.com/details.asp?ArticleID=1141)

41. ASTM E8-04, "Standard Test Methods for Tension Testing of Metallic Materials," ASTM International

42. R. C. Juvinall, et al., "Stress Concentration Factors for Grooved Shafts with Axial Loading," Fundamentals of Machine Component Design, pp. 144 (1999)

43. ASTM G49-85 (2000), "Standard Practice for Preparation and Use of Direct Tension Stress-Corrosion Test Specimens," ASTM International

44. Constant Load/Deflection Tests, Corrosion Source Website (http://www.corrosionsource.com/handbook/testing/cld.htm)

45. Cortest, Incorporated Website (www.cortest.com)

46. ASTM G129-00, "Standard Practice for Slow Strain Rate Testing to Evaluate the Susceptibility of Metallic Materials to Environmentally Assisted Cracking," ASTM International

47. Slow-Strain-Rate Testing, Corrosion Source Website http://www.corrosionsource.com/handbook/testing/ssrt.htm

48. A. K. Roy, et al., "Cracking of Titanium Alloys under Cathodic Applied Potential," Framatone Cogema Fuels (1999)

49. Polarization Behavior, Corrosion Doctors Website (http://www.corrosion-doctors.org/Kinetics/Polarization.htm)

50. Potentiostat, Corrosion Doctors Website (http://www.corrosion-doctors.org/Instrumentation/potentiostat.htm)

51. ASTM G5-94 (1999) e1, "Standard Reference Test Method for Making Potentiostatic and Potentiodynamic Anodic Polarization Measurements," ASTM International

52. Hydrogen Embrittlement, Metallurgical Consultants Website (http://www.materialsengineer.com/CA-hydrogen.htm)

53. G. P. Tiwari, et al., "A Study of Internal Hydrogen Embrittlement of Steels," *Materials Science and Engineering*, **A286**, pp. 269-281 (2000)

54. A.R. Troiano, *Transactions of the American Society of Metals*, **52**, pp. 54 (1960)

55. R.A. Oriani, *Annual Review of Materials Science*, **8**, pp. 327 (1978)

56. P. Hirth, *Metallurgical Transactions*, **11A**, pp. 861, (1980)

57. Hydrogen Embrittlement, Corrosion Doctors Website (http://www.corrosion-doctors.org/Forms/embrittlement.htm)

58. Hydrogen Embrittlement, Corrosion Source Website (http://www.corrosionsource.com/handbook/CPS/cps_a_hic.htm)

59. A. K. Roy, et al., "Cracking of Titanium Alloys under Cathodic Applied Electrochemical Potential," *Micron*, **32**, No. 2, pp. 211-218 (2001)

60. I. Azkarate, et al., "Hydrogen Assisted Stress Cracking of Titanium Alloys in Aqueous Chloride Environments," Progress in the Understanding and Prevention of Corrosion, 2, Spain, pp. 1573-1580 (1993)

61. A. K. Roy, et al., "Effect of Controlled Potential on SCC of Nuclear Waste Package Container Materials," *Proceedings of NACE Corrosion 2000*, Paper No. 00188, Orlando, FL (2000)

62. A. K. Roy, et al., "Localized Corrosion of Candidate Container Materials in Ferric Chloride Solutions," Proceedings of NACE Corrosion 1999, Paper No. 463 (1999)

63. Heat Treating Terms, Engineers Edge Website (http://www.engineersedge.com/heat_treat.htm)

64. A. K. Roy, et al., "Stress Corrosion Cracking of Martensitic Stainless Steel for Transmutation Applications," *Proceedings of IHLRWM 2003*, Las Vegas, NV, pp. 838-843 (2003)

65. A. K. Roy, et al., "Environment-Induced Degradation of Spallation Target Materials," *Proceedings of ANS AccApp'03*, San Diego, CA, pp. 893-899 (2003)

66. A. K. Roy, et al., "Effect of Environmental Variables on Cracking of Martensitic Stainless Steels under Different Loading Conditions, *Proceedings of ANS Global 2003*, New Orleans, LA, pp. 1824-1829 (2003)

67. General Information on Stainless Steels, efunda (Engineering Fundamentals) Website (http://www.efunda.com/materials/alloys/stainless_steels/stainless.cfm)

68. A. U. Malik et al., "The Influence of pH and Chloride Concentration on the Corrosion Behavior of AISI 316L Steel in Aqueous Solutions," *Corrosion Science*, **33**, No. 11, 1809 (1992) (it was 9 before)

69. J-H. Wang et al., "Effects of Cl^- Concentration and Temperature on Pitting of AISI 304 Stainless Steel," *Corrosion*, **44**, No. 10, 732 (1988)

70. W. Bogaerts et al., "Passivity of Austenitic Stainless Steel in High Temperature-High Pressure Aqueous Solutions," *Proc. 8th Int. Cong. Metallic Corrosion*, **1**, pp 31-36, Mainz, West Germany (1981)

71. P. E. Manning and D. J. Duquette, "The Effect of Temperature (25-289°C) on Pit Initiation in Single Phase and Duplex 304L Stainless Steels in 100 ppm Cl^- Solution," *Corrosion Science*, 20, 597 (1980)

72. Stress Corrosion Cracking, Metallurgical Consultants Website (http://www.materialsengineer.com/CA-scc.htm)

73. Corrosion, ASM International, 13(9)

74. R. J. H. Wanhill, "Aqueous Stress Corrosion in Titanium Alloys," *Br. Corros. J.*, **10**, No. 2, pp. 69-78 (1975)

75. J. Brettle, "Stress Corrosion of Titanium and its Alloys in Aqueous Chloride Environments," *Met. Mater.*, pp. 442-451 (1972)

76. Corrosion Resistant Alloys, Goodwin Steel Castings Limited Website (http://www.goodwin.co.uk/gsc/app_corrosion.htm)

77. A. K. Roy, et al., "Effect of Environmental Variables on Localized Corrosion of High-Performance Container Materials," Proceedings of the 5th International Conference on Nuclear Engineering, Paper No. ICONE5-2093, pp. 1-11, ASME/SFEN/JSME, Nice, France (1997)

78. A. K. Roy, et al., "Localized Corrosion Behavior of Candidate Nuclear Waste Package Container Materials," Materials Performance, 37, No. 3, NACE International, pp. 54-58 (1998)

79. M. G. Fontana, et al., Corrosion Engineering, McGraw-Hill Book Company, New York (1978)

80. R. M. Hudson, "Hydrogen Absorption by and Dissolution Rate of Low-Carbon Steel in Sulfuric, Hydrochloric, Phosphoric and Nitric Acids," Corrosion, 20, pp. 245 (1969)

81. J. Gu, et al., "Effect of Hydrogen on Structure and Slow Strain Rate Embrittlement of Mill Annealed Ti6Al4V," *Materials Science and Technology*, **12**, No. 10, pp. 802-807 (1996)

82. L. C. Covington, "Factors Affecting the Hydrogen Embrittlement of Titanium," *Proceedings of NACE Corrosion 1975*, Toronto, Canada (1975)

83. N. E. Paton, et al., "Effect of Hydrogen on Titanium and its Alloys," Titanium and Titanium Alloys Source Book, American Society of Metals, pp. 185-207 (1982)

84. A. K. Roy, et al. "Stress Corrosion Cracking Evaluation of Candidate Container Alloys by Double Cantilever Beam Method," *Proceedings of NACE Corrosion 2000*, Paper No. 00189 (2000)

85. A. K. Roy, et al. "Stress Corrosion Cracking of Alloy C-22 and Ti Gr-12 using Double-Cantilever-Beam Technique," *Micron*, **30**, No. 6, pp. 649-654 (1999)

86. Metals Handbook, Fractography, ASM International, 9th Edition, pp. 396 and 453 (1987)

VITA

Graduate College
University of Nevada, Las Vegas

Ramprashad Prabhakaran

Local Address:
4223 Cottage Circle, Apt # 1
Las Vegas, NV 89119

Permanent Address:
9199 Muir Lane
Fishers, IN 46038

Degree:
Bachelor of Engineering, Mechanical Engineering, 2001
University of Madras, Chennai, India

Special Honors and Awards:

- Received 3 scholarships (US DOE, ASME, ORAU) to attend and present technical papers at conferences
- Member of Tau Beta Pi (Engineering Honor Society), Phi Kappa Phi (National Honor Society), National Dean's List
- Secretary, UNLV American Nuclear Society Student Section
- Awarded graduate research assistantship at UNLV to pursue M.S. program in Mechanical Engineering

Selected Publications:

- Ajit K. Roy, Ramprashad Prabhakaran, et al., "Stress Corrosion Cracking of Nuclear Transmutation Structural Materials," *Materials Performance*, NACE International, September 2004, Vol. 43, No. 9, pp. 52-56 (2004)
- Ajit K. Roy, Ramprashad Prabhakaran, "Stress Corrosion Cracking of Type 422 Stainless Steel for Transmutation Applications," *Proceedings of IYNC 2004*, Paper No. 119, Toronto, Canada (2004)
- Ramprashad Prabhakaran, Ajit K. Roy, "The Effect of Environmental and Mechanical Variables on Stress Corrosion Cracking of a Martensitic Stainless Steel for Transmutation Applications," *Proceedings of ASME ICONE12*, Paper No. 49399, Arlington, VA (2004)

- Ajit K. Roy, Ramprashad Prabhakaran, et al., "Cracking of Target Structural Materials for Transmutation Applications," *Proceedings of NACE Corrosion 2004*, Paper No. 4559, New Orleans, LA (2004)
- Ajit K. Roy, Ramprashad Prabhakaran, et al., "Effect of Environmental Variables on Cracking of Martensitic Stainless Steels under Different Loading Conditions," *Proceedings of ANS Global 2003*, Paper No. 87869, New Orleans, LA (2003)
- Ajit K. Roy, Ramprashad Prabhakaran, et al., "Environment-Induced Degradation of Spallation Target Materials," *Proceedings of ANS AccApp'03*, Paper No. 79416, San Diego, CA (2003)

Thesis Title: Environment-Induced Degradations in a Target Structural Material for Transmutation Applications

Thesis Examination Committee:
Chairperson, Dr. Ajit K. Roy, Ph. D.
Committee Member, Dr. Anthony E. Hechanova, Ph. D.
Committee Member, Dr. Brendan J. O'Toole, Ph. D.
Graduate College Representative, Dr. Satish C. Bhatnagar, Ph. D.